Cell culture-based production of influenza A virus-derived defective interfering particles

Dissertation
zur Erlangung des akademischen Grades

Doktoringenieur
(Dr.-Ing)

von Marc Dominique Hein (M.Sc.)
geb. am 26. März 1994 in Berlin

genehmigt durch die Fakultät für Verfahrens- und Systemtechnik
der Otto-von-Guericke-Universität Magdeburg

Promotionskommission:	Prof. Dr. rer. nat. Nora Kulak	(Vorsitz)
	Prof. Dr.-Ing. Udo Reichl	(Gutachter)
	Prof. Dr.-Ing. Ralf Pörtner	(Gutachter)
	Dr. rer. nat. Ingo Jordan	(Gutachter)

eingereicht am: 28.01.2022

Promotionskolloquium am: 24.06.2022

ABSTRACT

With annual epidemics and occasionally severe pandemics, influenza A virus (IAV) represents a major human pathogen. Additional to the prevention of viral infections using vaccines, antiviral drugs represent a treatment option. However, resistances against currently used antivirals have already been reported, demonstrating the need for novel treatment modalities. An approach that was previously suggested is the use of defective interfering (DI) particles (DIPs) as antiviral agents. IAV DIPs are naturally occurring virus variants, typically characterized by a large internal deletion in one of their eight genomic viral RNA (vRNA) segments. Recently, a novel type of DIP, called OP7, which contains nucleotide substitutions in segment 7 vRNA instead of deletions was discovered. Due to deletions or mutations in the viral genome, DIPs express only truncated or mutated forms of functional proteins essential for viral replication. Therefore, DIPs can only propagate in a co-infection with infectious standard viruses (STVs), compensating for their defect. In such a co-infection scenario, DIPs interfere with and suppress STV replication and almost exclusively replication deficient DIPs are released, which constitutes their antiviral potential. In the presented PhD work, cell culture-based production processes for the recently discovered OP7 and a conventional DIP with a deletion in segment 1 vRNA, called DI244, were established.

In the first part of this work, a cell culture-based production process for OP7 was investigated in shake flasks. A seed virus containing infectious STVs and the desired OP7 was used. First, the interplay of STV and OP7 was assessed by testing a range of multiplicities of infection (MOIs). Here, an intermediate production MOI of 1E−2, showing a good balance between OP7 vRNA replication and an acceptable suppression of overall virus production, resulted in highest OP7 yields, determined by quantitative PCR. Further, to identify the production MOI yielding the highest biological efficacy, an *in vitro* interference assay was used. More specifically, STV-infected cells were co-infected with DIP material, and the reduction of released infectious virus particles was determined. Here, OP7 material produced at MOI 1E−2 showed the highest interfering efficacy and reduced the infectious virus titer by approximately four orders of magnitude. Next UV-irradiation was used, to inactivate infectious STVs in the produced OP7 material, which are unwanted for a potential application. Finally, the production process was transferred to a laboratory-scale stirred tank bioreactor (STR). Results obtained showed a very high comparability to small scale experiments in shake flasks.

In the second part of this PhD work, a system for production of purely clonal DI244 without contaminating STVs was investigated. DI244 has a deletion in vRNA segment 1 encoding for the viral polymerase basic protein 2 (PB2). Therefore, a genetically modified suspension cell line expressing PB2 and a purely clonal DI244 seed virus (both provided by a collaboration partner) were used. First, the impact of the multiplicity of DIP (MODIP) on DI244 yield was investigated in batch cultivations in shake flasks. Here, the highest interfering efficacy was observed for material produced at MODIP 1E−2, which reduced the infectious virus titer by approximately one order of magnitude. Lower interfering efficacies observed for lower production MODIPs were likely caused by the increased formation of virus particles lacking the DI244 vRNA. The produced DI244 did not require UV-irradiation, as it did not contain any STVs. Next, the production process was transferred from shake flask to a laboratory-scale STR. Here, very similar virus replication dynamics were observed independent of the production scale.

Finally, process intensification strategies were applied to improve the DI244 yield in the STR. Here, a perfusion process using an alternating tangential flow filtration (ATF) system for cell retention was used. DIP titers more than 10-fold higher than for batch cultivations were observed. Next, the perfusion rate was controlled using a capacitance probe measuring the viable cell volume in the cultivation vessel. The control resulted in sufficient metabolite concentrations and low waste product levels over the entire cultivation time. Furthermore, a novel tubular cell retention membrane was investigated for its potential for continuous virus harvesting into the permeate. In contrast to a commonly used hollow fiber membrane, the tubular membrane showed no significant retention of the produced virus particles and offers interesting possibilities for establishment of advanced process integration strategies.

Furthermore, DIP material produced in the context of this PhD work was used by collaboration partners for animal experiments. Here, the administration of the produced OP7 or DI244 protected mice against an otherwise lethal dose of IAV STVs, clearly demonstrating its antiviral potential.

Summarized, cell culture-based production processes were successfully established for both DIPs, DI244 and OP7, yielding material with a high DIP titers and high interfering efficacies. Further, the successful scale-up to a laboratory-scale STR could be shown for both production processes and process intensification strategies were applied for DI244 production. Overall, the presented work exhibits the feasibility of cell culture-based production of DIP material for antiviral therapy.

KURZFASSUNG

Mit jährlichen Epidemien und gelegentlich schweren Pandemien ist das Influenza-A-Virus (IAV) eines der bedeutendsten humanen Krankheitserreger. Die Behandlung mit antiviralen Medikamenten stellt eine Ergänzung zur Prävention mit Impfstoffen dar. Allerdings wurden bereits Resistenzen gegen derzeit verwendete antivirale Medikamente beobachtet, was die Notwendigkeit neuer Behandlungsmodalitäten aufzeigt. Ein Ansatz, der bereits früher diskutiert wurde, ist die Verwendung von defekten interferierenden (DI) Partikeln (DIPs) als antivirales Medikament. IAV DIPs sind natürlich entstehende Virusvarianten, die typischerweise durch eine große interne Deletion in mindestens einem ihrer acht genomischen viralen RNA (vRNA)-Segmente charakterisiert sind. Zusätzlich wurde kürzlich ein weiterer DIP entdeckt, genannt OP7, welcher sich anstelle von Deletionen nur durch Nukleotid-Substitutionen in vRNA-Segment 7 auszeichnet. Aufgrund der Deletion oder der Mutationen im viralen Genom exprimieren DIPs nur verkürzte oder mutierte Formen von funktionellen Proteinen, welche für die virale Replikation essentiell sind. Daher können DIPs in der Regel nur in einer Ko-Infektion mit infektiösen Standardviren (STV) replizieren, die ihren Defekt kompensieren. In einer solchen Ko-Infektion stören und inhibieren DIPs die STV-Replikation und es werden fast ausschließlich DIPs gebildet, was ihr antivirales Potenzial begründet. Die vorliegende Doktorarbeit befasst sich mit der Etablierung von zellkulturbasierten Produktionsprozessen zur Herstellung des kürzlich entdeckten OP7 und eines konventionellen DIPs mit einer Deletion in vRNA-Segment 1, genannt DI244.

Im ersten Teil dieser Arbeit wurde ein zellkulturbasierter Produktionsprozess für OP7 im Schüttelkolben untersucht. Hierfür wurde ein Saatvirus verwendet, das eine Mischung aus infektiösem STV und OP7 enthält. Zunächst wurde die Interaktion von STV und OP7-vRNA beleuchtet, indem verschiedene Multiplizitäten der Infektion (MOI) getestet wurden. Dabei führte eine mittlere MOI von 1E−2 zu den höchsten OP7-Ausbeuten, da diese ein gutes Gleichgewicht von OP7- Replikation und einer akzeptablen Unterdrückung der gesamten Virusproduktion erlaubte. Um die Produktions-MOI zu ermitteln bei der Material mit der höchsten biologischen Wirksamkeit erzeugt wird, wurde ein *in-vitro*-Interferenzassay durchgeführt. Dafür wurden STV-infizierte Zellen mit DIP-Material koinfiziert und die Reduktion der freigesetzten infizierenden Viruspartikel bestimmt. Hier zeigte OP7-Material, das mit einer MOI von 1E−2 hergestellt wurde, die höchste interferierende Wirksamkeit und reduzierte den Titer des infektiösen STV um etwa vier

Größenordnungen. Anschließend wurde eine UV-Bestrahlung durchgeführt, um infektiöses STV im produzierten OP7-Material zu inaktivieren, welches in einer potenziellen Anwendung unerwünscht wäre. Im Anschluss wurde der Produktionsprozess auf einen Rührkessel-Bioreaktor (STR) im Labormaßstab übertragen. Hier zeigte sich eine sehr hohe Vergleichbarkeit zu den Versuchen in Schüttelkolben.

Im zweiten Teil dieser Arbeit wurde ein Produktionssystem zur Herstellung von reinem DI244, ohne Kontamination mit STV, untersucht. DI244 hat eine Deletion im vRNA Segment 1, dass das virale Polymerase-Basisprotein 2 (PB2) kodiert. Daher wurden eine gentechnisch veränderte Suspensionszelllinie, die PB2 exprimiert, und ein rein klonales DI244-Saatvirus verwendet (beides bereitgestellt von einem Kooperationspartner). Zunächst wurde die Auswirkung der Multiplizitäten der DIPs (MODIP) auf die DI244-Ausbeute in Batch-Kulturen in Schüttelkolben untersucht. Dabei wurde die höchste interferierende Wirksamkeit für Material produziert mit MODIP 1E−2 beobachtet, welches den infektiösen Virustiter um etwa eine Größenordnung reduzierte. Die geringeren interferierenden Wirksamkeiten, die für Material produziert bei niedrigeren MOIs beobachtet wurden, sind wahrscheinlich auf eine vermehrte Bildung von Viruspartikeln zurückzuführen, denen die DI244 vRNA fehlte. Das produzierte DI244-Material benötigte keine UV-Inaktivierung, da es keine STV enthielt. Als Nächstes wurde der Produktionsprozess vom Schüttelkolben auf einen STR im Labormaßstab hochskaliert. Unabhängig vom Produktionsmaßstab wurde eine sehr ähnliche Virusreplikationsdynamik beobachtet.

Schließlich wurden Prozessintensivierungsstrategien angewendet, um die DI244 Ausbeute im STR zu erhöhen. Unter Verwendung eines alternierenden Tangentialflussfiltrationssystems (ATF) zur Zellrückhaltung wurde ein Perfusionsprozess etabliert. Hier wurden 10-mal höhere DIP-Titer als bei vorherigen Batch-Kulturen erreicht. Als nächstes wurde die Perfusionsrate unter Zuhilfenahme einer Kapazitätssonde, deren Signal zum Volumen der Zellen im Kultivierungsgefäß korreliert werden konnte, geregelt. Diese Reglung resultierte in Substrat- und Nebenproduktkonzentrationen, die ein exponentielles Zellwachstum und effiziente Virusreplikation erlaubten. Des Weiteren wurde eine neuartige tubulare Zellrückhaltemembran auf ihr Potenzial zur kontinuierlichen Virusernte untersucht. Im Gegensatz zu einer üblicherweise verwendeten Hohlfasermembran zeigte die tubulare Membran keine signifikante Rückhaltung der produzierten Viruspartikel und bietet interessante Möglichkeiten für Prozessintegrationsstrategien.

Darüber hinaus wurde das im Rahmen dieser Doktorarbeit hergestellte DIP-Material von Kooperationspartnern für Tierversuche verwendet. Hier schützte die Verabreichung des produzierten OP7 oder DI244 Mäuse vor einer andernfalls tödlichen Dosis von IAV STV, was eindeutig ihr antivirales Potenzial belegt.

Zusammengefasst konnten für beide DIPs, OP7 und DI244, zellkulturbasierte Prozesse etabliert werden, die die Produktion von Material mit hohen DIP-Titern und hohen antiviralen Wirksamkeiten ermöglichen. Für beide Produktionssysteme konnte erfolgreich die Skalierbarkeit auf einen STR im Labormaßstab gezeigt werden. Für die DI244-Produktion wurden Prozessintensivierungsstrategien angewandt und ermöglichten sehr hohe DI244-Titer. Die vorliegende Arbeit zeigt deutlich das Potenzial der zellkulturbasierten Produktion von DIPs für eine antivirale Therapie.

Table of content

LIST OF ABBREVIATIONS

Abbreviation	Description
ATCC	American-Type Culture Collection
ATF	Alternating tangential flow filtration
BPE	Bioprocess Engineering
cRNA	Complementary RNA
cRNP	Complementary ribonucleoprotein
CSVY	Cell-specific virus yield
DI	Defective interfering
DIP	Defective interfering particle
DPZ	German Primate Center
dsDNA	Double-stranded DNA
ECACC	European Collection of Cell Cultures
FL	Full-length
GMEM	Glasgow minimal essential medium
GMP	Good manufacturing practice
HA	Hemagglutinin
HA assay	Hemagglutination activity assay
HCD	High cell density

HFM	Hollow fiber membrane
hpi	Hours post infection
HZI	Helmholtz Centre for Infection Research
IAV	Influenza A virus
IB	Infection Biology
IG	Department of Infection Genetics
M1	Matrix protein 1
M1-OP7	Mutated matrix protein 1
M2	Matrix protein 2
MDCK	Madin-Darby canine kidney
MDCK(adh)	Parental adherent MDCK
MDCK.Xe.E	Parental suspension MDCK
MDCK-PB2(adh)	Adherent MDCK cells expressing PB2
MDCK-PB2(sus)	Suspension MDCK cells expressing PB2
MPI	Max Planck Institute
MS	Mass spectrometry
NA	Neuraminidase
NC	Negative control
NP	Nucleoprotein

NS1	Nonstructural protein 1
PA	Polymerase acidic protein
PB1	Polymerase basic protein 1
PB2	Polymerase basic protein 2
PBS	Phosphate buffered saline
PFU	Plaque forming units
DO	Dissolved oxygen
PR8	Influenza virus strain A/PR/8/34 (H1N1)
real-time RT-qPCR	Real-time reverse transcription-quantitative PCR
RIG-I	Retinoic acid inducible gene I
RSD	Relative standard deviation
RT	Reverse transcription
RV	Reactor volume
SARS-CoV-2	Severe acute respiratory syndrome coronavirus 2
Seg1–8	Segment 1–8
Seg7 OP7	Segment 7 vRNA of OP7
segment-specific RT-PCR	Segment-specific reverse transcription-PCR
STR	Stirred tank bioreactor
STV	Standard virus

SXC	Steric exclusion chromatography
$TCID_{50}$	50% tissue culture infectious dose
TFF	Tangential flow filtration
VAM	Department of Vaccinology and Applied Microbiology
VHU	Virus harvest unit
vRNA	Viral RNA
vRNP	Viral ribonucleoproteins

LIST OF SYMBOLS

Symbol	Description	Unit
μ	Cell-specific growth rate	1/h
b	Y-offset of the calibration curve of the vRNA standards	-
BVSPR	Biovolume-specific perfusion rate	pL/µm^3/d
$C_{PFU,cPerm}$	Virus concentration in the collected permeate	PFU/mL
$C_{PFU,Perm,t}$	Virus concentration in the permeate at sample time point t	PFU/mL
$C_{PFU,STR}$	Virus concentration in the STR	PFU/mL
$C_{PFU,STR,t}$	Virus concentration in the STR at sample time point t	PFU/mL
C_s	Metabolite concentration in the STR	mmol/mL
$C_{s,Med}$	Metabolite concentration in the medium	mmol/mL
CSPR	Cell-specific perfusion rate	pL/cell/d
$CSVY_{PFU}$	Cell-specific virus yield based on PFU	PFU/cell
$CSVY_{vRNA}$	Cell-specific virus yield based on vRNA	vRNA/cell
C_T	Cycles before signal intensity surpasses the threshold	-
d_{vc}	Average diameter of a viable cell	µm
F_{RT}	Coefficient of dilution of the RT	-
k	Average mass of a base	g/mol/bp
m	Slope of the calibration curve of the vRNA standards	-

MODIP	Multiplicity of DIP	PFU/cell
MOI	Multiplicity of infection	PFU/cell or $TCID_{50}$/cell
m_{Std}	Weight of one vRNA molecule in the standard	g
N_A	Avogardo constant	1/mol
n_{Base}	Fragment length	bp
$n_{mol,Sample}$	Number of vRNA molecules in the sample	-
$n_{mol,Std}$	Number of vRNA molecules in the standard	-
Q	Perfusion rate	mL/h
Q_{Est}	Estimated perfusion rate	mL/h
q_s	Cell-specific metabolite uptake rate	mmol/cell/h
r_c	Growth rate	cells/mL/h
STY	Space-time yield	PFU/h/mL
t	Cultivation time	h
t_i	Time post inoculation	h
t_P	Total process time	h
VCC	Viable cell concentration	cells/mL
VCC_0	Viable cell concentration at time of inoculation	cells/mL
VCC_{max}	Maximum cell concentration	cells/mL
V_{cPerm}	Volume of the collected permeate after infection	mL

VCV	Viable cell volume	$\mu m^3/mL$
V_{Sample}	Total volume of the vRNA sample	µL
V_{WV}	Working volume of the STR	mL
Δ_{Perm}	PFU in permeate line/ PFU in STR	%

1 INTRODUCTION

Infections with influenza viruses cause respiratory disease and are considered a major threat to human health. It was estimated that seasonal epidemics caused by influenza viruses result in approximately 300,000–650,000 death worldwide annually (Iuliano et al. 2018). Influenza virus pandemics even led to millions of deaths in the past, e.g. approximately 40 million death were attributed to the "Spanish flu" from 1918 (Johnson and Mueller 2002; Taubenberger et al. 2000). Further, circulating influenza strains continuously evolve and individuals that already have been infected by previous influenza strains are often susceptible to newly emerging circulating virus strains. Consequentially, the vaccine formulation needs to be adapted annually (Krammer et al. 2018).

Despite the high demand of millions of doses every year, influenza vaccines are still mainly produced in chicken eggs (Harding and Heaton 2018). Here, the influenza virus is propagated in the allantoic cavit of embryonated hens' eggs. However, this holds several disadvantages, such as (i) a high probability of mutations in the surface proteins of the produced virus, (ii) reduced virus replication rates and virus titers for some influenza strains, (iii) a high probability of contaminations, (vi) the dependency of a reliable supply of chicken eggs, and (v) a limited capability to expand the production capacity in case of a pandemic. Therefore, cell culture-based processes, where mammalian cells are cultivated and infected in a defined growth medium at large scale, are an alternative. The advantages of this production platform include (i) a reduced response time, due to the independence of chicken eggs, (ii) an improved flexibility in regards to production time and scale and, (iii) and an improved sterility and process control, due to a closed production chain. Here, it is generally desirable to use suspension cell lines rather than adherent cells (Warnock and Al-Rubeai 2006), as they allow an easier scale-up and implementation of process intensification strategies (Gallo-Ramirez et al. 2015; Tapia et al. 2016). However, despite the huge potential of cell culture-based processes for pandemic preparedness, the development and production of a new vaccine remains a time-consuming task. Consequentially, antivirals could prevent thousands of death in an acute pandemic situation until a vaccine is available. Further, antivirals represent a treatment option for persons that cannot be vaccinated due to medical reasons.

Currently used antiviral compounds against influenza, e.g. oseltamivir and zanamivir, are small molecules that inhibit the virus release from their host cell. However, the emergence and spreading of influenza virus strains resistant against these antivirals was already observed in the past (Han et al. 2018; Lackenby et al. 2018; Meijer et al. 2009) and demonstrates the need for novel treatment modalities. An approach that was suggested previously is the use of defective interfering (DI) particles (DIPs) (Dimmock et al. 2008). DIPs are naturally occurring virus variants with deletions or point mutations in their genome. Consequentially, DIPs only express truncated or mutated forms of functional proteins essential for replication and only propagate in a co-infection with infectious standard virus (STV), providing the missing gene functions. In such a co-infection scenario, DIPs interfere with and suppress STV replication and almost exclusively replication deficient DIPs are produced. The antiviral effect of influenza DIP material produced in chicken eggs was demonstrated previously in animal experiments (Dimmock et al. 2008). Here, it was reported that the DIP material protected against a variety of influenza strains. This indicates that influenza DIPs can have a very broad efficacy and consequentially no annual adaptation, as needed for vaccines, may be required. Therefore, it would be possible to generate and stockpile large quantities of DIP material for an improved pandemic preparedness.

So far, influenza DIP material investigated in animal experiments was always produced in chicken eggs. As cell culture-based processes hold several advantages, the present PhD work focused on the development of production processes for DIPs using cell culture technologies. Here, production processes for two different types of DIPs, characterized either by a large internal deletion or several point mutations, were developed. For this, different production conditions and their impact on the DIP yield were investigated. The DIP yield was determined by PCR measurements and virus quantification assays. Further, the antiviral potency of the produced material was assessed by an *in vitro* interference assay. Here, STV-infected cells were co-infected with the produced DIP material, and the reduction in the release of infectious virus particles was quantified. Next, the established processes were scaled up from shake flasks to laboratory-scale bioreactors. Further, process intensification strategies were applied. More specifically, perfusion cultivations utilizing a membrane-based cell retention device, were implemented to allow for higher cell concentrations and consequentially higher DIP titers. DIP material produced in the context of this PhD work was used by collaboration partners for animal experiments.

2 THEORETICAL BACKGROUND

The first section of the following chapter introduces the influenza A virus (IAV). In particular, the morphology and the virus replication of IAV and how it gives rise to and is influenced by DIPs are described. Subsequently, established IAV production systems and possible adaptations for DIP production are outlined. Finally, process intensification strategies for improved IAV production are introduced.

2.1 Influenza A virus morphology and replication

Influenza viruses belong to the *Orthomyxoviridae* family and can be divided into four species, namely A, B, C, and D (Shaw and Palese 2013). Of those, only influenza viruses of species A and B are known to cause annual epidemics (Krammer et al. 2018). However, influenza C virus infections causing influenza-like illness and hospitalization were observed as well (Matsuzaki et al. 2006). The symptoms of an influenza virus infection range from mild respiratory diseases, characterized by fever, sore throat, runny nose, cough, headache, muscle pain, and fatigue to a severe and in some cases lethal pneumonia (Krammer et al. 2018). Infections with influenza C virus are relatively rare and also influenza B virus infections only account for approximately 25% of the annual influenza-related hospitalizations (Tan et al. 2018). Thus IAV represents the greatest threat to human health of all influenza species. Furthermore, only influenza viruses of species A circulate in humans as well as in domestic animals, pigs, horses, poultry, and wild birds (Krammer et al. 2018). Here, more than 100 wild bird species are considered a neutral reservoir for a variety of IAV subtypes (Olsen et al. 2006; Webster et al. 1992).

Further, IAV has a high mutation rate and the accumulation of point mutations can lead to alterations in the surface proteins, known as antigenic drift. On the other hand, different IAV subtypes can exchange parts of their genetic information when they infect one host simultaneously. This phenomenon, known as antigenic shift, is facilitated by the segmented genome of IAV (further discussed in section 2.1.1) and can give rise to new virus strains. Both, antigenic drift and antigenic shift, can enable IAV strains which formerly circulated in animals to infect humans. These virus mutants have a potential to cause a pandemic due to the lack of pre-existing immunity in humans

(Krammer et al. 2018). Four IAV pandemics, all associated with an antigenic shift, have been observed in the past (Hampson and Mackenzie 2006; Rumschlag-Booms and Rong 2013; Smith et al. 2009).

2.1.1 Morphology

IAV is an enveloped negative-sense single-stranded RNA virus. IAV particles are mostly described as spherical particles with a diameter between 80 and 120 nm, but also filamentous elongated particles have been observed (Calder et al. 2010; Harris et al. 2006). The IAV genome consists of eight vRNA segments, ranging from 0.9 to 2.3 kb and each encoding for at least one viral protein. By utilizing alternative splicing, multiple open reading frames, and ribosomal frameshifts up to 18 different viral proteins can be encoded in the viral genome (Vasin et al. 2014). Yet, not all proteins appear to be essential as not all of them are expressed by every IAV strain.

The vRNA segments are located inside the virus particle and each segment is bound by multiple copies of the viral nucleoproteins (NP) and the viral RNA-dependent RNA polymerase (Noda et al. 2006; Zheng and Tao 2013) to form a rod-shaped complex (Compans et al. 1972), called viral ribonucleoprotein (vRNP) (Fig. 2.1). The vRNPs are arranged in a “1+7” pattern with one central vRNP surrounded by the other seven vRNPs (Fournier et al. 2012; Harris et al. 2006; Nakatsu et al. 2016; Noda et al. 2006). The viral RNA polymerase consists of three polymerase subunits; polymerase basic protein 1 and 2 (PB1 and PB2) and polymerase acidic protein (PA), encoded by vRNA segment 1–3 (Seg1–3), respectively. The virus particle obtains its structure from the matrix protein 1 (M1), which forms a capsid and separates the core of the virus from its lipid bilayer envelope (Krammer et al. 2018). The envelope is originated from the host cell membrane and contains the viral matrix protein 2 (M2), as well as the two glycoproteins haemagglutinin (HA) and neuraminidase (NA). HA and NA are the main antigens. Here, a total of 18 antigenically different HA and 11 antigenically different NA subtypes have been identified, which can reassort and give rise to new IAV subtypes (Jang and Bae 2018).

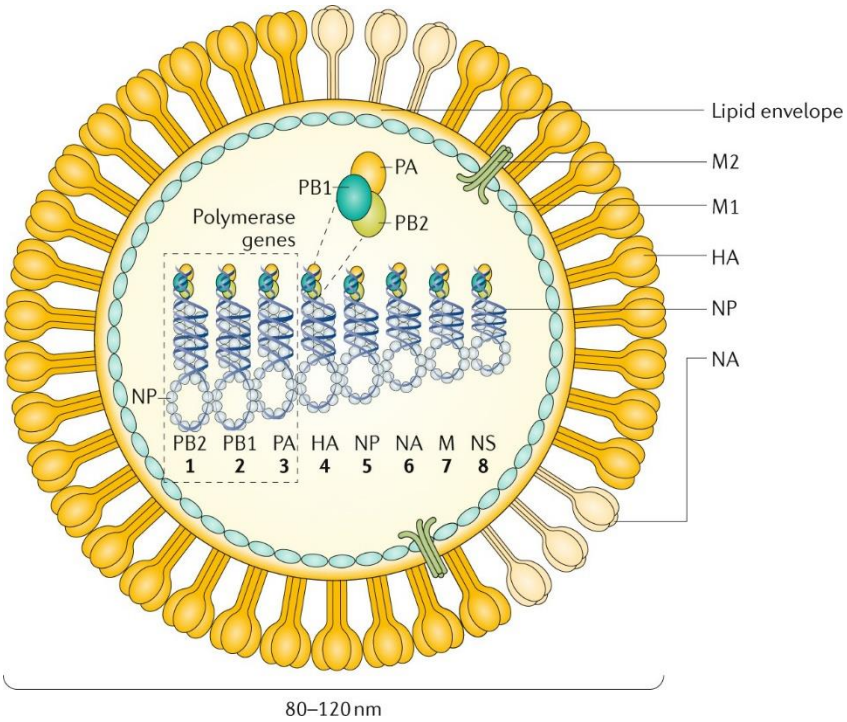

Fig. 2.1 General structure of an IAV particle. IAV is an enveloped negative-sense RNA virus with eight single-stranded RNA segments located inside the virus particle and bound by the viral nucleoprotein (NP, encoded by Seg5) and one viral polymerase. The matrix protein 1 (M1, Seg7) separates the virus envelope from the core and gives the virus particle its structure. The envelope is a lipid bilayer, originated from the host cell membrane, in which the viral surface proteins haemagglutinin (HA, Seg4), neuraminidase (NA, Seg6), and matrix protein 2 (M2, Seg7) are embedded. The three largest RNA segments encode for the subunits of the viral RNA-dependent RNA polymerase (PB2, Seg1; PB2, Seg1; PA, Seg3). Seg8 encodes for the nonstructural protein (NS1) and the nuclear transport protein (NEP). NS1, NEP, and other accessory viral proteins that can be expressed by IAV are not present in the virus particle. Illustration reprinted (Krammer et al. 2018) by permission of the Springer Nature Group.

Different IAV strains are named based on their HA and NA subtypes, as well as their species, the host the virus was isolated from (if none is specified, it is considered to be isolated from human), the place of isolation, the number of the isolate, and the year of isolation (Krammer et al. 2018). Accordingly, the model influenza virus strain A/Puerto Rico/8/1934 (H1N1), hereafter called PR8, widely used for research and manufacturing purposes, was the eighth isolate from human origin, taken in Puerto Rico in 1934 with the species A and the subtype HA1 and NA1.

2.1.2 Virus replication cycle

The IAV replication starts with the virus attachment (Fig. 2.2). Here, IAV attaches to the host cell by binding of the HA protein to sialic acid sugars of host cell proteins, present on the cell surface (Skehel and Wiley 2000). In a next step, the virus particle is taken up into the cell by receptor-mediated endocytosis (Matlin et al. 1981). The endosome containing virus eventually undergoes acidification resulting in a conformational change of the viral HA protein, inducing the fusion of the viral and the endosomal membrane (Krammer et al. 2018; Shaw and Palese 2013). Ultimately, the vRNPs are released into the cytosol and transported into the nucleus by the import machinery of the host cell (Cros and Palese 2003). Here, transcription and replication take place. The vRNA replication involves the generation of a positive-sense intermediate complementary RNA (cRNA), serving as a template for subsequent vRNA synthesis. Analogous to vRNA, the cRNA is bound by NPs and RNA polymerases to form a complementary ribonucleoprotein (cRNP) complex (Fodor 2013). The synthesis of vRNA from cRNA and *vice versa* are both carried out by the viral RNA polymerases and are primer-independent processes (Jorba et al. 2009).

In contrast, the vRNA transcription resulting in a positive-strand mRNA is initiated by a mechanism known as cap-snatching, where the viral RNA polymerase cleaves the 5’ cap and 10–15 nucleotides of a host cell pre-mRNA and uses it as a primer (York and Fodor 2013). Further, approximately 16 nucleotides from the 5’ end of the vRNA template are 5–7 uridine residues resulting in a stuttering of the RNA polymerase and the generation of a poly(A) tail on the mRNA transcript (Robertson et al. 1981). Utilizing these strategies, IAV mRNA synthesis results in transcripts structurally indistinguishable from host mRNA (5’ cap and 3’ poly(A) tail) and misleads the host cell into recognizing viral transcripts as native (York and Fodor 2013). The viral mRNA is exported into the cytoplasm and is translated into viral proteins by taking over the cellular translation machinery (Yanguez and Nieto 2011).

The newly synthesized viral polymerase subunits and the viral NP are imported into the nucleus and further increase vRNA replication and transcription rate. Via the endoplasmatic reticulum and the Golgi apparatus, virus membrane proteins (HA, NA, and M2) are transferred to and inserted into the cellular plasma membrane (Krammer et al. 2018). At late infection stages, M1 and NEP mediate the export of vRNPs from the nucleus to the cytoplasm through interactions with recycling endosomes (Cros and Palese 2003; Shaw and Palese 2013). Here, the vRNPs are transported to the cell membrane

and arrange to a "1+7" pattern, with one copy of each vRNA segment. This is facilitated by segment-specific genome packaging signals at both ends of the vRNA segment (Chou et al. 2012; Fujii et al. 2003; Hutchinson et al. 2010; Noda and Kawaoka 2012). Finally, budding of new virus particles takes place. This is initiated by the viral HA, NA and M2 (Nayak et al. 2004; Shaw and Palese 2013). Lastly, the virus particle must be released from the cell surface, which is facilitated by the viral NA, which cleaves sialic acid residues at the cell surface and prevents HA binding and aggregation of released viruses (Nayak et al. 2004).

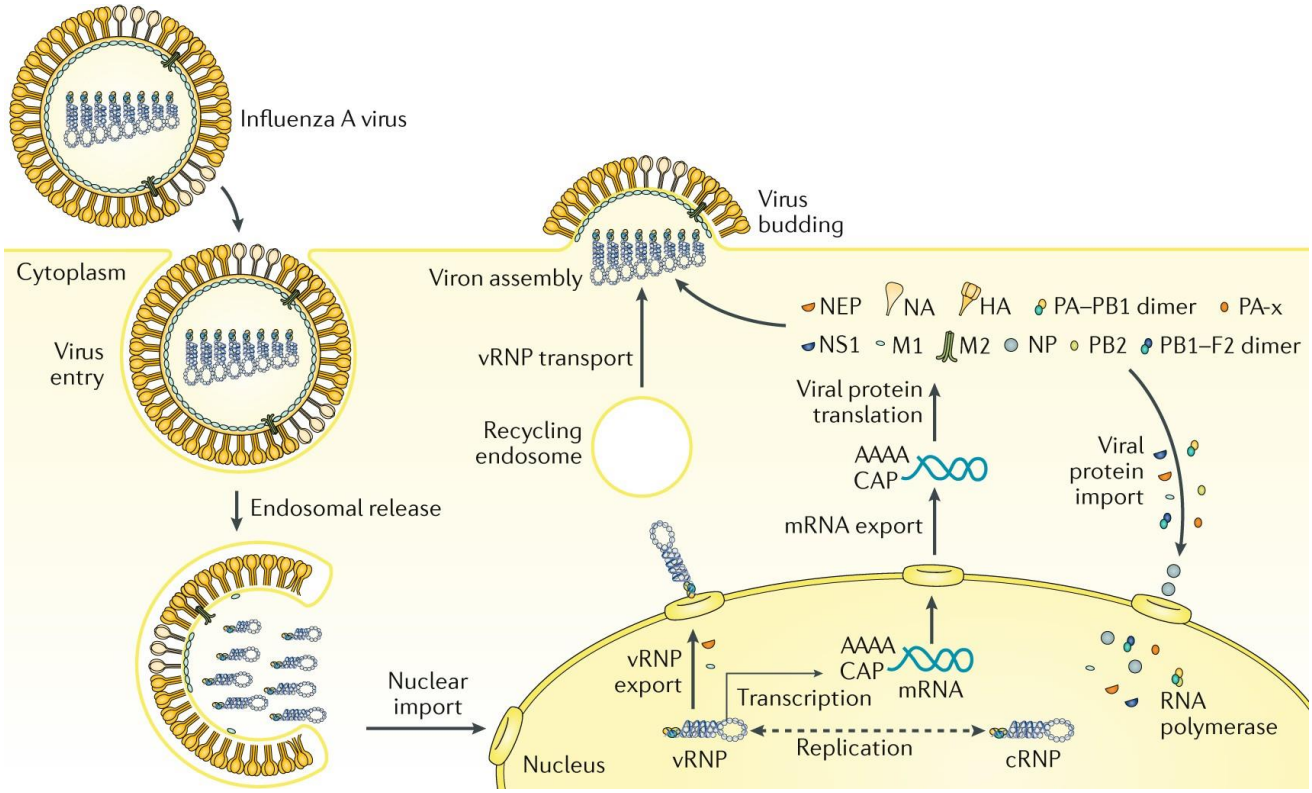

Fig. 2.2 Scheme of the IAV replication cycle. IAV enters the cell by receptor-mediated endocytosis and viral ribonucleoprotein (vRNPs) are released into the cytosol. vRNPs are imported into the nucleus for (i) replication through a positive-sense complementary ribonucleoprotein (cRNP) intermediate and for (ii) transcription of mRNA. Viral mRNA is translated in the cytoplasm, and the resulting proteins are assembled into virus particles. The synthesized proteins include haemagglutinin (HA), matrix protein 1 (M1), matrix protein 2 (M2), neuraminidase (NA), nuclear export protein (NEP), nucleoprotein (NP), nonstructural protein (NS1), and the viral polymerase subunits (PB1, PB2 and PA). Newly synthesized vRNPs are transported to the cell membrane, through interactions with recycling endosomes, and incorporated in the new virus particles. Illustration reprinted (Krammer et al. 2018) by permission of the Springer Nature Group.

2.2 Defective interfering particles

Already in 1951, the existence of “incomplete” IAV particles was supposed by von Magnus (Von Magnus 1951). He discovered that these particles accumulated during undiluted serial passages of IAV in embryonated chicken eggs. One of his observations was that the ratio of infectious to total virus particles decreased with each passage (Von Magnus 1951). In the following years, similar observations were made for other viruses and the terminology “defective interfering particle” was proposed, together with first hypotheses on the origin and mode of action of DIPs (Huang and Baltimore 1970).

2.2.1 Origin and morphology

By now, DIPs have been described for most single- and double-stranded DNA and RNA viruses, including herpes simplex virus (Harty et al. 1993), poliovirus (Lundquist et al. 1979), measles virus (Cattaneo et al. 1988), vesicular stomatitis virus (Giachetti and Holland 1988), dengue virus (Li and Aaskov 2014), severe acute respiratory syndrome coronavirus (Raman and Brian 2005), and influenza virus (Von Magnus 1951). DIPs are naturally occurring virus variants with the same structural features as their STV counterpart that typically contain a truncated form of the viral genome (Huang and Baltimore 1970). The *de novo* generation of DIPs is a random process caused by erroneous translocation of the viral polymerase, e.g. the polymerase skips from one part of the template to another part and resumes elongation at the 3’ end of the nascent chain (Lazzarini et al. 1981; Perrault 1981). This would result in the formation of the simplest form of a DIP with an internal deletion in the genome (Jaworski and Routh 2017; Perrault 1981). Other mechanisms can lead to the formation of copyback or snapback DI genomes, where parts of the genome are copied in reverse complement sequence orientation (Fodor et al. 1994; Schubert and Lazzarini 1981) or mosaic or complex DI genomes, where various genome regions are reordered or even host cell RNA is incorporated (Mura et al. 2017).

For IAV, the simplest form of DI genome is typically observed. It is characterized by a large internal deletion, where up to 90% of the genomic information of the respective vRNA segment is missing. The deletions are observed most frequently for Seg1–3 (Baum and Garcia-Sastre 2011; Dimmock and Easton 2015). In addition, it was recently hypothesized that DI vRNAs of other segments are

inefficiently packaged into virus particles (Alnaji et al. 2021; Mendes and Russell 2021). Further, the 5’ and 3’ termini of the vRNA containing the packaging signal and the promotor are usually retained in the DI vRNA and are therefore considered crucial for DIP propagation (Nayak et al. 1985). One “conventional” IAV DIPs with a deletion in Seg1, called DI244, was thoroughly characterized before (Dimmock et al. 2008; Easton et al. 2011; Scott et al. 2011) and often used as a model DIP. The Seg1 vRNA of DI244 has a length of 395 nucleotides and compromises the nucleotides 1 to 244 and 2191 to 2341 of the full-length Seg1 vRNA, thus retaining the packaging signal at both termini (Dimmock et al. 2008) (Fig. 2.3).

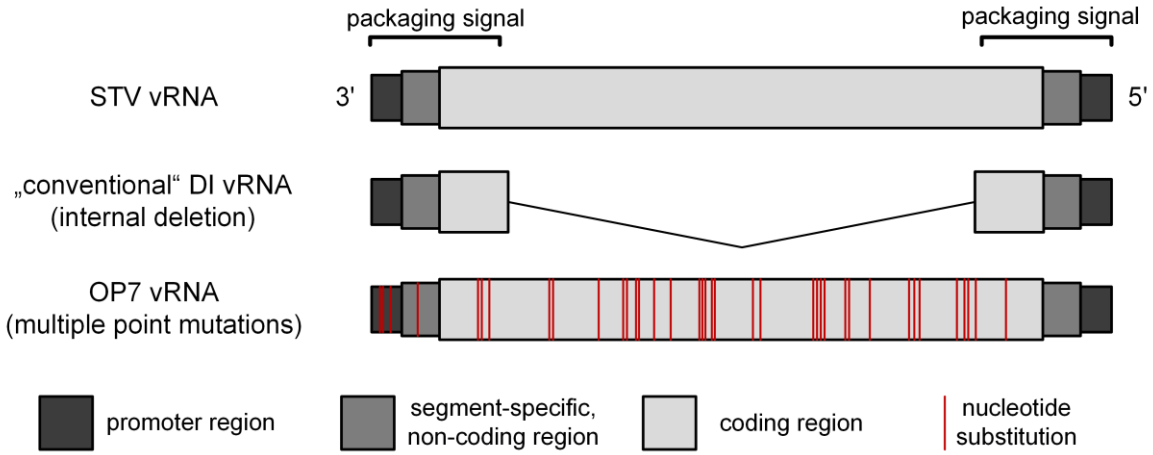

Fig. 2.3 Different IAV defective interfering (DI) vRNAs. Standard virus (STV) particles incorporate a set of eight vRNA segments without deletions or excessive mutations. “Conventional” DIPs, like DI244, contain an internal deletion in at least one of their vRNA segments (most commonly in Seg1–3). A recently discovered DIP, called OP7, has 37 point mutations in its segment 7 vRNA. Illustration adapted (Kupke et al. 2019).

Recently, a novel type of IAV DIP, called “OP7”, was discovered in the Bioprocess Engineering (BPE) group at the Max Planck Institute (MPI) in Magdeburg. Instead of deletions, OP7 contains 37 point mutations in Seg7 vRNA in relation to the reference sequence of PR8 STV (from the National Center for Biotechnology Information) (Kupke et al. 2019). These point mutations affect the promoter region, encoded proteins and the packaging signal sequence (Fig. 2.3). In a co-infection with STVs, the OP7 phenotype is characterized by an over-proportional level of the mutated Seg7 vRNA. This might be caused by a previously described “superpromotor” mutation (Belicha-Villanueva et al. 2012) found on the Seg7 vRNA of OP7 (Seg7 OP7). Furthermore, OP7 particles appear to miss other vRNA segments, which might explain the observed defect in virus replication. Despite the different

structures of the DI genomes, both DIP types (“conventional” DIPs with a deletion and OP7) show similar characteristics in a co-infection with STVs, described in the following.

2.2.2 Interference of IAV DIPs with STV replication

Due to the missing or mutated part of the vRNA, IAV DIPs express only a truncated or mutated protein essential for replication (White and Morris 1994). Consequentially, they are unable to propagate, unless the functional protein is provided, for example by a co-infection with STVs. However, in such a co-infection scenario, the DI vRNA interferes with and suppresses STV replication. One explanation for the interference of conventional DIPs is the shorter DI vRNA, which is amplified faster compared to the full-length (FL) vRNA (Mendes and Russell 2021). Thus, the DI vRNAs might outcompete STV vRNAs for limited cellular or viral resources (Dimmock and Easton 2014; Laske et al. 2016; Nayak et al. 1985). Likewise, a faster accumulation of Seg7 OP7 vRNA was observed, possibly mediated by the presence of a superpromoter (Kupke et al. 2019). Further, a preferential packaging of the DI vRNA over the FL counterpart into progeny virus particles was observed (Duhaut and McCauley 1996; Odagiri and Tashiro 1997), similarly OP7 vRNA appears to be preferentially packaged (Kupke et al. 2019). However, the preferential packaging of DI RNAs was recently challenged by two research groups (Alnaji and Brooke 2020; Mendes and Russell 2021). Still, DIP co-infections result in a drastic decrease in released infectious STV particles, as mainly replication deficient DIPs are produced (Frensing 2015; Tapia et al. 2019). Here, it was speculated that the existence of DIPs might offer an evolutionary advantage and promotes viral spread either by protecting the host from lethal damage or by leading to a more persistent infection (Barrett and Dimmock 1986; De and Nayak 1980; Huang and Baltimore 1970). It should be mentioned that not all vRNAs with a deletion interfere with the replication of their FL equivalent. However, the criteria rendering a deleted vRNA interfering are still elusive (Brooke et al. 2013).

2.2.3 Potential applications of IAV DIPs

The interfering properties of DIPs fueled the discussion about their potential use as novel antiviral agents (Dimmock and Easton 2014). It was speculated that the administration of DIPs to prevent IAV infection might have several benefits compared to vaccines (Dimmock and Easton 2015). First, DIPs show a fast mode of action, as their protective ability does not depend on the adaptive immune system, which can take up to 2–3 weeks to establish full protection in the case of vaccine administration.

Because of their mode of action, DIPs could be used either prophylactically or even therapeutically (Dimmock et al. 2008). Specifically, it was shown that egg-derived DI244 material administered seven days before infection still protected mice from a lethal dose of IAV STVs (Dimmock and Easton 2015). Moreover, mice infected with a lethal dose of IAV and treated with DI244 24 h after the challenge survived (Dimmock et al. 2008). Partial protection was observed, when DIPs were administered 48 h after the infection (Dimmock et al. 2008). Furthermore, an antiviral effect of conventional DIPs against a variety of IAV strains (i.e. H2N2, H3N2, and H3N8) was shown (Dimmock et al. 2012; Dimmock et al. 2008) including pandemic and highly pathogenic avian strains (Dimmock et al. 2012; Huo et al. 2020; Zhao et al. 2018). Also for OP7, the interference with a variety of IAV subtypes could be shown (Kupke et al. 2019). This suggests that IAV DIPs, in contrast to currently used vaccines, might have the potential to act universally against IAV strains (Dimmock and Easton 2015). Additionally, an antiviral effect even against non-homologous influenza B virus and pneumovirus was demonstrated (Easton et al. 2011; Scott et al. 2011). This might be explained by an unspecific protection due to an enhanced stimulation of the innate immune response upon DIP co-infection (Killip et al. 2013; Lopez 2014; Strahle et al. 2006). More specifically, it was shown that retinoic acid inducible gene I (RIG-I) preferentially associates with IAV DI vRNA over FL vRNA and leads to an increased interferon induction in DIP treated cells (Baum and Garcia-Sastre 2011; Linder et al. 2021; Rehwinkel et al. 2010).

IAV DIPs may even act like a live attenuated vaccine. For instance, mice infected with a lethal dose of STVs and treated with DI244 did not show symptoms of disease, but still developed an immunity to the pathogenic STVs (Dimmock et al. 2008). Here, it was speculated that DIP co-treatment results in the release of replication deficient particles carrying the surface proteins of the pathogenic virus (Dimmock and Easton 2015). In line with this, it was shown that compared to an untreated control group (STV infection only), DI244 co-treatment did not influence the amount of specific IAV antibodies produced in ferrets. In contrast, reduced antibody titers were detected in ferrets treated with conventional antivirals (NA inhibitors) (Dimmock et al. 2012), emphasizing potential advantages of DIPs over such antivirals. Furthermore, while different antivirals were found to offer protection in the past, resistances against those antivirals became prevalent (Colman 2009; Deyde et al. 2007; Gubareva et al. 2010; Oxford 2007; Smith et al. 2006) and since 2009 only NA inhibitors have been able to provide protection (Krammer et al. 2018). Two currently available NA inhibitors are oseltamivir and zanamivir. However, the emergence and spread of an oseltamivir resistant IAV strain was already observed in the past (Han et al. 2018; Lackenby et al. 2018; Meijer et al. 2009). In

contrast, it is highly unlikely that resistances against DIPs arise: the RNA-dependent RNA polymerase complex (comprising the polymerase subunits PB2, PB1, and PA proteins) would need to mutate to not recognize and replicate the DI vRNA anymore (Dimmock and Easton 2015). However, the same polymerase complex replicates all eight vRNA segments (Cianci et al. 1995; Hagen et al. 1994; Tiley et al. 1994). Thus, in addition to mutation of the viral polymerase complex, it would be necessary that mutations of the polymerase recognition sequences of all eight STV vRNA segments arise simultaneously. Only under these circumstances, STV replication without DIP replication could take place (Dimmock and Easton 2015). The probability that this happens is extremely low and was previously estimated to be around 1:1E45 (Dimmock and Easton 2015). In conclusion, IAV DIPs with their unique antiviral mechanism are very interesting candidates for prophylactic and therapeutic treatments showing advantages over currently used small molecule antivirals.

2.3 Influenza A virus production

Until today vaccination is considered the most effective countermeasure to prevent the spread of influenza viruses (Grohskopf et al. 2020; Noh and Kim 2013; Plotkin 2014; Shaw 2012). Most currently used IAV vaccines rely on the production of whole virus particles. In the following section, currently used platforms for IAV production and how they can be adapted for DIP production are outlined.

2.3.1 The development of vaccine production

In 1796, Edward Jenner demonstrated the use of a vaccinia virus for protection against smallpox. This discovery should ultimately lead to the eradication of smallpox almost 200 years later (Baxby 1999; Strassburg 1982). Since Jenner´s first discoveries, new vaccine types and production technologies have emerged. Early vaccines (e.g. smallpox, rabies, tuberculosis, yellow fever) were based on attenuated viruses isolated from animal tissue or embryonated chicken eggs. In the 1940s, the discovery that animal cells could be cultured *in vitro* and used as a substrate for viral growth revolutionized vaccine manufacturing. It was shown that many viruses, including polio and measles, could replicate in cell culture (Enders et al. 1949). The production method was quickly taken up by some vaccine developers, leading first to an inactivated polio vaccine and later a live attenuated oral

vaccine (Blume and Geesink 2000; Rey and Girard 2008). The use of cell culture-based technologies led in the second half of the 20th century to the development of new vaccine candidates for a variety of viruses (e.g. measles, mumps, rubella) (Zahoor et al. 2016). More recently, improvements in genetic engineering gave rise to a new generation of vaccines, no longer relying on virus inactivation or attenuation. For instance, novel vaccine candidates include recombinant proteins, virus like particles, and chimeric viruses (Cox et al. 2008; Guy et al. 2010; Henao-Restrepo et al. 2017; Kirnbauer et al. 1992; Valenzuela et al. 1982). The latest innovation in the vaccine field was the formulation of RNA- and DNA-vaccines, solely based on DNA or mRNA administration to the patient to result in the expression of immunologically relevant antigens *in situ* (Ulmer et al. 2012; Ulmer et al. 1996). The first commercial products based on this technology were the vaccine candidates for SARS-CoV-2 in 2020 (Golob et al. 2021).

2.3.2 Influenza vaccine manufacturing

The first influenza vaccine was licensed during World War II in 1945 in the United States. Unfortunately, the vaccine did not protected well against newly arising virus strains, which was later explained by changes in the circulating virus (Salk and Suriano 1949). These changes were caused by the high mutation rate of IAV, which results in a high variability of the viral antigens. As a consequence, the vaccine formulation needs annual adaptations until today. Despite the resulting high demand of hundreds of millions of vaccine doses every year, manufacturing processes remained largely unchanged for over 60 years. During this period, influenza virus propagation in embryonated chicken eggs followed by an inactivation with chemicals was the sole production platform. The only mentionable change in the production process was in 1970. Here, a reassortment of up to six vRNA segments of the high-yielding influenza strain PR8 with the vRNA segments encoding for HA and NA of the circulating virus improved the vaccine production by increasing the obtainable virus titers (Krammer et al. 2018). The first cell culture-based human influenza vaccine was only approved in 2001 in the Nethelands, but was never commercially distributed owing to manufacturing delays (Doroshenko and Halperin 2009). In 2007, the European Medicines Agency approved a cell culture-based vaccine, called Optaflu (Doroshenko and Halperin 2009). The same production cell line (MDCK 33016, see section 2.3.3) is still used today for the production of the influenza vaccine Flucelvax (Perez Rubio and Eiros 2018). Despite the advances in cell culture-based vaccine

manufacturing (Genzel and Reichl 2009), the platform still has not been able to play a major role in the global manufacturing capacity for IAV production (Harding and Heaton 2018).

However, the virus production in cells rather than in eggs holds several advantages. Egg-based manufacturing relies on the availability of tremendous amounts of chicken eggs (approximately one egg per vaccine dose) and slowing production due to the shortage of eggs already occurred in the past. In contrast, cell culture-based manufacturing is more flexible as the production only depends on the capacity of available bioreactors (Milian and Kamen 2015). Furthermore, viruses that are considered for human vaccines that are produced in avian cells (i.e. embryonated chicken eggs) exhibit substantially different glycosylation profiles. This may negatively affect immunogenicity (Zost et al. 2017) compared to viruses produced in mammalian cells (An et al. 2013; Hutter et al. 2013). Another important advantage for cell culture-based manufacturing is the reduction of the egg selective pressure resulting in HA mutations. Today, seed viruses used for cell culture-based vaccine production are generated by reverse genetics to completely omit egg-adaptation (Paules et al. 2018; Ping et al. 2015). Further, cell culture-based processes allow for a better process control and increased sterility, due to a closed production chain. However, there are also some drawbacks for cell culture-based manufacturing processes. Most importantly, the infrastructure to manufacture enough doses for an entire season does not exist yet. Additionally, it was estimated that currently cell-based influenza vaccines cost approximately 40% more than egg-based influenza vaccines (Harding and Heaton 2018). However, the cost-effectiveness of cell culture-based production processes might be further improved by process intensification strategies (section 2.4).

While the influenza vaccine market is currently still dominated by egg-based formulations, this might change in the future as alternatives are slowly entering the market. One such alternative are cell culture-based processes, which offer a multitude of advantages especially in terms of flexibility and scalability. Consequentially, further research and improvements of the infrastructure of cell culture-based processes is indispensable for pandemic preparedness (Fineberg 2014; Hegde 2015).

2.3.3 MDCK cells for influenza A virus production

A variety of cell lines were characterized as potential substrate for influenza virus manufacturing (Genzel et al. 2013; Lohr et al. 2010; Lohr et al. 2009; Naruse et al. 2015; Pau et al. 2001). However, Madin-Darby Canine Kidney (MDCK) cells are currently the only cell line used for commercial

production of a human influenza vaccine (Flucelvax). MDCK cells were isolated by S.H. Madin and N.B. Darby from the kidney epithelium of a female adult cocker spaniel in 1958. Very early on, MDCK cells were considered for virus production, as their susceptibility to many human viruses could be shown (Gaush et al. 1966; Nerome and Ishida 1978; Tobita 1975; Tobita et al. 1975). MDCK cells became the most important cell line for the production of influenza viruses, mainly due to their superior growth properties and high virus yield (Genzel and Reichl 2009; Liu et al. 2009). Different MDCK cells can be obtained from cell culture collections such as the European Collection of Cell Cultures (ECACC) or the American-Type Culture Collection (ATCC). In addition, many MDCK cells of unknown histories are used in research laboratories (Genzel and Reichl 2009). Initially, adherent MDCK cells grown on microcarriers were used for large scale influenza virus production (Bock et al. 2009; Genzel et al. 2006; Hu et al. 2008). In 1997, the adherent MDCK cell line CCL-34 (from ATCC) was adapted to suspension growth and was afterwards named MDCK 33016. This cell line was first used for production of the vaccine Optaflu and is currently still used for production of Flucelvax (Doroshenko and Halperin 2009; Gröner and Vorlop 1996; Perez Rubio and Eiros 2018). The first suspension MDCK cell line available for research purposes was developed approximately ten years later (Chu et al. 2009; Lohr et al. 2010; van Wielink et al. 2011). However, the suspension MDCK cell lines used in industry and academia showed low specific growth rates, low maximum cell concentrations and formed aggregates (Bissinger et al. 2019; Castro et al. 2015). Consequentially, this resulted in limitations for the implementation of large scale or intensified processes (Castro et al. 2015; Peschel et al. 2013; Tapia et al. 2014). Only recently, a new cultivation medium (Xeno™ medium) was developed, allowing MDCK cells to grow in single cells with high specific growth rates (Huang et al. 2015; Huang et al. 2011). It was shown that MDCK cells (descendent of a MDCK cell line originally obtained from ATCC) grown in Xeno™ medium could reach up 40.0E+06 cells/mL, when process intensification strategies were applied (Wu et al. 2021). Additionally, another MDCK cell line originally obtained from ECACC and adapted to suspension growth (Lohr et al. 2010) was further adapted to grow in Xeno™ medium. This cell line showed good growth in shake flask experiments (Bissinger 2020; Bissinger et al. 2019) and was further investigated in this PhD work.

2.3.4 Production of defective interfering particles

The first IAV DIP preparations for antiviral use were generated by multiple high multiplicities of infection (MOI) passages of a seed virus in embryonated chicken eggs (Dimmock et al. 1986). DIP

formation was tracked by a decreasing ratio of infectious to total virus. However, this production approach resulted in the random formation of many different DI vRNAs with many different deletion sites. Consequentially, the product could not be generated reproducibly (Duhaut and Dimmock 1998; Jennings et al. 1983). This was later circumvented by the generation of seed viruses with only one defined deletion in one segment, using reverse genetics (Dimmock et al. 2008; Hoffmann et al. 2000). One such well-characterized seed virus contained the DIP DI244 and was used for production in eggs (Dimmock et al. 2008) and later in cell culture (Wasik et al. 2018). However, since DIP propagation usually relies on STV co-infections, these DIP preparations were a mixture of the desired DIPs and infectious STVs, where the latter needed to be inactivated. For this, UV-irradiation, introducing photodimeric lesions (Remsen et al. 1970) or unspecific chain breaks (Coahran et al. 1962; Jericevic et al. 1982) was used, before testing in animal experiments (Dimmock and Easton 2014; Dimmock and Easton 2015). The extent of how strongly the DIP interference was affected by this inactivation was uncertain. Further, questions regarding the safety of such preparation remained unanswered. In an attempt to overcome the necessity of a STV co-infection for DIP propagation, adherent 293T and MDCK cells were genetically modified to express the viral polymerase subunit PB2, encoded by Seg1 vRNA (Bdeir et al. 2019). Using this cell line in a previously reported reverse genetics system for IAV (Hoffmann et al. 2000), it was possible to generate a pure DI244 seed, without any STV contamination (Bdeir et al. 2019). Further, with the aim to generate a production cell line, a MDCK suspension cell line (adapted to Xeno™ medium; section 2.3.3) was genetically modified to express PB2. The pure DI244 seed virus as well as the genetically modified MDCK suspension cell line, both provided by a collaboration partner (Infection Biology (IB) Unit at the German Primate Center (DPZ), Germany), were used in the present PhD work in an attempt to establish a production process for large DIP quantities for antiviral therapy.

2.4 Process intensification strategies

Since the first *in vitro* cultivation of mammalian cells in the 1940s, cell culture techniques have drastically improved. The development of genetically engineered cell lines and new chemically defined media allowed cells to grow in suspension and to much higher cell concentrations than before. This resulted in production processes with very high productivities (Kelley 2009). However, lately the biopharmaceutical industry is facing new challenges including an increased need for “speed-to-market”, cost efficiency, and flexibility of the production process (Chen et al. 2018). These challenges

can be addressed by applying process intensification strategies. In upstream bioprocessing this includes all efforts with the aim to increase the space-time yield (STY) of the cultivation vessel (Chen et al. 2018). The STY describes the amount of product produced per bioreactor volume and time. For vaccine production, process intensification strategies focused on increased cell concentrations, improved cell-specific virus yields (CSVYs) (mainly facilitated by media optimization and cell line development), improved process control, and the optimization of infection conditions (Gallo-Ramirez et al. 2015; Tapia et al. 2016). In the following, process intensification strategies relevant for the present work are introduced.

2.4.1 Virus manufacturing in adherent and suspension cells

Until today, viral vaccines are often produced using adherent cells. In large scale production processes adherent cells are grown on microcarriers (Barrett et al. 2009; Hundt et al. 2011; Rourou et al. 2014; Thomassen et al. 2012) or macrocarriers (Hassanzadeh et al. 2011; Rajendran et al. 2014) to increase the available surface area.

Adherent cells grown on microcarriers (typically beads made of glass, plastic, or dextran) are usually cultivated in stirred tank bioreactors (STRs) or in wave bioreactors in quasi suspension (Rourou et al. 2014; Thomassen et al. 2012). Here, cells can be easily separated from the medium by reducing the agitation speed to allow bead sedimentation. This enables advanced process operations, like medium exchanges or volume reduction prior virus infection that can result in increased virus titers (Pohlscheidt et al. 2008; Thomassen et al. 2014). However, there are also several drawbacks for microcarrier-based processes. One being poor cell attachment often observed when serum-free medium is used (Frazzati-Gallina et al. 2001), resulting in the necessity to add recombinant adhesion factors. This, in combination with the comparatively expensive microcarriers, which can often not be recycled, results in increased process costs (Gallo-Ramirez et al. 2015). However, the main drawback of microcarrier-based processes is the challenging scale-up, which involves trypsinization and harvest of confluent cells and a bead-to-bead transfer to initiate the next scale-up step. Lastly, to increase the maximum cell concentration, the available surface area and therefore the bead concentration needs to be increased (Warnock and Al-Rubeai 2006). Here, a higher power input is needed to keep the microcarriers in suspension, resulting in increased shear stress. Further, increasing microcarrier concentrations is limited, as friction between the beads can cause cell abrasion (Reiter and Mundt 2005).

Alternatively, adherent cells can be grown on macrocarriers (typically highly porous polyester microfiber carriers) in fixed-bed bioreactor systems (Hassanzadeh et al. 2011; Rajendran et al. 2014). The macrocarriers provide a large surface area allowing cell growth to very high cell densities (HCD). One drawback of this system is the difficult harvest of viable cells from the carrier material, excluding it from seed train purposes (Silva et al. 2015) and complicating the harvesting of intracellular viruses (Gallo-Ramirez et al. 2015). Lastly, inhomogeneous growth, where cells do not colonize the entire fixed-bed, can occur and will result in reduced virus titers (Losa 2018).

Due to the drawbacks of adherent cells, suspension cells are preferred for large-scale production of viral vaccines (Warnock and Al-Rubeai 2006). Usually, suspension cell lines are generated by adaptation of adherent cells. Here, cells eventually lose their anchorage dependence and start to propagate as single cells in the medium, when grown over a long period in a cultivation system for suspension cells (e.g. shake flasks). The main advantage of suspension cells is their easy expansion, allowing the development of a simple seed train and scale-up beyond 10,000 L. Furthermore, the process parameters can be better controlled and process intensification strategies, such as the increase of the maximum cell concentration can be applied (Warnock and Al-Rubeai 2006; Zhang et al. 2015).

2.4.2 High cell density perfusion processes

Traditionally, suspension animal cells were cultivated in batch mode. Here, a STR was inoculated and the process was terminated when the substrates of the culture medium were depleted. This production process was improved by the addition of a concentrated medium feed. The additionally supplied nutrients resulted in increased maximum cell concentrations and product titers. This cultivation method is called fed-batch. Currently, it is the most commonly used process regime in industry (Chen et al. 2018). However, in an attempt to improve the STY of existing production facilities, perfusion processes got in the focus of research and industry. Perfusion processes are characterized by a continuous feed of cell culture medium and a continuous harvest coupled with a cell retention device. Thus, sufficient substrate concentrations and low waste product concentrations can be ensured while cells are accumulated in the STR. Consequentially, this setup allows much higher cell concentrations than usually achieved for batch or fed-batch processes (Bielser et al. 2018). The increased cell concentrations result in higher product titers, given the cell-specific product yield can be maintained. Currently, several companies use perfusion cultivations for the production of certain biopharmaceuticals (Konstantinov and Cooney 2015).

Cell retention devices

All perfusion cultivations rely on some sort of cell retention. Several cell retention devices, utilizing different separation principles have been evaluated in the past. Usually, these devices are mounted externally to the bioreactor and integrated in a recirculation loop. The cell culture broth is circulated in this loop and the separation device allows the removal of cell-free medium. The separation devices mostly used today are based either on filtration or sedimentation (Chotteau 2015).

Filtration-based separation devices have been commercially most successful for recombinant protein production in the last decade. However, filter fouling is an inherent drawback in any filtration technology. To mitigate this, the flow of the cell culture broth is tangential to the filter surface (Kawahara et al. 1994; Velez et al. 1989). The tangential flow reduces filter fouling since particles are not pressed into the filter membrane. Currently, two filter-based systems are frequently used in research and industry, the tangential flow filtration (TFF) and the alternating tangential flow filtration (ATF) system (Fig. 2.4). In the TFF system, the cell culture broth is pumped unidirectional in a loop by a peristaltic or a centrifugal pump. The used filters are almost exclusively hollow fiber membranes (HFMs). The HFM is integrated in the loop and the cell culture broth passes through the lumen of the membrane. The cell-free supernatant is removed through the membrane in orthogonal direction. While this system was proven to reduce filter fouling, retention of the protein of interest (associated with filter fouling) could still be observed, even with more advanced pumping regimes (Hiller et al. 1993; Zhang et al. 1993). As an alternative to the TFF, the ATF system was introduced in 2000 (Shevitz 2000). Here, a diaphragm pump alternatingly pulls cell culture broth from the bioreactor into the lumen of the HFM and pushes it back into the bioreactor. The alternating flow generates a backflush in the filter membrane, which is causative for a reduced filter fouling. Consequentially, a reduced retention of the proteins of interest was observed (Clincke et al. 2013; Karst et al. 2016). While protein harvest through a filter membrane was repeatedly demonstrated (Chotteau 2015; Su et al. 2021), it was so far not possible to continuously harvest virus particles through a membrane during a perfusion process (Genzel et al. 2014; Nikolay et al. 2020b).

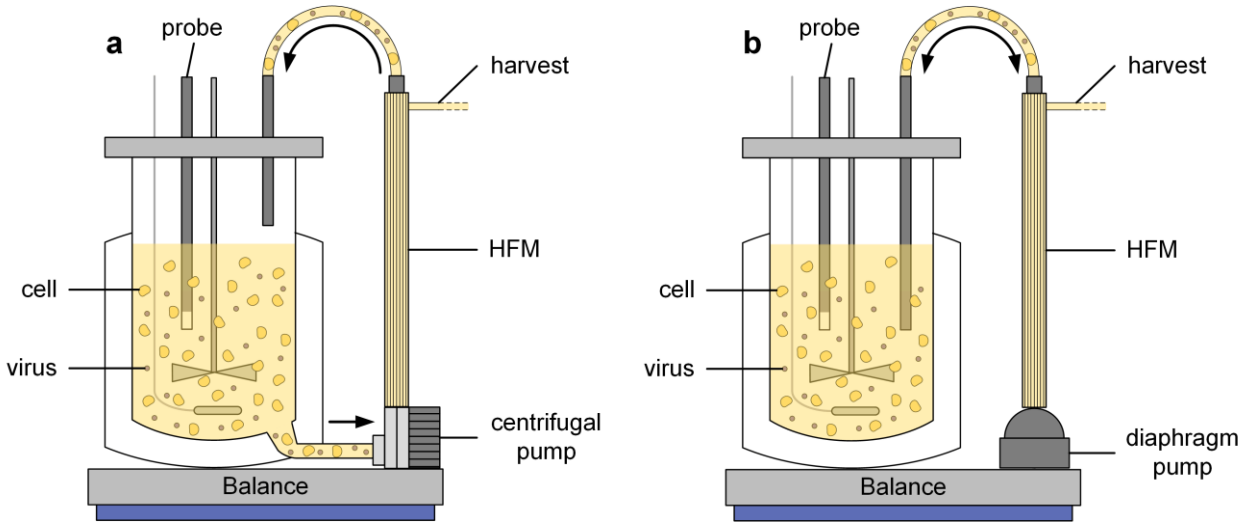

Fig. 2.4 Schematic representation of two different membrane-based perfusion systems. (a) Tangential flow filtration (TFF) and (b) alternating tangential flow filtration (ATF). In the TFF system, the cell culture broth is pumped unidirectional in a loop by a peristaltic or a centrifugal pump. In the ATF system, a diaphragm pump alternatingly pulls cell culture broth from the bioreactor into the lumen of the hollow fiber membrane (HFM) and pushes it back into the bioreactor.

One alternative to the previously described filter-based cell retention devices are separation devices based on sedimentation, e.g. acoustic settler and inclined settler. The latter includes several inclined plates, which favor cell sedimentation due to the convection phenomenon, called Boycott effect (Boycott 1920). The cell culture broth is pumped into the settler, where cells eventually settle at the lower part. The cell-free supernatant is pumped from the top of the settler into the harvest, while the sedimented cells are pumped back to the bioreactor. The inclined settler shows lower shear stress compared to other retention methods. However, there are also several drawbacks, mainly due to prolonged recirculation times and limitations in the maximum perfusion rate (Coronel et al. 2020).

Another cell retention system utilizing cell sedimentation is the acoustic settler. Here, cell culture broth is pumped into a chamber to which an acoustic wave is applied. The cells are concentrated at the nodes of the acoustic wave. When the wave is interrupted the aggregated cells sediment quickly and the cell-free supernatant can be removed, while the cells are pumped back into the bioreactor (Chotteau 2015; Shirgaonkar et al. 2004). The major drawback of the acoustic settler is that the power needed to generate the acoustic wave results in heating of the chamber and can damage some cells. This issue has currently only been solved for small scale productions (Granicher et al. 2020; Shirgaonkar et al. 2004; Trampler et al. 1994).

Finally, devices which rely either on filtration (spin-filter) or sedimentation (centrifuge and hydrocyclone), exist. These separation devices were intensively investigated in the past but all show some severe drawbacks. For spin-filters, filter fouling was reported frequently (Esclade et al. 1991; Mercille et al. 1994), while hydrocyclones display high pressure drops, which can cause cell damage (Elsayed and Wagner 2011; Pinto et al. 2008). While centrifugation offers interesting possibilities for cell separation, the devices are very expensive and also here cell damage was observed (Chotteau 2015; Johnson et al. 1996). Due to these disadvantages these separation devices are not discussed in detail here.

When ATF, TFF, inclined settler, and acoustic settler are compared, the filter-based devices appear to be superior. Here, it was described that they have a better separation efficacy of viable cells, allow for higher perfusion rates (and consequentially higher maximum cell concentrations), are simpler to operate and optimize, are available as single-use systems, and show a better scalability (Chotteau 2015). The inclined settler and the acoustic settler have the advantage that they both allow continuous virus harvesting. This opens up possibilities for process integration strategies, where the harvested material is immediately transferred to subsequent purification steps (Coronel et al. 2020; Granicher et al. 2020). In the last years, several HFM were investigated for their potential to continuously harvest virus particles (Genzel et al. 2014; Nikolay et al. 2020b), but so far no continuous virus harvesting could be established for a membrane-based perfusion cultivation. It was concluded that the membrane material and with this, its inner surface and structure, porosity, and hollow fiber wall thickness largely influence the retention of virus particles. The identification of a membrane allowing for continuous virus harvesting is very desirable as it would combine the advantages of membrane-based perfusion cultivations with the possibilities for process integration strategies. Recently, a novel tubular cell retention membrane, called virus harvest unit (VHU), was developed (Cattaneo and Spanjaard 2017). This membrane was tested in the presented PhD work for its potential to enable a continuous IAV DIP harvest during a membrane-based perfusion process.

Perfusion rate control

A perfusion process can be set up in different ways to either ensure a stable or an increasing cell concentration over the process time. While it is for production of recombinant proteins often desirable to maintain a stable cell concentration to prolong the production time (Ahn et al. 2008; Heidemann et al. 2000), this can be rarely applied for virus production processes, since virus replication is usually

associated with cell lysis. Consequentially, a virus production process comprises typically two phases: the cell growth phase and the virus replication phase (Nikolay et al. 2020a). Here, different strategies to ensure high cell concentrations can be applied for the perfusion rate control during the cell growth phase.

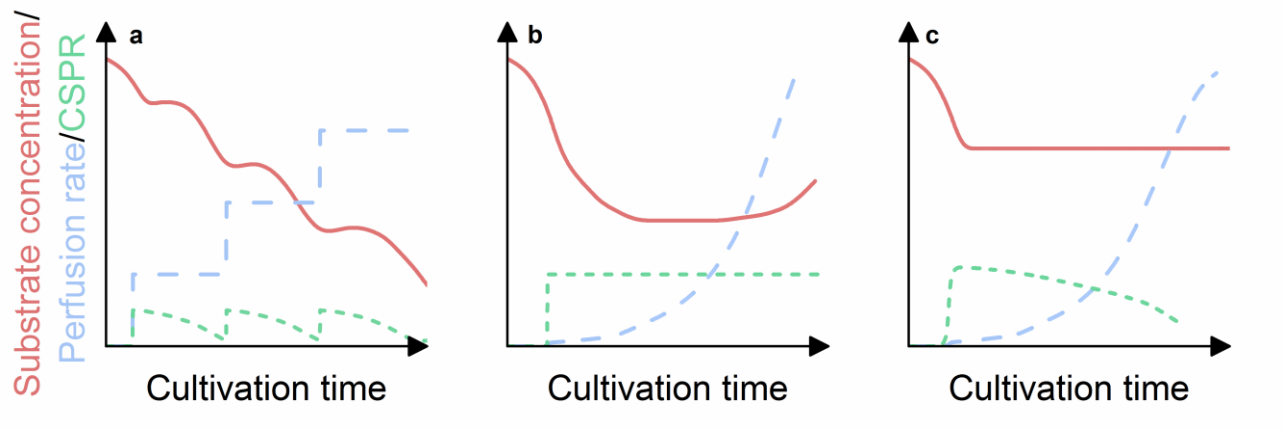

Fig. 2.5 Perfusion rate control strategies. (a) Reactor volume exchange regime, (b) cell-specific perfusion rate (CSPR) control, (c) metabolite-based perfusion rate control. (b and c) Substrate concentration, perfusion rate and CSPR are shown for a controlled process. Illustration adapted (Nikolay et al. 2020a).

The simplest control strategy is the reactor volume (RV) exchange regime. Here, the exchange rate of the medium is either fixed or follows a time regime to meet cellular demands. In the latter, the perfusion rate is often changed step-wise based on the cell growth and metabolite uptake known from previous cultivations. The pre-calculated profiles do not take the biological status of the system into account and consequentially this control strategy cannot cover biological variations (e.g. cell growth, substrate uptake rates, waste product release) and can therefore lead to overfeeding or limitations. Further, cell-specific perfusion rate (CSPR) and metabolite concentrations might fluctuate using this control regime (Fig. 2.5a). However, for well-characterized and robust production systems, the RV exchange regime can be a valuable strategy as it requires minimum technical effort (Karst et al. 2017b; Nikolay et al. 2020a).

Alternatively, the perfusion rate can be adjusted based on the viable cell concentration or the viable cell volume present in the bioreactor. Here, a certain amount of medium is added per cell or cell volume in a fixed time period, resulting in a constant CSPR or biovolume-specific perfusion rate (BVSPR) (Konstantinov et al. 2006; Ozturk 1996). The perfusion rate can be changed manually, based on offline measurements for example by an automated cell counter. Additionally, it is possible

to program the perfusion pump rate to increase according to the predicted cell growth. Furthermore, the perfusion rate can be controlled based on the measurements of an online biomass probe measuring the cell volume in the bioreactor (Dowd et al. 2003). The CSPR-based control allows an adequate supply of substrates with increasing cell concentrations and is able to cover biological variations. Consequentially, stable substrate levels can be achieved (Fig. 2.5b)

Lastly, the perfusion rate can also be controlled based on metabolite measurements. As for the CSPR-based control, the perfusion rate can be adjusted manually based on offline measurements and programmed to fulfill the predicted medium requirements. For the latter, the cell-specific growth rate and substrate uptake rate needs to be considered. It is also possible to control the perfusion rate based on online metabolite measurements. Typically, key substrates (e.g. glucose or glutamine) are used for a metabolite-based perfusion control (Dowd et al. 2001; Meuwly et al. 2006; Wang et al. 2002). However, the perfusion rate can also be controlled based on waste product concentrations (e.g lactate or ammonium) (Clincke et al. 2013; Handa-Corrigan et al. 1992). This control strategy results in a constant concentration of the chosen metabolite and equally allows a robust process control (Fig. 2.5c).

Online cell measurements

Information about the current cell concentration in the used cultivation system are of interest for any cultivation system. Online measurements can be especially valuable for systems were no offline measurements are possible (e.g. fixed-bed bioreactors). Furthermore, online cell measurements can be used to establish a controlled feeding strategy (e.g. CSPR control) (Dowd et al. 2003). The cell concentration can be estimated by monitoring the consumption of oxygen or glucose (Kyung et al. 1994; Meuwly et al. 2006). In addition, probes which measure the cell concentration based on the optical density or dielectric properties of the cells are commercially available. Optical density probes measure the turbidity in the cultivation vessel. The correlation of the turbidity to the viable cell concentration was found to be satisfying up to a concentration of 20E+06 cells/mL. For higher cell concentrations the presence of cell debris seemed to have a high impact on the measurement (Gorenflo et al. 2005; Wu et al. 1995). Further, this detection method does not allow do differentiate between live and dead cells. A more advanced detection method is utilized by biomass capacitance probes. Here, an electric field is applied resulting in the polarization of cells with an intact cell membrane, which can be measured as a change in capacity. Using the capacity to evaluate the biomass

in the bioreactor is more reliable than the optical density, since dead cells, gas bubbles or other particles like microcarrier are not polarizable and do not interfere with the measurement. Consequentially, capacitance probes are frequently used to monitor the biomass in perfusion processes up to high concentrations (Ducommun et al. 2002; Karst et al. 2017a; Noll and Biselli 1998; Petiot et al. 2012; Zhang et al. 2015). In the presented PhD work, a capacitance probe was used to control the perfusion rate based on the viable cell volume (VCV) in the cultivation vessel.

2.4.3 Other process intensification strategies

Next to the increase of the maximum viable cell concentration by the implementation of a perfusion strategy, other process intensification methods can be applied to increase the virus yield. One such strategy would be the increase of the CSVY, often facilitated by medium optimization. In this PhD work a recently developed chemically defined medium was used (Xeno™ medium), which allowed MDCK cells to grow in single cells to higher cell concentrations, while maintaining their CSVY (Bissinger 2020; Huang et al. 2015; Huang et al. 2011; Wu et al. 2021).

Further, advanced process control strategies can be applied to achieve higher virus titers. For example, the cells need to be metabolically active and supplied with sufficient nutrient concentrations over the cultivation time to ensure a high CSVY. For this, a medium exchange prior infection and high rate of medium renewal during the cell growth phase were proven to be effective measures (Bock et al. 2011; Pohlscheidt et al. 2008; Thomassen et al. 2014). The exchange of medium at time of infection also reduces the concentration of metabolic waste products and consequentially, very comparable CSVYs compared to batch processes could be achieved for HCD cultivations (Tapia et al. 2014).

Lastly, the infection conditions can be optimized. For an IAV production process these conditions include the trypsin activity, the MOI, the chosen harvest time point, and the temperature during the virus replication phase. These parameters were already addressed for IAV STV production (Bissinger 2020; Genzel and Reichl 2009; Wu et al. 2021) and were further investigated in the present PhD work.

3 MATERIALS AND METHODS

In the following chapter, the materials and methods used in this work are provided. The used consumables (Table C.1), reagents (Table C.2), and the equipment (Table C.3) are listed in the Appendix. The first sections of this chapter focuses on the cell maintenance, cell cultivation in different cultivation vessels and the general procedure for IAV infection experiments. The later sections describe the analytical assays used for this PhD work including cell concentration measurements, metabolite measurements, virus quantification assays and other assays to characterize the produced virus material.

3.1 Viruses

In this PhD work, two DIPs were produced; OP7 and DI244. The OP7 seed virus was a mixture of the desired OP7 and infectious A/Puerto Rico/8/1934 (H1N1) (PR8) STV, acting as a helper virus. This seed virus was a descendent of a previously reported virus preparation (Kupke et al. 2019), originally obtained from the National Institute for Biological Standards and Control (NIBSC; #99/716). The MOI was calculated based on the infectious virus titer (1.3E+8 $TCID_{50}$/mL) of the seed virus. The DI244 seed virus was generated using an eight-plasmid DNA transfection system (Bdeir et al. 2019) and therefore not contaminated with any STVs. This seed virus was provided by a collaboration partner (IB unit at the DPZ) and the multiplicity of DIP (MODIP) used for infections was calculated based on the DI244 titer (1.01E+8 PFU/mL).

For DIP-free control infections and as a challenge virus in the interference assay (section 3.11) pure STV seeds were used. The STV strain was an influenza PR8 seed virus strain of the subtype H1N1 originally obtained from the Robert Koch Institute (RKI; Amp. 3138). Here, two different seed virus preparations were used. For control infections, a seed virus adapted to suspension MDCK cells grown in Xeno™ medium (see section 3.2) was used (5.6E+8 $TCID_{50}$/mL). In the interference assay, a seed virus adapted to adherent MDCK cells was used (1.1E+9 $TCID_{50}$/mL).

As a negative control for mass spectrometry analysis, a plaque-purified STV preparation devoid of OP7 was used (Kupke et al. 2019). Here, plaques from a STV (NIBSC; #99/716) infection were

picked and reseeded in three consecutive assays and then multiplied on adherent MDCK cells (see section 3.2) for generation of a seed virus (5.8E+8 $TCID_{50}$/mL). For the different quantification methods of DIPs and infectious viruses, consult section 3.8.

3.2 Cells

For production of OP7, an MDCK cell line (ECACC, No. 84121903) adapted to suspension growth (Lohr et al. 2010) and subsequently further adapted to grow in chemically defined Xeno™ medium (Bissinger 2020) was used (MDCK.Xe.E). For production of purely clonal DI244, the Xeno™ medium-adapted MDCK.Xe.E cell line was genetically modified by retroviral transduction to stably express the viral PB2, encoded by the IAV vRNA Seg1. This genetically modified suspension cell line, hereafter called MDCK-PB2(sus), was provided by a collaboration partner (IB unit at the DPZ) (Hein et al. 2021c).

For virus quantification assays, innocuity assays, and interference assays, adherent MDCK cells (ECACC, No. 84121903) were used, hereafter called (MDCK(adh). Further, MDCK(adh) cells, genetically modified by retroviral transduction to stably express the viral PB2, were utilized for DIP quantification. This genetically modified adherent cell line, hereafter called MDCK-PB2(adh), was provided by a collaboration partner (IB unit at the DPZ) (Bdeir et al. 2019).

3.2.1 Cell maintenance

MDCK.Xe.E and MDCK-PB2(sus) cells were cultivated in shake flasks (125 or 250 mL baffled polycarbonate Erlenmeyer Flask, 4116-0125 or 4116-0250, Thermo Fisher Scientific) at 37°C, 5% CO_2 and 185 rounds per minute (rpm) (Multitron Pro, Infors HT, 50 mm shaking orbit) in chemically defined Xeno™ medium. The cells were maintained in their exponential growth phase by passaging them thrice a week. On Monday and Wednesday, the cells were diluted with fresh medium to a cell concentration of 1.0E+06 cells/mL, on Friday to 0.5E+06 cells/mL. For MDCK-PB2(sus), 0.5 µg/mL puromycin (Thermo Fisher Scientific, #A1113803) was added to the cultivation medium as a selective pressure, to ensure that only cells expressing the viral PB2 could replicate. Puromycin was only added to the medium for cell maintenance, but not for experiments.

MDCK(adh) and MDCK-PB2(adh) cells were cultivated in tissue culture flasks (175cm², C7231 or C7481, Greiner BioOne) in Glasgow minimum essential medium (GMEM) containing 1% peptone and 10% fetal bovine serum (cultivation medium) at 37°C and 5% CO_2. The cells were passaged weekly. For passaging, the monolayer was first washed twice with phosphate buffered saline (PBS), before 4.0 mL trypsin (porcine trypsin, 500 U/mL, Gibco) was added. After incubation (37°C, 5% CO_2, 25 min) the monolayer was detached and the reaction was stopped by addition of 6.0 mL cultivation medium. The cells were separated by repeated pipetting and cells were seeded into new tissue culture flasks with 7.0E+6 cells/flask. For MDCK-PB2(adh), 1.5 µg/mL puromycin (Thermo Fisher Scientific, #A1113803) was added to the cultivation medium. Puromycin was only added to the medium for cell maintenance, but not for virus quantification assays.

3.2.2 Cell-specific parameters

The growth rate of a cell line (r_c) can be correlated to the viable cell concentration (VCC) to obtain the proportionality factor, also called cell-specific growth rate (µ). The maximum cell-specific growth rate at optimal cultivation conditions is called μ_{max} (Eq. 1).

$$\frac{dVCC}{dt} = r_c = \mu_{max} \times VCC \qquad \text{Eq. 1}$$

VCC	Viable cell concentration [cells/mL]
t	Cultivation time [h]
r_c	Growth rate [cells/mL/h]
μ_{max}	Maximum cell-specific growth rate [1/h]

The cell-specific uptake rates (q_s) for the different metabolites can be calculated as followed (Eq. 2).

$$\frac{dC_s}{dt} = -q_s \times VCC - C_s \times Q + C_{s,Med} \times Q \qquad \text{Eq. 2}$$

C_s	Metabolite concentration in the STR [mmol/mL]
t	Cultivation time [h]
q_s	Cell-specific metabolite uptake rate [mmol/cell/h]
VCC	Viable cell concentration [cells/mL]
Q	Perfusion rate [mL/h]
$C_{s,Med}$	Substrate concentration in the medium [mmol/mL]

For batch cultivations, the perfusion rate was 0 mL/h. The setup of the perfusion cultivations is explained in section 3.4.2.

3.3 Infection experiments in shake flasks

Suspension cells grown in shake flasks (as described in section 3.2.1) were expanded to the required amount prior the experiment, if necessary by increasing the number of shake flasks cultivated in parallel. First, the culture broth was centrifuged (300×g, room temperature, 3 min) and the medium was exchanged with fresh medium. Next, the cell concentration was adjusted to the desired VCC and cells were transferred to new shake flasks with 50 mL working volume (125 mL baffled polycarbonate Erlenmeyer Flask, 4116-0125, Thermo Fisher Scientific). For most infection experiments in shake flasks, the cells were infected at time of inoculation (deviations will be pointed out in the results part). For this, trypsin (5000 U/mL in PBS; 27250018, Gibco) was added to a final activity of 20 U/mL, before the cells were infected with a seed virus at the desired MOI or MODIP, usually between 1E−1 and 1E−4. After infection, cells were incubated (37°C, 5% CO_2, 185 rpm) and samples were taken every 6–12 h until the VCC reduced below 0.5E+06 cells/mL. For sampling, the VCC was measured (section 3.6) and the remaining sample volume was centrifuged (3000×g, 4°C, 10 min). Aliquots of the supernatant were stored at −80°C to be analyzed later.

3.4 Bioreactor cultivations

To investigate the scalability of established production processes and for the implementation of process intensification strategies, bioreactor cultivations were conducted.

3.4.1 Bioreactor setup

For bioreactor cultivations, a 1 L-STR glass vessel (with working volumes ranging from 500 to 700 mL) and a digital control unit (DASGIP® Parallel Bioreactor System, 76DG04CCBB, Eppendorf AG) were used. The STR was equipped with one inclined blade impeller (three blades, 30° angle, 50 mm diameter) with an impeller to vessel diameter ratio of 0.5. Further, probes for the measurement temperature (78103304, Eppendorf AG), dissolved oxygen (DO) (78108039, Hamilton®), and pH value (78103230, Hamilton®) were used. Additionally, a capacitance probe (Incyte, Hamilton) for the online monitoring of cell growth was utilized. For aeration, the STR could be equipped with a macro-sparger and/or a micro-sparger. For trypsin addition and infection, a small septum in the top plate or a bigger septum on the side lid of the STR was used. Finally, a dip tube for sampling (inner diameter 6 mm), short tubes for addition of fluids (e.g. base or medium), and sterile connectors were utilized. The additional equipment needed for perfusion cultivations is described in section 3.4.2. Before STR assembly, the DO-probe and pH-probe were calibrated. The DO-probe was calibrated from 0% (nitrogen gassing) to 100% (air in the room). Here, the 100% DO was later recalibrated shortly before inoculation, to represent the maximum solvable oxygen in the cultivation medium. The pH-probe was calibrated with buffer solutions in the range from 7.00 (51350006, Mettler Toledo) to 9.21 (51350008, Mettler Toledo). After calibration and assembly, the STR was filled with 500 mL PBS and autoclaved. Afterwards, the PBS was removed and the STR was filled with Xeno™ medium. Next, the STR was connected to the control unit and the process control was started, before the bioreactor was inoculated.

3.4.2 Bioreactor cultivations in perfusion mode

For IAV production with high cell densities, membrane-based perfusion cultivations were carried out. Here, an additional continuous medium feed and harvest (coupled with a cell retention device) was required. As cell retention device an alternating tangential flow filtration system (ATF 2, Repligen) was used. The ATF was connected to the STR with a dip tube (inner diameter 10 mm). The perfusion rate was either adjusted manually or was controlled based on online cell measurements.

Alternating tangential flow filtration system

The flow rate of the diaphragm pump was set to 0.9 L/min, other parameters of the ATF controller were kept as given by the supplier. Two different cell retention membranes were tested. One was a commonly used polyethersulfone HFM (0.2 µm pore size, 470 cm^2 surface area, Spectrum Labs), the other one was the tubular VHU (~10 µm pore size, 62 cm^2 surface area, Artemis Biosystems). Neither membrane needed any pretreatment. The VHU was gamma sterilized before delivery and could not be autoclaved. Therefore the VHU was only attached to the autoclaved bioreactor under sterile conditions. Further, for removal of cell-free supernatant (hereafter called permeate flow) a peristaltic pump (120 U, Watson-Marlow) was used.

Control strategies for the perfusion rate

The feed of cultivation medium (Xeno™ medium) was controlled by a balance under the STR to maintain a constant working volume. Therefore, the feed flow rate always equaled the permeate flow rate. The permeate flow rate was increased over the process time either manually or was controlled based on online cell measurements. For the manually adjusted perfusion rate (RV exchange regime), the required set point was calculated based on the cell-specific growth rate and the glucose consumption rate in the exponential phase determined in previous batch cultivations (according to Eq. 3). Here, the perfusion rate was increased stepwise every 12 h according to a chosen CSPR (Eq. 4) or BVSPR. Please note, that Eq. 4 can be easily modified to calculate the BVSPR, by using the VCV (Eq. 5) instead of the VCC.

$$Q_{Est} = \frac{VCC_0 \times e^{\mu \times t_i} \times V_{WV} \times q_s}{C_{s,Med}} \quad \text{Eq. 3}$$

Q_{Est}	Estimated perfusion rate [mL/h]
VCC_0	Viable cell concentration at time of inoculation [cells/mL]
μ	Cell-specific growth rate [1/h]
t_i	Time post inoculation [h]
V_{WV}	Working volume of the STR [mL]
q_s	Cell-specific metabolite uptake rate [mmol/cell/h]
$C_{s,Med}$	Metabolite concentration in the medium [mmol/mL]

$$CSPR = \frac{Q * 10^9 * 24}{VCC \times V_{WV}} \quad \text{Eq. 4}$$

CSPR	Cell-specific perfusion rate [pL/cell/d]
Q	Perfusion rate [mL/h]
VCC	Viable cell concentration [cells/mL]
V_{WV}	Working volume of the STR [mL]

For the controlled perfusion (CSPR control), a previously reported approach was used (Nikolay et al. 2018). Here, a multi-frequency capacitance probe was connected to a controller (ArcView Controller 265, Hamilton), which converted the measured capacity to a permittivity signal. The permittivity signal correlates to the VCV in the STR and was forwarded to an analog 4–20 mA output box (Hamilton), which was connected to the peristaltic pump (120 U, Watson-Marlow) controlling the permeate flow. The desired BVSPR was realized by adjusting the specific cell factor stored in the ArcView controller. Here, a cell factor of 1.18 was used to achieve a BVSPR of 0.12 pL/µm^3/d, equaling a CSPR of 200 pL/cell/d, when a cell is assumed to be a sphere with a diameter of 15 µm. A scheme of the bioreactor setup for (controlled) perfusion cultivations is shown in Fig. 3.1. The perfusion rate control could only be used prior the virus infection, as the permittivity signal was drastically disturbed by the virus addition and replication. Therefore, the perfusion rate was kept constant after infection.

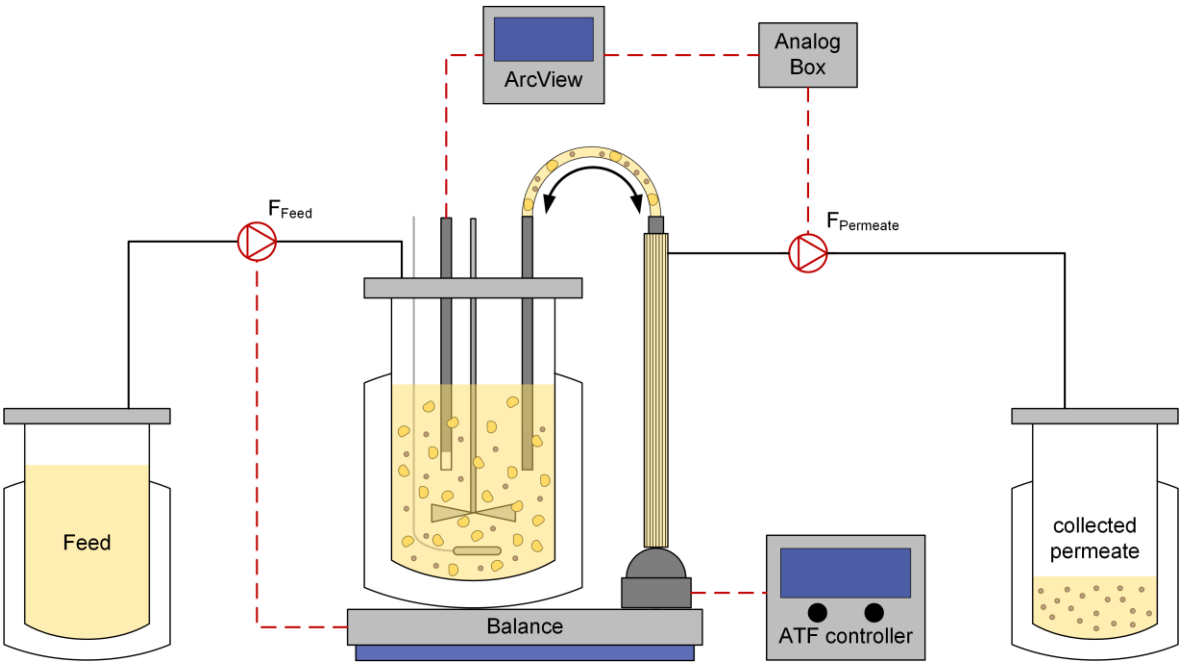

Fig. 3.1 Scheme of the bioreactor setup for perfusion cultivations. A stirred tank bioreactor (STR) was coupled with an alternating tangential flow filtration system (ATF) for cell retention. For on-line monitoring of the viable cell volume a capacitance probe could be used. The signal was converted by the ArcView and an analog box to control a peristaltic pump. Depending on the membrane used for cell retention, virus particles could be either found exclusively in the STR or additionally in the collected permeate. Black lines indicate the flow of fresh medium (F_{Feed}) and cell-free permeate ($F_{Permeate}$). Red dashed lines indicate different types of signal transmission. Illustration adapted (Nikolay et al. 2018).

3.4.3 Parameter setpoints and process control

A DO level of 40% was maintained by the aeration control. Here, with increasing oxygen demand, the flow of air was increased up to 6.0 L/h, before gassing with pure oxygen was started. The used DO control did not allow a reduction of the dissolved oxygen, when concentrations higher than the desired setpoint were present. The temperature setpoint was 37°C (or 32°C for the virus replication phase of perfusion cultivations) and was controlled by a heat sleeve. The pH setpoint depended on the experiment purpose and was controlled by addition of CO_2 and a 7.5% $NaHCO_3$ solution.

3.4.4 Bioreactor inoculation

Before inoculation, cells grown in shake flasks (as described in section 3.2.1) were centrifuged (300×g, room temperature, 3 min) and the spent medium was discarded. Fresh medium was added and the VCC was adjusted to 5.0E+06, 10.0E+06, or 20.0E+06 cells/mL (depending on the desired VCC in the STR). This cell pool was transferred to a bottle, which could be connected to the STR via a sterile connector. The cell pool volume was chosen to result in a 1:10 dilution and consequentially the STR was inoculated with 0.5E+06, 1.0E+06, or 2.0E+06 cells/mL.

3.4.5 Bioreactor infections

For perfusion cultivations, a complete medium exchange was performed prior to infection to facilitate virus replication. This was realized by manually increasing the perfusion rate. For HFMs, the perfusion rate was increased to 100 RV/d (50 mL/min). For the VHU, the perfusion rate was only increased to 15 RV/d (7.5 mL/min), as damage to the VHU membrane was observed for higher rates. After the medium exchange, the cultivation temperature was changed to 32°C, as this was shown to have a positive impact on virus replication (Wu et al. 2021). For batch cultivations, cells were infected shortly after inoculation to allow comparison to small scale infection experiments. At time of infection, trypsin (5000 U/mL in PBS; 27250018, Gibco) was diluted in 5 mL Xeno™ medium and added to the STR with a syringe using a septum (final activity 20 U/mL). Afterwards, the necessary amount of seed virus (to realize the desired MOI/MODIP) was diluted in 5 mL Xeno™ medium and added to the STR with a syringe.

3.4.6 Bioreactor sampling

For dead volume-reduced sampling, a T-piece connecting a one-way sampling valve (78510145, Eppendorf AG) and an air filter (17573----------Q, Sartorius AG) was used. This allowed to push the cell culture broth, remaining in the tubing, back into the STR. Samples were taken with a syringe via the sample valve. It was possible to take samples from the STR exclusively or additionally from the tubing behind the cell retention membrane (permeate line). The samples were analyzed for their VCCs (section 3.6), the rest was centrifuged (3000×g, 10 min, 4°C) and the supernatant was stored at -80°C for subsequent analysis.

3.5 UV-irradiation of virus preparations

UV-irradiation was used to (i) inactivate the STVs present in OP7 preparations or (ii) to inactivate DIPs in produced material (e.g. as negative control for animal experiments). Here, the inactivation efficacy was highly dependent on the irradiation time. To expose the virus preparation directly to the UV light while keeping a sterile environment, a laminar hood equipped with UV lamps (Safe 2020, Thermo Fisher Scientific) was used. For inactivation, 45 mL virus preparation were transferred into an open tray (250 cm^2 surface area) that was continuously shaken by a mixer (Duomax 1030, 543-32205-00 Heidolph). Thus, a thin film layer (approximately 2 mm) and a homogenous inactivation were ensured.

3.6 Offline cell concentration measurements

The cell concentration, average cell diameter, and viability of adherent and suspension cells were determined using an automated cell counter (Vi-CELL XR, Beckman Coulter, 731050). Different settings were used for the cell count of suspension and adherent cells (Table 3.1). The cell counter took a set of 100 pictures for the analysis. The differentiation of live and dead cells was achieved by a preceding trypan-blue dye staining. Cells incapable of dye exclusion were considered dead. The relative standard deviation (RSD) of the cell concentration measurements was $\leq 5\%$ (given by the supplier).

Table 3.1 Vi-CELL XR settings for suspension and adherent MDCK cells

	Suspension MDCK cells	**Adherent MDCK cells**
Min. diameter [µm]	7	8
Max. diameter [µm]	50	25
Cell brightness [%]	85	85
Cell sharpness	80	80
Viable cell spot brightness [%]	90	90
Viable cell spot area [%]	4	4
Min. circularity	0	0
Decluster degree	Medium	Medium

The cell counter measurements for cell concentration and average diameter were used to calculate the VCV, assuming the cells to be a perfect sphere (Eq. 5).

$$VCV = {d_{vc}}^3 \times \frac{\pi}{6} \times VCC \qquad \text{Eq. 5}$$

VCV Viable cell volume [µm^3/mL]

d_{vc} Average diameter of a viable cells [µm]

VCC Viable cell concentration [cells/mL]

3.7 Metabolite measurements

The concentrations of glucose, lactate, glutamine, ammonium, and glutamate in cell-free samples were measured with a Bioprofile 100 Plus (Nova Biomedical). If necessary, the samples were diluted with PBS to perform the measurements in the validated range. Additionally, virus-containing samples were heat inactivated prior measurement (80°C, 3 min). All samples of one experiment were collected and measured at the same time, together with in-house standards. For each metabolite, standards in four concentrations were prepared. Next, the measured metabolite concentrations of the standards were correlated against their actual concentrations. The resulting linear regressions were used to determine the sample metabolite concentrations. The average RSD depended on the measured metabolite: glucose (≤ 4.40%), lactate (≤ 2.57%), glutamine (≤ 3.06%), ammonium (≤ 1.90%), and glutamate (≤ 2.55%).

3.8 Virus quantification assays

3.8.1 Hemagglutination activity assay

The total amount of IAV particles was estimated by a hemagglutination activity assay (HA assay) as described previously (Kalbfuss et al. 2008). Briefly, virus samples were prepared in two serial 2-fold dilutions with PBS in a 96-round-bottom well plate, shifted by a factor of $1:2^{0.5}$. Each well contained 100 µL diluted sample to which 100 µL of a chicken erythrocyte solution with a concentration of 2.0E+07 erythrocytes per mL were added and incubated (room temperature, 3–8 h). The erythrocytes were cross-linked by the HA protein on the virus surface, consequentially agglutination would occur only up to a certain dilution, observable by the sedimentation of the agglutinated erythrocytes. Agglutination was evaluated photometrically by a plate reader (Infinite® 36M200 microplate reader, Tecan Group) measuring the extinction at 700 nm. Using a curve fitting function of the resulting extinction data, the transition in the sedimentation behavior was determined. HA titers were expressed as $\log_{10}$ HA units per 100 µL ($\log_{10}$ HAU/100 µL). The RSD of the HA assay was ≤ 9.7% for technical triplicates.

3.8.2 Plaque assay

For quantification of infectious, IAV particles, a plaque assay was used. For this, 6-well plates were seeded with MDCK(adh) cells (0.8E+6 cells per well) and incubated (37°C, 5% CO_2, 48 h). Samples were prepared in serial 10-fold dilutions in GMEM containing 1% peptone and 5 U/mL trypsin (infection medium for adherent cells). Cells were washed twice with PBS and for each dilution 250 µL/well were added and incubated (37°C, 5% CO_2, 1 h). Next, the supernatant was removed and cells were overlaid with 2 mL of 1% agar in infection medium. After incubation (37°C, 5% CO_2, 4 d), the agar was removed and the cells were fixed with methanol and stained with a 0.2% crystal violet solution. Finally, the plaque count was determined by light microscopy and the virus titer was calculated as plaque forming units (PFU) per mL (PFU/mL).

Further, the plaque assay was modified to detect DI244 particles. For this, MDCK-PB2(adh) cells instead of the parental MDCK(adh) cells were used. MDCK-PB2(adh) cells allowed replication of DIPs with a deletion in Seg1 vRNA, but also infectious STVs could propagate. Consequentially, only the DI244 titers of pure DIP preparation could be measured. The procedure of the plaque assay was identical regardless of the used MDCK cell line. The RSD of the plaque assay was ≤ 43.8% for technical duplicates.

Using the plaque assay and offline cell concentration measurements (section 3.6), it was possible to calculate the CSVY based on PFU ($CSVY_{PFU}$, Eq. 6). Please note that Eq. 6 can be easily modified to calculate the CSVY based on vRNA ($CSVY_{vRNA}$) by using the DI244 vRNA level (section 3.10.2) instead of the virus concentration. The error for the CSVY was calculated by error propagation of the individual assays, specifically plaque assay, quantitative PCR and offline cell measurements. The calculated RSD was ≤ 44.1% and ≤ 52.7% for the $CSVY_{PFU}$ and the $CSVY_{vRNA}$, respectively.

Further, the STY of a STR could be calculated (Eq. 7). The RSD of the STY corresponds to the error of the assay used for virus quantification. Here, the plaque assay was used to calculate the STY. Consequentially, the RSD of the STY was ≤ 43.8%.

$$\mathrm{CSVY}_{PFU} = \frac{C_{PFU,STR} \times V_{WV} + C_{PFU,cPerm} \times V_{cPerm}}{VCC_{max} \times V_{WV}} \quad \text{Eq. 6}$$

$$\mathrm{STY} = \frac{C_{PFU,STR} \times V_{WV} + C_{PFU,cPerm} \times V_{cPerm}}{t_P \times V_{WV}} \quad \text{Eq. 7}$$

$CSVY_{PFU}$	Cell-specific virus yield based on PFU [PFU/cell]
$C_{PFU,STR}$	Virus concentration in the STR [PFU/mL]
V_{WV}	Working volume of the STR [mL]
$C_{PFU,cPerm}$	Virus concentration in the collected permeate [PFU/mL]
V_{cPerm}	Volume of the collected permeate after infection [mL]
VCC_{max}	Maximum viable cell concentration [cells/mL]
STY	Space-time yield [PFU/h/mL]
t_P	Total process time [h]

Further, sampling the STR and the permeate line, allowed to measure and calculate the percentage of PFU in permeate line relative to PFU in the STR for each sampling time point (Eq. 8). The calculation allows to assess if any virus retention by the used cell retention membrane (section 3.4.2) occurred. Please note that Eq. 8 can be easily modified to calculate the "DI244 vRNA in permeate line / DI244 vRNA in STR" by using the DI244 vRNA level instead of the virus concentration.

$$\Delta_{Perm} = \frac{1}{n} \sum_{t=0}^{t=n} \left(\frac{C_{PFU,STR,t}}{C_{PFU,Perm,t}} \right) \times 100\% \quad \text{Eq. 8}$$

Δ_{Perm}	PFU in permeate line / PFU in STR [%]
$C_{PFU,STR,t}$	Virus concentration in the STR at sample time point t [PFU/mL]
$C_{PFU,Perm,t}$	Virus concentration in the permeate line at sample time point t [PFU/mL]

3.8.3 Tissue culture infectious dose assay

In addition to the plaque assay, the 50% tissue culture infectious dose assay ($TCID_{50}$) assay (Genzel and Reichl 2007) was used to determine the concentration of infectious IAV particles. Briefly, 96-well plates were seeded with MDCK(adh) cells (2.0E+4 cells per well) and incubated (37°C, 5% CO_2, 48 h). The confluent MDCK(adh) cells were infected with 100 µL/well of 10-fold serially diluted virus samples and incubated (37°C, 5% CO_2, 48 h). Subsequently, the cells were fixed with an 80% acetone solution and stained with an anti-IAV PR8 (H1N1) HA serum (#03/242, NIBSC) and an Alexa Fluor donkey anti-sheep IgG antibody (#A11015, Thermo Scientific) as a secondary fluorescence label. Each sample was processed in an 8-fold measurement. Using a fluorescence microscope (AxioObserver.A1, Zeiss) the fluorescence positive wells were determined and infectious titers were calculated with the Spearman-Kärber method (Kärber 1931; Spearman 1909). The RSD of the assay $TCID_{50}$ was $\leq$ 41.2% for technical triplicates.

3.9 Innocuity assay

For identification of residual infectious STVs in inactivated virus preparations (i.e. after UV-irradiation), an innocuity assay was conducted. Here, MDCK(adh) cells were cultivated in T75-flasks to a confluence of about 80%. Next, the cells were washed with PBS and the cultivation medium was replaced with 45 mL infection medium for adherent cells. A sample volume of 100 µL/flask was added and the cells were incubated (37°C, 5% CO_2, 72 h). Next, 1 mL of the supernatant was transferred to another T75-flasks with 80% confluent MDCK(adh) cells and 45 mL infection medium. After incubation (37°C, 5% CO_2, 72 h), the supernatant was analyzed in the HA assay. Samples without a detectable HA titer in the second passage were considered inactive and devoid of infectious STVs. Each sample was analyzed in triplicate, a STV preparation was used as positive control, and PBS as negative control.

3.10 PCR measurements

PCR-based measurements were used to analyze the vRNA concentrations of virus samples. The vRNA of collected samples was purified using the NucleoSpin® RNA virus kit (740956, Macherey-Nagel) according to manufacturer´s instructions. For identification of vRNAs with a deletion, a segment-specific reverse transcription-PCR (segment-specific RT-PCR) was used (section 3.10.1). For quantification of vRNAs of IAV Seg1 DI244, Seg5, Seg7, Seg7 OP7, and Seg8, a real-time reverse transcription quantitative PCR (real-time RT-qPCR) was used (section 3.10.2).

3.10.1 Segment-specific RT-PCR

The reverse transcription (RT) of isolated vRNAs and segment-specific PCR amplification of the resulting cDNAs was performed as described previously (Frensing et al. 2013; Kupke et al. 2019). Briefly, for the RT a universal primer (Uni12), which hybridized to the conserved 3’ region of all eight vRNA segments, was utilized. This allowed the cDNA generation of all segments in a single reaction (Hoffmann et al. 2001). For the subsequent PCR, individual segment-specific primers were used. The primer sequences comprise the conserved 3’ or 5’ terminal vRNA ends in conjunction with a segment-specific portion to allow for the specific amplification of the complete genome segment (Table 3.2).

For the RT, 10 µL extracted vRNA were mixed with 1 µL dNTPs (10 mM), 1 µL Uni12 primer (10 µM) and 3 µL with nuclease-free water. The mix was first incubated (65°C, 5 min) and then cooled (4°C, 5 min). Afterwards, 4 µL of “5x Reaction Buffer”, 0.5 µL “RevertAid H Minus Reverse Transcriptase” (100 U), 0.5 µL “RiboLock RNase Inhibitor” (40 U/µL) (all reagents were obtained from Thermo Fisher Scientific) were added and the mix was incubated (42°C, 60 min). Next, the RT was terminated (70°C, 10 min) and the generated cDNA could be stored at −20°C.

Table 3.2 Primers for segment-specific reverse transcription-PCR

Reaction	Target	Primer name	Sequence (5' -> 3')
RT	All segments	Uni 12	AGCAAAAGCAGG
PCR	Seg1	S1 Uni for	AGCGAAAGCAGGTCAATTAT
		S1 Uni rev	AGTAGAAACAAGGTCGTTTTTAAAC
	Seg2	S2 Uni for	AGCGAAAGCAGGCAAACCAT
		S2 Uni rev	AGTAGGAACAAGGCATTTTTTCATG
	Seg3	S3 Uni for	AGCGAAAGCAGGTACTGATCC
		S3 Uni rev	AGTAGAAACAAGGTACTTTTTTGG
	Seg4	S4 Uni for	AGCAAAAGCAGGGGAA
		S4 Uni rev	AGTAGAAACAAGGGTGTTTT
	Seg5	S5 Uni for	AGCAAAAGCAGGGTAGATAATC
		S5 Uni rev	AGTAGAAACAAGGGTATTTTTC
	Seg6	S6 Uni for	AGCGAAAGCAGGGGTTTAAAATG
		S6 Uni rev	AGTAGAAACAAGGAGTTTTTTGAAC
	Seg7	S7 Uni for	AGCGAAAGCAGGTAGATATTG
		S7 Uni rev	AGTAGAAACAAGGTAGTTTTTTAC
	Seg8	S8 Uni for	AGAAAAAGCAGGGTGACAAA
		S8 Uni rev	AGTAGAAACAAGGGTGTTTT

For the subsequent PCR, 2 µL cDNA was mixed with 4 µL "5x Phusion HF Buffer", 2 µL $MgCL_2$ (10 mM), 1 µL dNTP (10 mM), 1 µL of the forward and reverse primers (each 10 µM), 0.2 µL "Phusion DNA Polymerase" (2 U/µL) and 8.8 µL nuclease-free water (all reagents were obtained from Thermo Fisher Scientific). Afterwards the mix was incubated according to the cycle program shown in Table 3.3.

Table 3.3 Cycler program for the segment-specific PCR

Repetitions	Purpose	Temperature	Time
1x	Initial Denaturation	98°C	3.0 min
25x	Denaturation	98°C	25 s
	Annealing	54°C	45 s
	Elongation	72°C	2.0 min for Seg1–3 1.5 min for Seg4–6 1.0 min for Seg7–8
1x	Final elongation	72°C	10.0 min

Amplified PCR products were visualized using gel electrophoresis and analyzed for the presence of shortened PCR products (in comparison to the PCR product of a full-length vRNA segment), which would indicate the presence of DI vRNAs. For this, a gel was prepared with 1% w/v of agarose in Tris-Phosphate-EDTA buffer and stained with "Roti-GelStain" (Roth). As loading dye "FastDigest Green Buffer" (Thermo Fischer Scientific) was used. "GeneRuler DNA Ladder Mix" (Thermo Fischer Scientific) was used as a DNA ladder. The electrophoresis was performed at 70 V for 40 min.

3.10.2 Real-time RT-qPCR

For the real-time RT-qPCR, a previously reported primer system (Kawakami et al. 2011) that allowed the specific detection and quantification of individual vRNA segments, was used. The *in vitro* generation of reference standards, reverse transcription, real-time qPCR, and calculation of absolute vRNA levels were described previously (Frensing et al. 2014; Kupke 2020; Kupke et al. 2019). New primer combinations and reference standards were established accordingly for quantification of Seg1 DI244 (Wasik et al. 2018) and Seg7 OP7 vRNA (Hein et al. 2021c) (established by S. Kupke from the BPE group at the MPI).

For the RT, tagged primers were used (Table 3.4). First, 1 µL RNA sample, 1 µL dNTPs (10mM), 1 µL RT primer (1 µM), 1 µL total RNA (350 ng/µL), and 10.5 µL nuclease-free water were mixed and incubated (65°C, 5min). During the next incubation step (55°C, 5 min) a pre-warmed mixture

(55°C) consisting of 4 µL "5x RT buffer", 0.5 µL "Maxima H Minus Reverse Transcriptase" (200 U/µL), 0.5 µL RiboLock RNase Inhibitor (40 U/µL), and 0.5 µL nuclease-free water (all reagents were obtained from Thermo Fisher Scientific) was added. Afterwards, the RT was carried out (60°C, 30 min), before the reaction was terminated (85°C, 5 min). RNA reference standards in a 10-fold dilution series (from 5.0E+0 ng/µL to 5.0E−7 ng/µL) were reverse transcribed in parallel to the RNA samples. After the RT, the generated cDNA was diluted to 80 µL in nuclease-free water and stored at −20°C.

Table 3.4 Tagged primers for reverse transcriptase (for quantification of viral RNAs)

Target	Primer name	Sequence (5' -> 3')
Seg1 DI244	Seg-1-tagRT-for	ATTTAGGTGACACTATAGAAGCGAGCGAAAGCAGGTCAATTATATTC
Seg5	S5 tagRT for	ATTTAGGTGACACTATAGAAGCGAGTGATTATGAGGGACGGTTGAT
Seg7 OP7	S7-OP7 tagRT for	ATTTAGGTGACACTATAGAAGCGACTGTGACTGCTGAAGTGGTG
Seg 8	S8 tagRT for	ATTTAGGTGACACTATAGAAGCGGATAGTGGAGCGGATTCTG

For the qPCR, a PCR cycler (Rotor-Gene Q real-time PCR cycler, Qiagen) and specific qPCR primers (Table 3.5) were used. The qPCR mix contained 5 µL"1x Rotor-Gene SYBR Green PCR Kit" (Qiagen), 0.5 µL reverse and forward primer (10µM), and 4 µL of the diluted cDNA. The cycler program involved an initial denaturation (95°C, 5 min), followed by 40 PCR cycles of: 95°C for 10 s and 62°C for 20 s. Afterwards, melting curve analysis from 65°C to 90°C was performed.

Table 3.5 Primers for quantitative PCR (for quantification of viral RNAs)

Target	Primer name	Sequence (5' -> 3')
Introduced tag sequence	vRNA tagRealtime for	ATTTAGGTGACACTATAGAAGCG
Seg1 DI244	DI244 Realtime rev	GGAATCCCCTCAGTCTTC
Seg5	Seg 5 Realtime rev	CGCACTGGGATGTTCTTC
Seg7 OP7	Seg 7 OP7 Realtime rev	CATTTGCCTAGCCCGAATC
Seg 8	Seg 8 Realtime rev	CACTTTCTGCTTGGGTATGA

For absolute quantification, the C_T values of the 10-fold dilution series of the RNA reference standard were plotted against their $\log_{10}$ number of RNA molecules in the measured volume to generate a calibration curve. The number of RNA molecules of each standard was calculated based on the quantity of the standard, fragment length and an average mass per base, as followed.

$$n_{mol,Std} = \frac{m_{Std} \times N_A}{n_{Base} \times k} \quad \text{Eq. 9}$$

$n_{mol,Std}$ Number of vRNA molecules in the standard [-]

m_{Std} Weight of one vRNA molecule in the standard [g]

n_{Base} Fragment length [bp]

k Average mass of a base [g/mol/bp]

N_A Avogardo constant [1/mol]

Using the calibration curve of the RNA reference standards, the number of viral RNA molecules of each sample could be calculated based on their C_T value according to Eq. 10. The RSD of the real-time RT-qPCR measurements was ≤ 52.5% for technical quadruplicates.

$$n_{mol,Sample} = 10^{(\frac{C_T - b}{m})}[\frac{1}{\mu L}] \times F_{RT} \times V_{sample} \quad \text{Eq. 10}$$

$n_{mol,Sample}$	Number of vRNA molecules in the sample [-]
C_T	Cycles before signal intensity surpassed the threshold [-]
b	Y-offset of the calibration curve of the vRNA standards [-]
m	Slope of the calibration curve of the vRNA standards [-]
F_{RT}	Coefficient of dilution of the RT [-]
V_{Sample}	Total volume of the vRNA sample [µL]

3.11 Interference Assay

The interfering efficacy of the produced DIPs was evaluated by an interference assay (adapted from (Kupke et al. 2019)). Here, the DIP-induced reduction in the release of infectious virus particles in a co-infection with STVs was determined. First, 6-well plates were seeded with MDCK(adh) cells (1E+6 cells per well) and incubated for 24 h (37°C, 5% CO_2). Before infection, cells were washed twice with PBS. Afterwards, cells were co-infected with infectious STVs at MOI 10 or 0.01 and 125 µL of DIP material. The DIP addition with a fixed volume allowed the identification of production conditions yielding the highest interfering efficacy per product volume. Infection medium was filled up to a total volume of 250 µL. After incubation (37°C, 5% CO_2, 1 h), cells were washed once with PBS. Next, infection medium was added (2 mL per well) and cells were incubated again (37°C, 5% CO_2). When STVs were added at MOI 10, cells were incubated for 16 h. For an infection with STVs at MOI 1E−2, the incubation time was 24 h. The supernatants were stored at -80°C and later analyzed for their HA titer, plaque titer, and vRNA concentration.

3.12 Matrix protein 1 analysis

Mass spectrometry (MS) measurements were carried out by S. Püttker (Bioprocess Engineering, Otto-von-Guericke-University Magdeburg) to determine the abundance of total and mutated M1 protein in the produced OP7 material. The work conducted by the colleague for the protein precipitation, tryptic digestion, liquid chromatography, MS measurements, and data analysis with Skyline are described in the publication investigating the production process of OP7 (Hein et al. 2021c).

The point mutations of the OP7 Seg7 vRNA likely result in the expression of a mutated M1 protein (M1-OP7). For quantification of "the abundance of M1-OP7", a peptide containing one of the OP7 mutations (EITFYGAK) was measured. To quantify "the abundance of total M1", a peptide without point mutations (TRPILSPLTK), which should be present in IAV STVs and OP7 particles, was measured. The "proportion of M1-OP7 to total M1" was estimated by dividing "the abundance of M1-OP7" by the respective "abundance of total M1". Subsequently, results were normalized to their corresponding maximum value.

3.13 Protein and DNA quantification

To investigate the protein and double stranded DNA (dsDNA) retention of different cell retention membranes, samples from the STR and the collected harvest were analyzed. The measurements were carried by P. Marichal-Gallardo (BPE group at the MPI). The protein content was determined by a Bradford assay (BioRad Laboratories, 500-0006). The standard calibration curve was generated with bovine serum albumin (Sigma-Aldrich Chemie GmbH, A3912). The RSD of technical triplicates was $\leq 6.3\%$. For dsDNA quantification a Quant-iT PicoGreen assay (Life Technologies GmbH, P7581) was used, as described previously (Opitz et al. 2007). The standard calibration curve was generated with lambda DNA (Promega, D1501). The RSD of technical duplicates was $\leq 2.1\%$.

4 RESULTS AND DISCUSSION

The following chapter is divided into two parts. In the first section, the establishment of a cell culture-based production system for the novel DIP OP7 is described (section 4.1). Here, the MOI screening in shake flasks, the UV-inactivation of STV by-product, and the scale-up to a STR is outlined (Hein et al. 2021c). In the second section, the development of a production process for pure DI244 preparations, using a genetically modified MDCK cell line, is described (section 4.2). Here, the DI244 production in shake flasks, scale-up to a STR (Hein et al. 2021a), and the establishment of a controlled high cell-density perfusion process with continuous virus harvesting (Hein et al. 2021b) are reported.

4.1 Establishment of a production process for OP7

Note, that major parts of the original research article from Hein *et al.* in *Applied Microbiology and Biotechnology* were used in the following section (Hein et al. 2021c). The novel DIP OP7, recently discovered in our research group, contains point mutations instead of internal deletions (Kupke et al. 2019). In the present PhD work, a small-scale cell culture-based production process of OP7 material was established. For production, the interplay of DIPs and STVs was assessed by testing a range of MOIs to obtain high OP7 yields (section 4.1.1). Next, the produced OP7 material was UV-irradiated, to ensure complete STV inactivation while maintaining a high interfering efficacy, as shown in an *in vitro* interference assay (section 4.1.2). Afterwards, the growth of MDCK.Xe.E cells in a STR was evaluated and optimized (section 4.1.3). Then, the production process for OP7 was scaled up from shake flasks to the STR (section 4.1.3).

4.1.1 MOI screening for OP7 production

A seed virus containing OP7 particles and STVs was used for cell culture-based production, since propagation of the defective OP7 relies on STV complementation. On the one hand, more STV and DIP co-infections were expected at higher MOIs, likely leading to an enhanced propagation of OP7 over STVs. However, it has to be considered that DIP co-infections also suppress virus replication, which may lead to an overall reduced virus titer (and thus, reduced OP7 yield) at higher MOIs. On the other hand, low MOIs should result in higher total virus titers, since cells are mostly infected by

single virus particles. Here, only STV-infected cells (but not OP7-infected cells) will produce progeny viruses. Therefore, OP7 propagation and interference with virus replication was expected to cease for lower MOIs. To test this supposed dependency of OP7 yield on MOI, four MOIs ranging from 1E−1 to 1E−4 were investigated in shake flask batch cultures. Therefore, MDCK.Xe.E cells in Xeno™ medium were infected with OP7 seed virus. The applied MOI was calculated based on $TCID_{50}$ measurements of the seed virus determining the amount of infectious STV particles. VCCs, HA titers, $TCID_{50}$ titers and vRNA levels of the mutated Seg7 OP7 of released virus particles were quantified over time post infection (Fig. 4.1).

Indeed, cell cultures infected at higher MOIs resulted in lower HA titers compared to those infected at lower MOIs (Fig. 4.1a), indicating an interfering effect of OP7 on virus propagation. In line with this observation, maximum $TCID_{50}$ titers were lower with higher MOIs (Fig. 4.1b). The vRNA levels of Seg7 OP7 showed a higher initial levels for higher MOIs (Fig. 4.1c); yet, the highest maximum vRNA levels were reached for infections at MOI 1E−2 and 1E−3. As a control, one cultivation was infected with a pure STV seed (devoid of OP7) at MOI 1E−4. As expected, the STV infection showed the fastest decrease in VCC (Fig. 4.1d) while resulting in the fasted increase in HA and $TCID_{50}$ titers.

For all infections, the $TCID_{50}$ titer decreased at late process times, in line with previous findings (Genzel et al. 2010). For instance, the infectious virus titer of the pure STV infection showed a decrease of approximately three orders of magnitude from 24 to 56 hours post infection (hpi). Since it needs to be assumed that OP7 particles may lose biological activity similarly, it was considered to harvest as early as possible. A harvest time point of 32 hpi was chosen, where the HA titers and Seg7 OP7 vRNA levels roughly reached their respective maximum value (Fig. 4.1a and c, black arrow). At the same time, $TCID_{50}$ titers were close to their maximum. $TCID_{50}$ titers, HA titers, and Seg7 OP7 vRNA levels for the different MOI at 32 hpi are shown in Table 4.1 (production replicate 1).

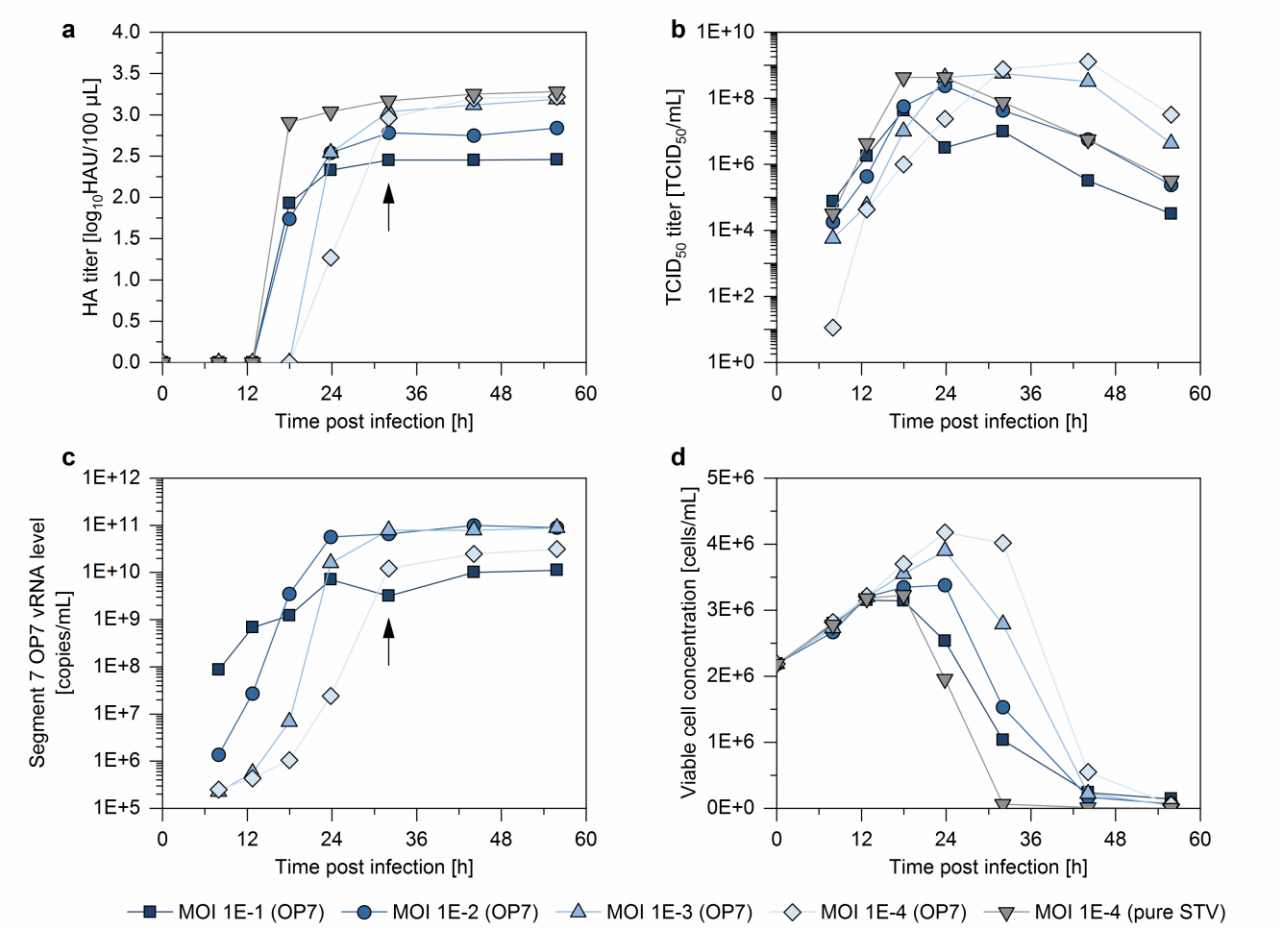

Fig. 4.1 MOI screening for batch mode production of OP7. MDCK.Xe.E cells were cultivated in shake flasks (50 mL working volume) and infected at a VCC of 2.0E+6 cells/mL with OP7 seed virus at different MOIs or pure STVs at MOI 1E−4. (a) HA titers, (b) $TCID_{50}$ titers, (c) vRNA levels of Seg7 OP7 and (d) VCCs. For the pure STV infection, no Seg7 OP7 could be detected. The black arrows indicate the chosen harvest time point (32 hpi) for following experiments.

To determine the production MOI yielding the highest biological efficacy, OP7 samples were compared in an *in vitro* interference assay. Here, the suppression of STV replication by OP7 co-infection was assessed. More specifically, STV-infected cells were co-infected with OP7 material, and the reduction of released infectious virus particles was compared to those of STV only infected cells. STVs were added at MOI 10 and harvested OP7 material with a fixed volume of 125 µL in order to identify a production condition showing the highest interfering efficacy per product volume. The $TCID_{50}$ titers, HA titers, and OP7 Seg7 vRNA levels for the OP7 preparations produced at different MOIs and tested in the interference assay are shown in Table 4.1 (production replicate 2).

Table 4.1 Virus quantification of different OP7 preparations produced at different MOIs

Assay	OP7 Preparation (32 hpi)	Production replicate 1	Production replicate 2	Production replicate 3
HA assay (log_{10} HA units/100 µL)	MOI 1E-1	2.45	2.23	2.61
	MOI 1E-2	2.78	2.81	
	MOI 1E-3	3.04	3.04	
	MOI 1E-4	2.96	2.74	
$TCID_{50}$ assay ($TCID_{50}$/mL)	MOI 1E-1	1.00E+07	5.6E+05	5.12E+07
	MOI 1E-2	4.30E+07	7.60E+07	
	MOI 1E-3	5.60E+08	4.30E+08	
	MOI 1E-4	7.60E+08	7.60E+08	
Real-time RT-qPCR (Seg7 OP7 vRNA copies/mL)	MOI 1E-1	3.19E+09	1.09E+10	2.20E+10
	MOI 1E-2	6.62E+10	3.43E+10	
	MOI 1E-3	7.80E+10	1.40E+10	
	MOI 1E-4	1.22E+10	2.37E+09	

Fig. 4.2a shows the results of the interference assay. OP7 material produced at MOI 1E−2 showed the strongest interference, when compared to the OP7 preparations produced at other MOIs ($p < 0.05$, unpaired two-tailed t-test), reducing the infectious virus titer (determined by plaque assay) by almost four orders of magnitude. Material produced at MOI 1E−1 or 1E−3 showed a less pronounced titer reduction, and OP7 produced at MOI 1E−4, decreased the plaque titer just marginally. Nevertheless, the reduction in the plaque titer was significant for all OP7 preparations, when compared to the negative control ($p < 0.001$). A similar trend could be observed for the reduction in total virus particle release, as indicated by the HA titers ($p < 0.05$ for MOI 1E–1, 1E–2, and 1E–3; $p=0.13$ for MOI 1E–4). For the HA titers, the observed differences were not as pronounced, as the release of replication deficient OP7 particles also contributed to total virus particle concentration. Please note that also OP7 material harvested at other time points was investigated (Fig. A1). However, no significant improvements in the interfering efficacy could be observed.

The interference of OP7 was further assessed in vRNA measurements of the released virus particles using real-time RT-qPCR (Fig. 4.2b). Material produced at any MOI induced an OP7 phenotype in the interference assay, indicated by an over-proportional level of Seg7 OP7 vRNA, as described previously (Kupke et al. 2019). While the maximum Seg7 OP7 vRNA levels were comparable, Seg5 and Seg8 vRNA levels showed a stronger reduction at higher interference.

The point mutations on Seg7 OP7 vRNA also affect the coding region, resulting in a mutated M1-OP7 protein, which is presumably incorporated into OP7 particles. To investigate this, MS was used to quantify M1-OP7 (Fig. 4.2c). The sample preparation and MS measurements were carried out by S. Püttker (Bioprocess Engineering, Otto-von-Guericke-University Magdeburg). Here, M1-OP7 was quantified by measuring the abundance of a fragment peptide that carried a mutation in the respective amino acid sequence. The abundance of total M1 protein was quantified by measurements of a fragment peptide that was identical for OP7 and wild type virus. In line with the results of the interference assay, the relative abundance of M1-OP7 was highest for OP7 produced at MOI 1E−2 and lowest for a production at MOI 1E−4. Next, the proportion of the M1-OP7 to total M1 protein was estimated. Here, higher production MOIs led to higher proportions of M1-OP7, with OP7 produced at MOI 1E−1 showing the highest proportion. However, the total amount of produced M1-OP7 was higher for material produced at MOI 1E−2, which may be explained by the decreased total virus titer for the production MOI 1E−1 (Fig. 4.1a). As a control, a plaque-purified STV sample (devoid of OP7) was used, which was tested negative for the presence of M1-OP7 (Fig. 4.2c). In contrast, the peptide for total M1 protein could be measured for all samples (Fig. 4.2d), confirming the validity of the measurements.

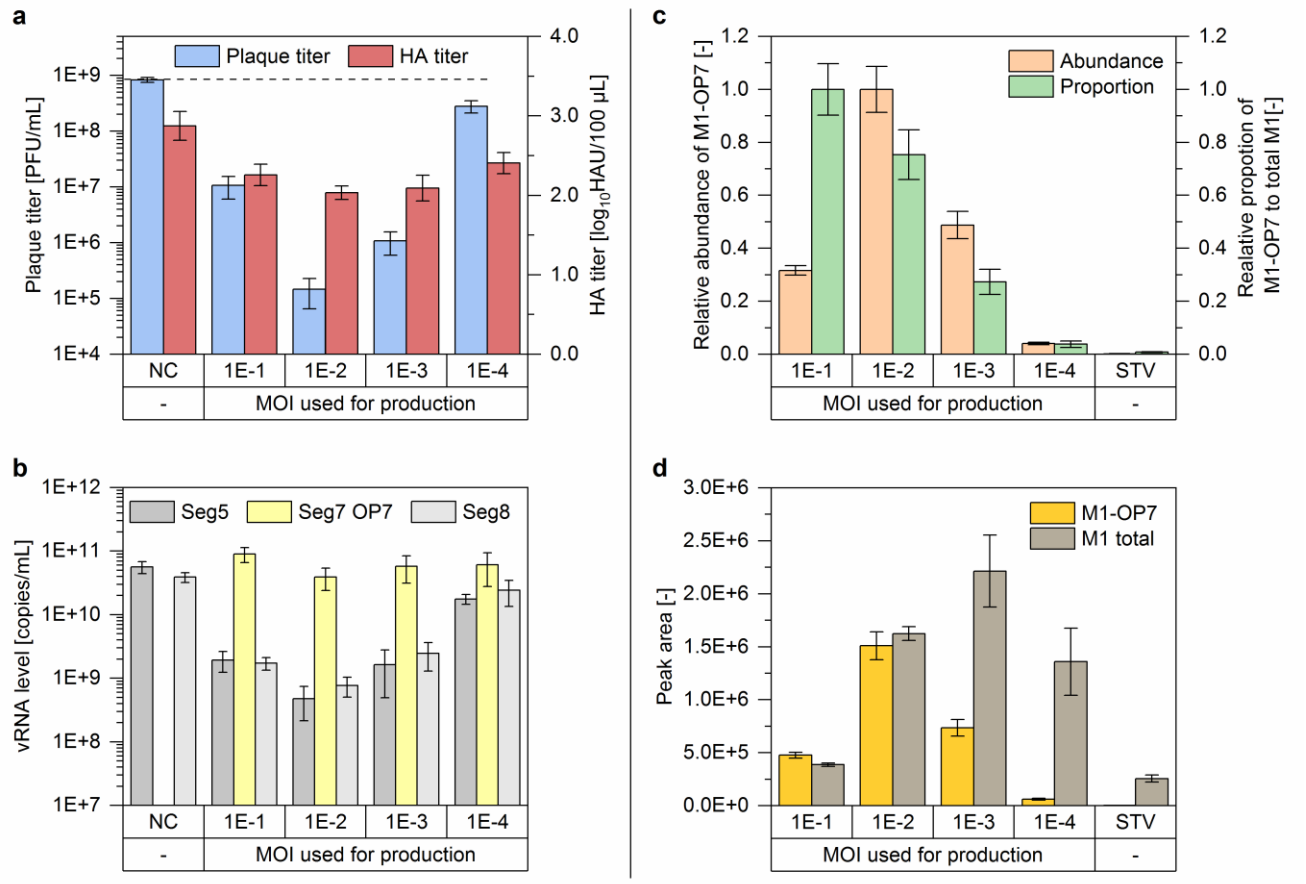

Fig. 4.2 Evaluation of OP7 material produced at different MOIs. (a and b) Interference assay. MDCK(adh) cells were infected at MOI 10 with STVs and co-infected with 125 µL of OP7 material, produced at a MOI ranging from 1E−1 to 1E−4 (Table 4.1, production replicate 2) or medium as negative control (NC). At 16 hpi, (a) virus titers and (b) vRNA levels of Seg5, Seg7 OP7, and Seg8 in the progeny virus particle were determined. (c and d) OP7 materials, produced at different MOIs analyzed by mass spectrometry (MS). As a control, a plaque-purified STV seed, devoid of OP7, was measured. (c) The relative abundance of M1-OP7 and the relative proportion of M1-OP7 to total M1 protein are shown. Results were normalized to the respective maximum value. (d) Peak area of M1-OP7 and total M1. The interference assay was performed in independent experiments (n=3) using one OP7 production sample. MS measurements were performed as technical replicates (n=3) of one production sample. Error bars indicate one standard deviation.

To ensure that observed interfering effects were not caused by conventional DIPs, a segment-specific RT-PCR was performed. The method was previously used to detect deleted (and therefore shorter) DI vRNAs of IAV of Seg1–8 in cell culture (Frensing et al. 2013; Tapia et al. 2019). No DI vRNAs were observed on any segment at any production MOI (Fig. 4.3).

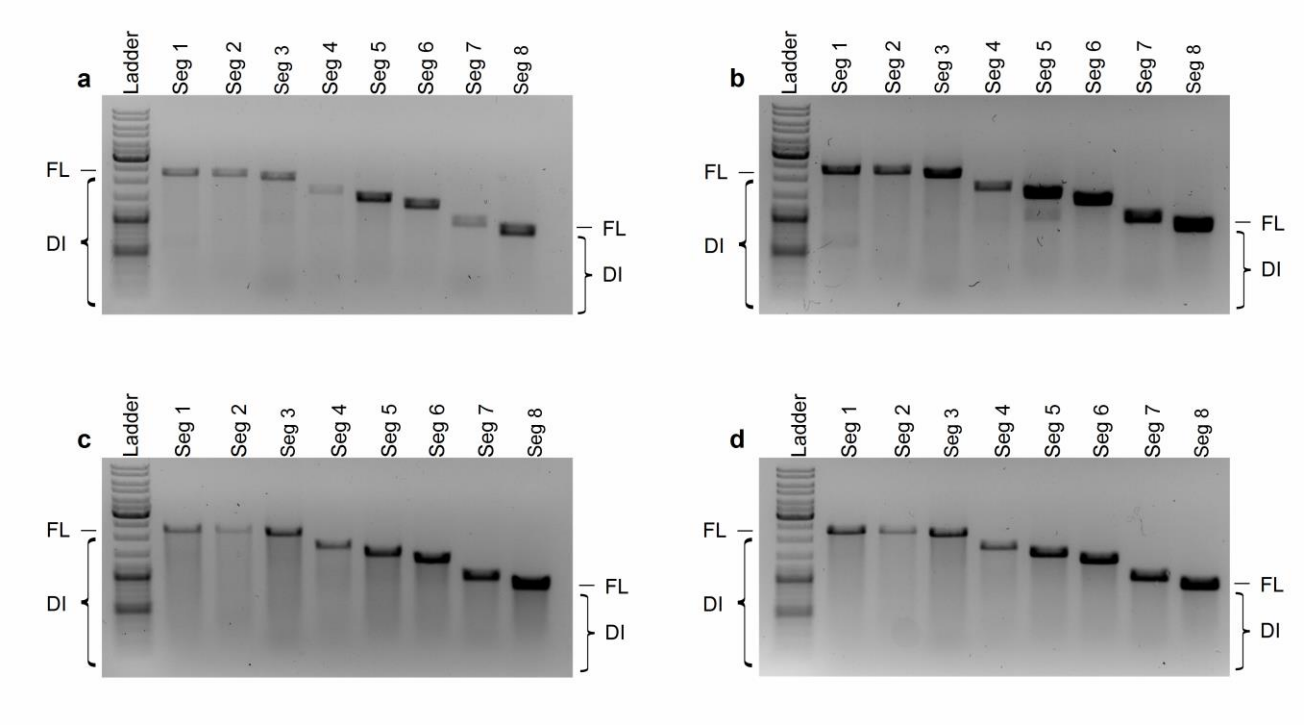

Fig. 4.3 Segment-specific RT-PCR of OP7 material. OP7 material produced at different MOIs (Table 4.1, production replicate 2) was analyzed by segment-specific reverse transcriptase-PCR for the presence of short vRNAs in Seg1–8. Results for (a) MOI 1E−1, (b) MOI 1E−2, (c) MOI 1E−3 and (d) MOI 1E−4 are shown. Signals corresponding to full-length (FL) and deleted (DL) vRNAs are indicated (FL size depends on the analyzed vRNA segment). Ladder: upper thick band 3.0 kb, middle thick band 1.0 kb, lower thick band 0.5 kb.

In summary, it appears that the MOI strongly affected the yield of OP7 (i.e., Seg7 OP7 vRNA). High MOIs resulted in lower virus titers, indicating suppression and interference of virus production by OP7. On the other side, low MOIs resulted in higher total virus particle concentrations. Therefore, intermediate production MOIs (i.e., MOI 1E−2 or 1E−3) seem to allow for high-yield OP7 production due to a good balance between Seg7 OP7 vRNA replication and an acceptable suppression of overall virus production. Here, the interference assay showed the highest interfering efficacy for material produced at MOI 1E−2, in line with MS measurements indicating the highest amount of M1-OP7.

4.1.2 UV-irradiation of OP7 preparations

In order to inactivate STVs in the produced OP7 material, which may cause harm in a potential application, UV-irradiation was used. However, short inactivation times were targeted to avoid a potential loss of interfering efficacy of OP7.

Fig. 4.4 shows the inactivation kinetics of a pure STV sample and of OP7 produced at MOI 1E−2. For the STV sample, infectious virus titers steadily decreased with irradiation time until 5 min. At 6 min, the detection limit of the plaque assay was reached. However, for the OP7 material, no infectious virus titer could be detected already after 2 min UV-irradiation. Here, it is likely that the quantification of STVs in the plaque assay (detecting only infectious viruses) was impeded by the suppression of virus replication by OP7 particles.

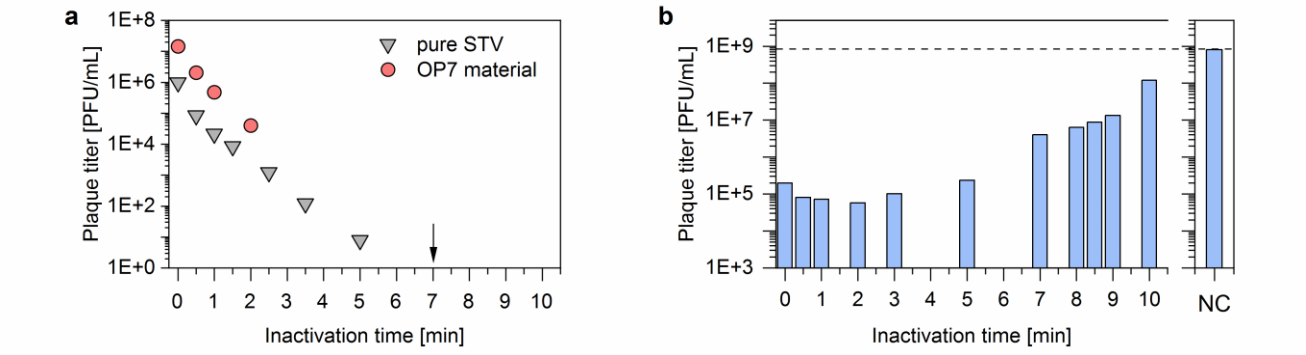

Fig. 4.4 UV-irradiation of produced OP7 material. Produced OP7 material (MOI 1E−2, 32 hpi; Table 4.1, production replicate 3) was irradiated with UV light. (a) Infectious virus titer in the sample at different UV-inactivation times, where 0 min corresponds to UV-untreated samples. As a control, the decrease in infectious virus titer of a pure STV preparation, devoid of OP7, was tested. The black arrow indicates the first time point where no infectious virus could be detected for the UV-treated OP7 material, as shown by an innocuity assay. (b) Interference assay. MDCK(adh) cells were infected at MOI 10 with STVs and co-infected with 125 µL of OP7 material, UV-inactivated for different durations. Medium was tested as a negative control (NC).

To demonstrate the absence of STVs for UV-treated OP7 material, an *in vitro* innocuity assay was performed. Here, a small sample volume was used for infection of a large number of cells, followed by another infection passage after three days. This complies with a low MOI scenario in which almost exclusively single-hit infections occur. Accordingly, these infection conditions allow for the propagation of residual STVs, which might have not been detectable by the plaque assay (Fig. 4.4a). Afterwards, virus accumulation was determined by hemagglutination assay. Indeed, OP7 material irradiated up to 6 min was tested positive in the presence of infectious STVs. The first time point

tested negative was 7 min of UV-irradiation (black arrow, Fig. 4.4a). Nevertheless, for safety reasons an inactivation time of 8 min was chosen for processing of OP7 material for subsequent animal experiments.

Next, the interfering efficacy was determined for OP7 material inactivated for different UV-irradiation times (Fig. 4.4b). With longer inactivation times, the interfering efficacy decreased, which can be explained by inactivation of OP7 particles. Interestingly, up until 1 min inactivation time, the interfering efficacy slightly increased, which may be explained by a faster inactivation of STVs compared to OP7.

Taken together, UV-irradiation resulted in a complete inactivation of STVs in the produced OP7 material after 7 min. Still, to a large degree, the interfering efficacy of OP7 was preserved. OP7 material was produced and processed according to the previously determined optimal process conditions (MOI 1E–2, harvest time 32 hpi, 8 min UV-inactivation) and the antiviral potential was evaluated in animal experiments with mice by a collaboration partner (Department of Infection Genetics (IG) at the Helmholtz Centre for Infection Research (HZI), Germany) (Hein et al. 2021c). Here, 100% of the mice infected with an otherwise lethal dose of IAV survived the infection, when treated with the produced OP7 material.

4.1.3 OP7 production in a STR batch cultivation

To investigate the scalability of the developed OP7 production process, first the cell growth of MDCK.Xe.E cells in a STR with a working volume of 500 mL was investigated. Here, the optimal agitation speed and pH setpoint were determined, before OP7 infection experiments were carried out.

First, four STRs were inoculated with MDCK.Xe.E cells with a VCC of 1.0E+06 cells/mL and operated with different agitation speeds ranging from 100 rpm to 220 rpm. Despite the different agitation speeds no altered cell growth could be observed (Fig. 4.5a). The maximum VCC was reached after 84 h, with approximately 6.0E+06 cells/mL for all cultivations. The pH setpoint was 7.4, but no base was connected to counteract a decreasing pH (Fig. 4.6b) and consequentially a shift in the pH to roughly 7.0 was observed at 72 h post inoculation. This might be explained by an increasing lactate concentration over the process time (Fig. 4.5e). Over the entire cultivation time, glucose concentrations sufficient to support cell growth were measured (Fig. 4.5c). However, glutamine was depleted at 72 h post inoculation (Fig. 4.5d). This possibly resulted in the observed

decreased cell growth. Here, it is unlikely that the secreted waste products influenced the cell growth, since lactate (Fig. 4.5e) and ammonium concentrations (Fig. 4.5f) were below 25 mmol/L and 5 mmol/L, respectively. In previous experiments, no reduction in virus titers of IAV produced with MDCK cells was observed at similar lactate and ammonium concentrations.

Overall, the screening revealed that the agitation speed (in the chosen range) did not impact the cell growth or metabolic uptake rates significantly. To avoid intensive foaming, observed for high agitation speeds or high gasing rates (required for low agitation speeds), an intermediate agitation speed of 150 rpm was chosen for subsequent experiments. Interestingly, a glutamine limitation was observed at 72 h post inoculation, likely resulting in a reduced maximum VCC. To potentially increase the maximum achievable VCC, glutamine was supplemented in the following pH screening.

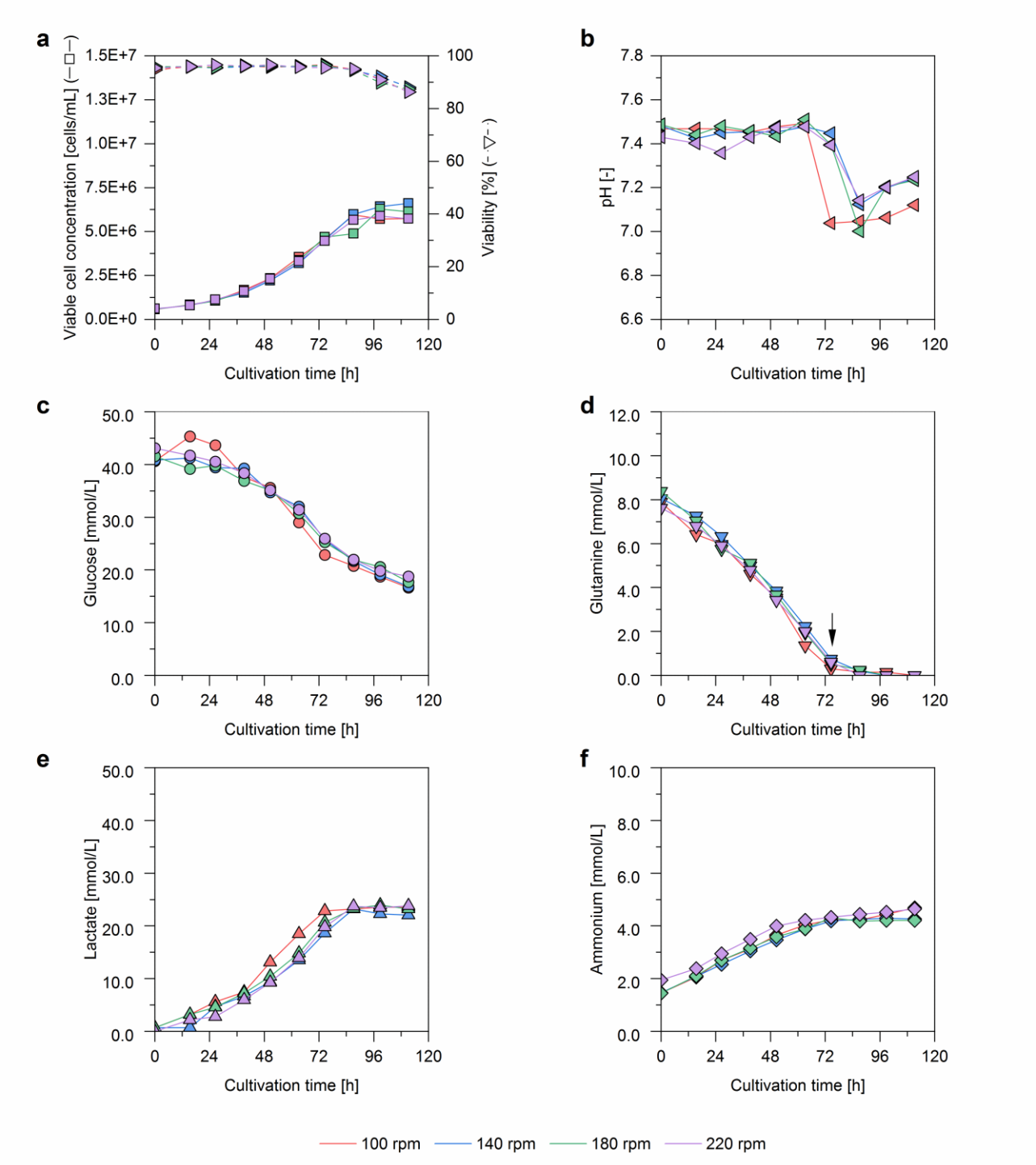

Fig. 4.5 Screening of agitation speeds for MDCK.Xe.E cells grown in a STR. Four STR (500 mL working volume) were inoculated with MDCK.Xe.E cells at a VCC of 1.0E+06 cells/mL and operated with different agitation speeds ranging from 100 rpm to 220 rpm. (a) VCCs and viabilities, (b) pH (setpoint 7.4; controlled by CO_2 addition only), (c) glucose concentrations, (d) glutamine concentrations, (e) lactate concentrations, (f) ammonium concentrations.

Next, the impact of the pH value on the cell growth was investigated. For this, four STRs with a working volume of 500 mL were inoculated with MDCK.Xe.E cells with a VCC of 1.0E+06 cells/mL and operated at different pH ranging from 6.8 to 7.4. The pH was controlled by addition of CO_2 or 7.5% $NaHCO_3$ solution. Additionally a shake flask cultivation was conducted in parallel for comparison.

The pH drastically impacted the cell growth (Fig. 4.6a). For cultivations with a pH setpoint of 6.8 and 7.0 almost no cell growth was observed and these are therefore not discussed in detail in the following. The highest specific growth rate in an STR was observed with a pH of 7.4. However, cells grown in shake flask grew faster and achieved higher maximum VCCs. The initial pH in the shake flask was 7.6, but decreased over the process time to 7.2 (Fig. 4.6). While it is possible that a pH higher than 7.4 (e.g. 7.6) would result in an improved cell growth in the STR, this possibility was not further investigated, as it would require the addition of large amounts of base to maintain such a high pH, especially for HCD cultivations.

The metabolite uptake rates for the cultivation with a pH of 7.4 were slightly reduced compared to previous cultivations (Fig. 4.5) and consequentially higher substrate levels were observed (Fig. 4.6c and d). This might be explained by biological variance. At 72 h post inoculation, glutamine was added to STR cultivations operated at pH 7.2 and 7.4, as well as to the shake flask to achieve a final concentration of approximately 10 mmol/L (initial concentration in the medium). Thus, a glutamine limitation was avoided (Fig. 4.6d) and higher maximum cell concentrations of up to 8.9E+06 cells/mL (compared to approximately 6.0E+06 cells/mL without glutamine supplementation) were observed (Fig. 4.6a). On the other hand, the glutamine addition resulted in a drastic increase of the release of ammonium, and concentrations above 7.0 mmol/L could be measured in the STRs (Fig. 4.6f). Such high concentrations would affect virus infection, as it is well known that high ammonium concentrations inhibit IAV replication (Eaton and Scala 1961). Therefore, the removal of ammonium appears to be indispensable for HCD cultivations. The maximum lactate concentration was very comparable to previous cultivations, when cells were cultivated at a pH of 7.4 (Fig. 4.6e). Surprisingly, the maximum lactate concentration for the shake flask cultivation was lower. This might be explained by higher shear stress in the bioreactor system. Previously, an increased lactate dehydrogenase activity was reported for Chinese hamster ovary cells exposed to shear stress (Shiragami and Unno 1994).

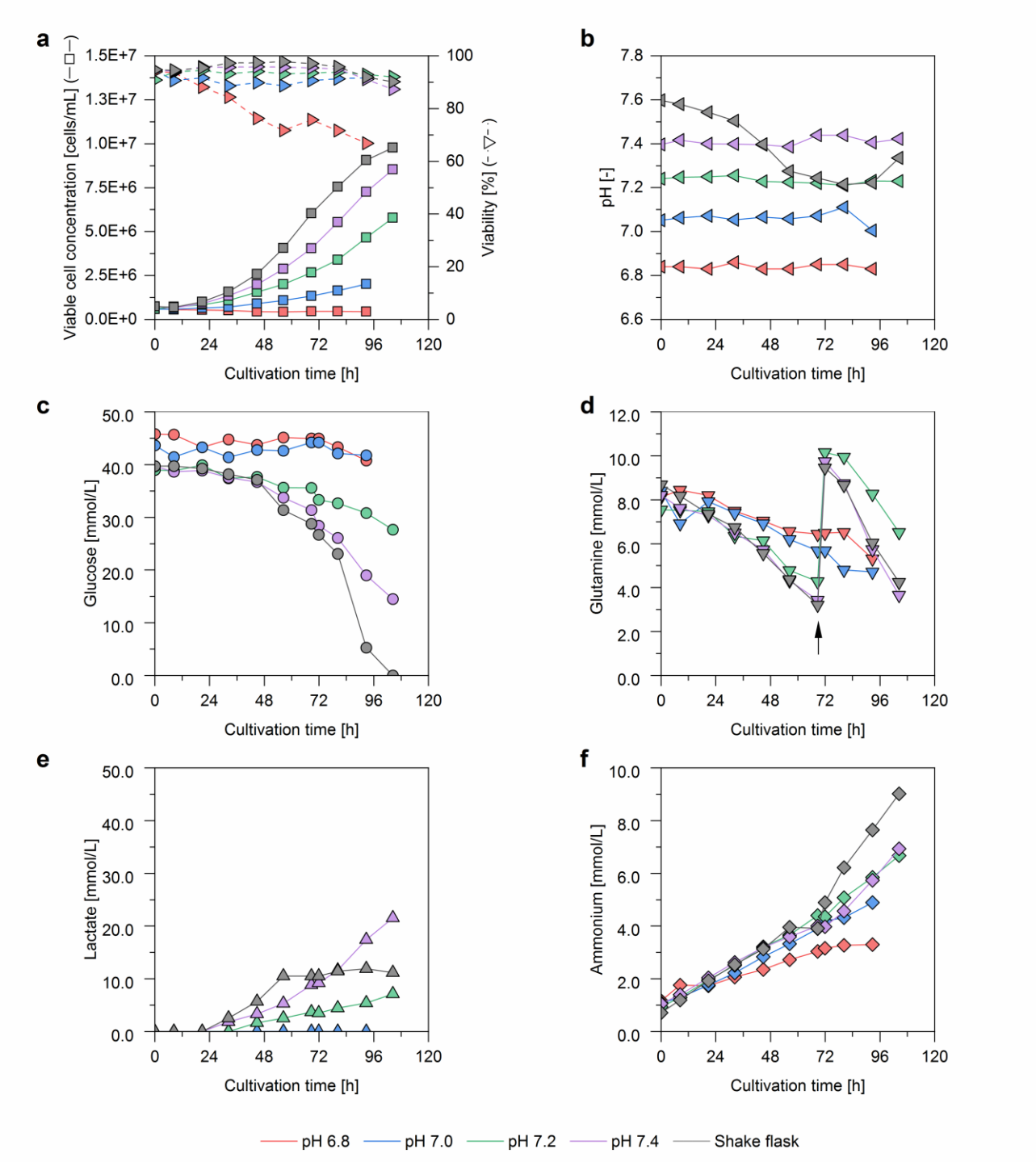

Fig. 4.6 Screening of pH setpoints for MDCK.Xe.E cells grown in a STR. Four STR (500 mL working volume) were inoculated with MDCK.Xe.E cells at a VCC of 1.0E+06 cells/mL and operated with different pH setpoints ranging from 6.8 to 7.4 (controlled by CO_2 and base addition). (a) VCCs and viabilities, (b) pH, (c) glucose concentrations, (d) glutamine concentrations, (e) lactate concentrations, (f) ammonium concentrations. The black arrow indicates time of glutamine addition to shake flask and STR operated at pH 7.2 and 7.4 (final concentration 10 mmol/L).

In summary, the MDCK.Xe.E cell line showed good cell growth in the STR with VCCs up to 8.9E+06 cells/mL and, therefore, has a great potential for HCD cultivations. The optimal agitation speed and pH setpoint (in the tested range) were 150 rpm and 7.4, respectively. These process parameter were used for subsequent infection experiments in the STR.

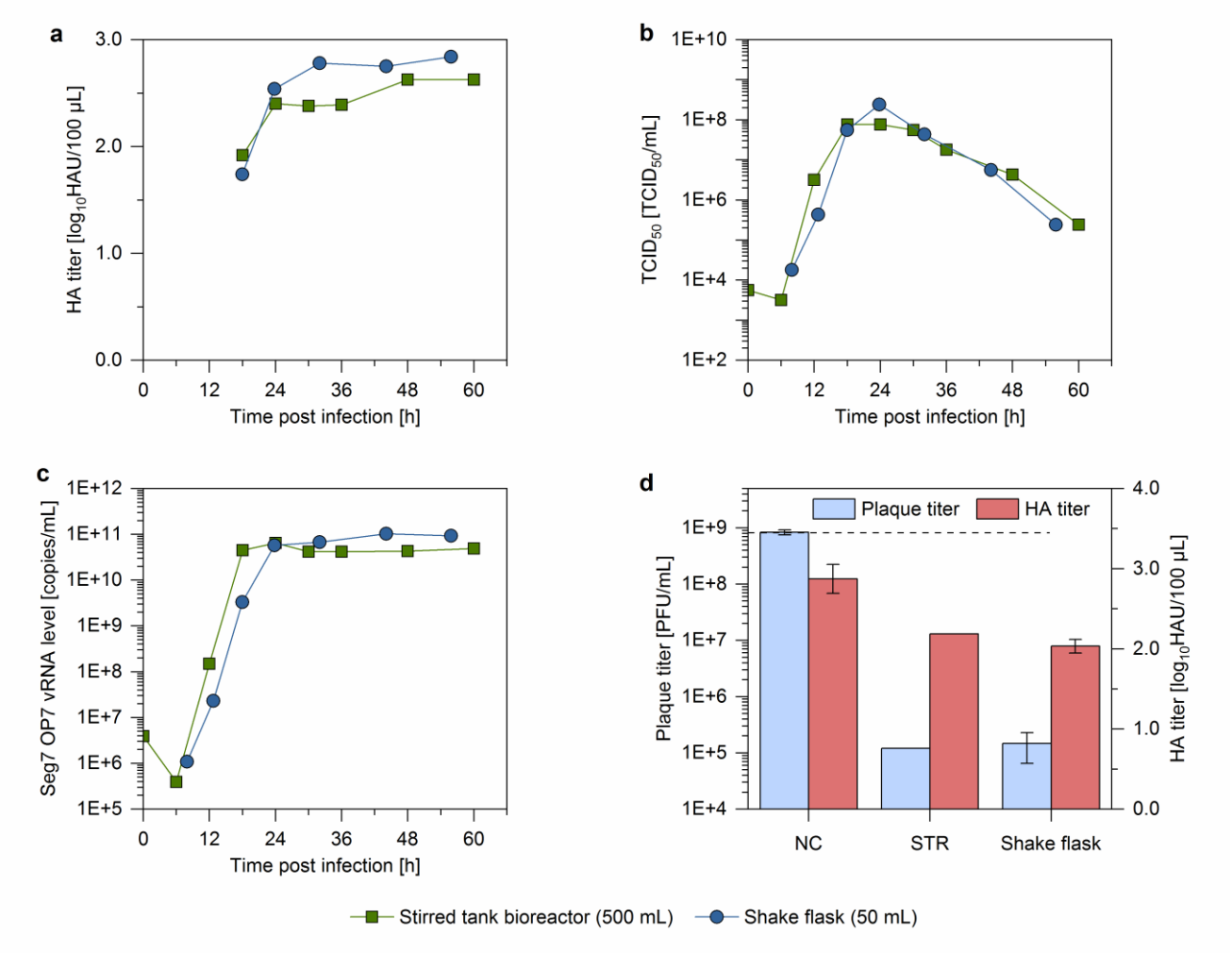

Fig. 4.7 Comparison of OP7 production in a STR and a shake flask. A STR (500 mL working volume) was inoculated with MDCK.Xe.E cells at a VCC of 2E+6 cells/mL and infected with OP7 seed virus at MOI 1E-2. For comparison, OP7 production at the same VCC and MOI in a shake flask and corresponding interfering efficacy (data from Fig. 4.1 and Fig. 4.2) is shown. (a) HA titers, (b) $TCID_{50}$ titers, (c) OP7 vRNA levels. (d) Interference assay. MDCK(adh) cells were infected at MOI 10 with STVs and co-infected with 125 µL of OP7 material, harvested at 32 hpi. Medium was tested as negative control (NC). (a, b, c) Illustrations include results of one experiment. (d) The interference assay was performed in independent experiments (NC and Shake flask n=3, STR n=1) using one OP7 production sample. Error bars indicate one standard deviation.

In order to investigate the scalability of the production process of OP7, shake flask (50 mL) production conditions were reproduced in bioreactor scale (500 mL). For this, the STR was inoculated with 2.0E+06 cells/mL and immediately infected with OP7 seed virus at MOI 1E–2. Despite the different production systems, very comparable replication dynamics and maximum virus titers were observed (Fig. 4.7a–c). Additionally, almost identical titer reductions were observed in the interference assay for OP7 produced in shake flask and STR. Afterwards, OP7 material produced in the STR was tested for its antiviral activity against SARS-CoV-2 (Rand et al. 2021). Here, the replication of SARS-CoV-2 *in vitro* was completely abolished upon co-infection with the produced OP7.

4.1.4 Discussion

A cell culture-based production process for OP7 material was established. First, the impact of the MOI on the interfering efficacy of the produced material was investigated in shake flasks. Here, an optimal production MOI of 1E–2 was determined. Next, an UV-irradiation procedure for OP7 material was established to inactivate potentially harmful STVs in the harvests. Finally, the production process was scaled up from shake flask to a laboratory-scale STR and very comparable results regarding cell growth, virus replication, and interfering efficacy of the produced material were observed.

Identification of the production conditions yielding a high interfering efficacy

First, the impact of the applied MOI, the harvest time, and the VCC at time of infection on OP7 yield was investigated in shake flasks. The interfering efficacy of material harvested at different time points or produced with different VCCs at time of infection did not show any significant differences (Fig. A1 − Fig. A5). However, as previous works suggested, the MOI had a large impact on the yield (Dimmock et al. 2008; Frensing 2015; Tapia et al. 2019; Wasik et al. 2018). The highest interfering efficacy was observed for material produced at MOI 1E−2. This can be explained as follows. On the one hand, the yield of Seg7 OP7 vRNA was very similar for production MOI 1E−2 and 1E−3, however, the production MOI 1E−3 resulted in a higher infectious STV titers. Here, the higher STV concentrations may have resulted in a reduced interfering efficacy in this sample, probably by a

stronger competition of STVs against OP7. As different vRNA segments compete for resources in translation, increased amounts of STV vRNA may have also had a negative impact on the amounts of produced M1-OP7. More specifically, MS measurements indicated reduced amounts of M1-OP7 for virions produced at MOI 1E−3 compared to those produced at MOI 1E-2. Here, it was speculated that M1-OP7 may also contribute to the interference of OP7 (Kupke et al. 2019), which could be an additional explanation for the lower interfering efficacy for material produced at MOI 1E-3.

Comparison of cell culture-based production processes for DIPs

The cell culture-based batch production process suggested here has advantages over a previously reported egg-based process for DIPs (Dimmock et al. 2008). The cell culture-based process allows for an improved scalability and flexibility. Furthermore, it allows for better defined process conditions and the possibility to monitor the cultivations. Therefore, the production process can be characterized in-depth and reproducible product quality can be ensured (Frensing et al. 2014; Swick et al. 2014; Tapia et al. 2019; Wasik et al. 2018). Previously, a cell culture-based process for continuous production of DIPs was reported (Frensing et al. 2013; Tapia et al. 2019). However, a batch process may hold several advantages. For example, the reproducibility and product quality are higher for a batch process. For instance, in continuous cultivations, the *de novo* generation and accumulation of conventional DI vRNAs was observed (Frensing et al. 2013; Tapia et al. 2019). This resulted in a mixture of a variety of DIPs and thus, a less-defined product. In contrast, no accumulation of conventional DI vRNAs was observed in the batch cultivations for any genome segment, probably due to a shorter cultivation time and a lower MOI (Fig. 4.3). Moreover, an oscillating titers and fluctuating DIP to STV ratios were observed in continuous cultivations (Frensing et al. 2013; Tapia et al. 2019), which might complicate the selection of an optimal harvest time point. In contrast, the batch process shown here resulted in very reproducible titers (Fig. 4.7 and Table 4.1).

The results obtained in this proof-of-concept study should facilitate further process improvements. The high comparability of a production in shake flasks and a STR indicates that production in larger scales is equally feasible. Furthermore, process intensification strategies could be applied similar to those that have already been widely explored for production of monoclonal antibodies in CHO cells (Pollock et al. 2013) or the production of flaviviruses (Nikolay et al. 2018). Please note that those process intensification strategies were explored in the section 4.2 for production of DI244 in the genetically modified MDCK-PB2(sus) cell line.

UV-irradiation for inactivation of STVs in OP7 manufacturing

For the inactivation of STVs in the produced material, a previously described UV-irradiation principle was applied (Dimmock et al. 2008). The UV-irradiation introduces photodimeric lesions (Remsen et al. 1970) or unspecific chain breaks (Coahran et al. 1962; Jericevic et al. 1982) in the vRNA. Here, a faster inactivation of STVs compared to DIPs was expected (Dimmock et al. 2008). In theory, a STV already loses its infectivity when only one segment is inactivated, while OP7 only loses its interfering efficacy when specifically Seg7 OP7 is inactivated. Moreover, Seg7 is rather small (~1 kb) compared to e.g., Seg1, Seg2 and Seg3 with more than 2 kb, decreasing the likelihood of its inactivation. Nevertheless, the UV-irradiation inactivated parts of the produced OP7 and resulted in a reduced interfering efficacy (Fig. 4.4). One approach to avoid the need of UV-irradiation may be the production of pure OP7 particles using a cell line that complements the defect in replication of OP7. Such a production system was already successfully developed for the propagation of the conventional DIP DI244, carrying a deletion on Seg1 vRNA. Here, a complementing cell line expressing the corresponding missing protein (PB2) and a purely clonal DI244 seed virus, generated by reverse genetics were utilized (Bdeir et al. 2019; Yamagata et al. 2019). This production system was further investigated in the present PhD work (section 4.2). A similar strategy might be used for the production of OP7, for example, by using a cell line expressing the wild-type M1 and/or M2 protein.

4.1.5 Subsequent experiments with produced OP7 material

The OP7 material produced in the context of this PhD work with the established cell culture-based process was used by colleagues or collaboration partners for subsequent experiments to investigate (i) the feasibility of virus purification methods (Hein et al. 2021c), (ii) the antiviral efficacy in animal experiments (mice) (Hein et al. 2021c), and (iii) the interfering efficacy against SARS-CoV-2 in vitro (Rand et al. 2021).

UV-irradiated OP7 material was purified and concentrated by membrane-based steric exclusion chromatography (SXC) (Marichal-Gallardo et al. 2021; Marichal-Gallardo et al. 2017). Here, two main peaks (80–95 nm) were detected by differential centrifugation sedimentation analysis of the SXC-purified sample, which were consistent with the reported size range for IAV particles of 80–120 nm (Pieler et al. 2017). The difference between both peaks might be due to previously observed size differences between STVs and OP7 (Kupke et al. 2019). The potential separation of STVs and

OP7 by SXC could be an interesting objective of future research. Further, SXC-purification was able to eliminate most UV-detected impurities as evidenced by analytical size exclusion chromatography fingerprints. Before SXC, the virus peak had an estimated purity of 2.7%, compared to 89.1% after SXC. Further, the SXC purification resulted in an approximately 13-fold increased concentration and consequentially a greatly improved interfering efficacy (Hein et al. 2021c).

Studies in a mouse infection model to evaluate the antiviral efficacy of OP7 material *in vivo* were performed by a collaboration partner (IG group at the HZI). The tested material was cell culture-derived unpurified OP7 produced in shake flasks, UV-inactivated for 8 min. Although the material tested in animal experiments was unpurified (cell culture supernatants may contain high amounts of impurities), no toxic or pathogenic effects could be observed upon OP7 administration to mice. Further, mice infected with an otherwise lethal dose of IAV showed no body weight loss and all mice survived the infection, when treated with OP7. This clearly demonstrated the antiviral potential of OP7 (Hein et al. 2021c).

Lastly, the antiviral efficacy of produced OP7 against SARS-CoV-2 was investigated by a collaboration partner (Department of Vaccinology and Applied Microbiology (VAM) at the Helmholtz Centre for Infection Research (HZI), Germany). Calu-3 cells were co-infected with SARS-CoV-2 STVs and SXC-purified OP7 produced in a STR. Depending on the applied amount of OP7 it was possible to completely abolish SARS-CoV-2 replication. Here, it was hypothesized that an unspecific stimulation of the innate immune response by IAV DIP co-infection was a major cause of the antiviral effect. This study suggested that IAV DIP treatment might also confer protection against a variety of other heterologous interferon-sensitive viruses (Rand et al. 2021). This would be in line with previous claims, where IAV DIP administration protected mice against a lethal dose of non-homologous influenza B virus and pneumovirus (Dimmock and Easton 2015; Easton et al. 2011; Scott et al. 2011). However, while these experiments emphasize the importance of the innate immune response it cannot solely explain the antiviral effects of IAV DIPs. More specifically, the *in vitro* interference assay used in this PhD work was carried out with adherent MDCK cells, which express a canine MX1 lacking activity against the human IAV strain PR8 (Seitz et al. 2010). Furthermore, trypsin added to the medium used in the interference assay degrades the secreted interferon (Seitz et al. 2012). Therefore, the interfering effects against IAV observed in the assay are most likely explained by DIPs interfering with the replication of the STVs, rather than induction of the innate immune response. In order to better understand the contribution of the innate immune response to the

interference of DIPs *in vitro*, additional experiments are necessary. For example, the interference assay could be carried out with a human cell line carrying a functional MX1 (e.g. A549 or HEK293 cells). Additionally, to avoid interferon degradation by trypsin, the virus strain A/WSN/33, which does not rely on trypsin addition for its propagation (Goto and Kawaoka 1998) could be used.

4.2 Establishment of a production process for DI244

Note, that major parts of the original research articles from Hein *et al.* in *BMC Biology* and *Applied Microbiology and Biotechnology* were used in this section (Hein et al. 2021a; Hein et al. 2021b). As DIP replication usually depends on STV co-infection, both the egg-derived and the cell culture-based produced IAV DIP material has so far always been a mixture of DIPs and infectious STVs (Dimmock and Easton 2015; Hein et al. 2021c). Moreover, to eliminate potentially harmful STVs in therapy, it was inactivated by UV-irradiation, as done for OP7 material. Yet, this also inactivated at least parts of the produced DIPs and consequently reduced their interfering efficacy (Dimmock et al. 2008; Hein et al. 2021c), as shown in section 4.1.2. Previously, methods for production of purely clonal DIP populations, overcoming the need of STV inactivation have been described (Bdeir et al. 2019; Yamagata et al. 2019). These were based on genetically modified adherent cell lines expressing the viral PB2 encoded by IAV Seg1 vRNA and purely clonal DIP preparations without STV contaminations, generated by reverse genetics.

For the development of a manufacturing process for pure DI244 particles it was desirable to switch to a suspension cell line, as this facilitates the implementation of process intensification strategies. Therefore, a collaboration partner (IB unit at the DPZ) genetically modified our MDCK.Xe.E cell line (Bissinger 2020) to express the viral PB2 (MDCK-PB2(sus)). In the present PhD work, this suspension cell line was used for the establishment of a production process for purely clonal DI244. Shake flask experiments demonstrated that the resulting DI244 yield and the interfering efficacy of the produced material depended on the MODIP applied for infection (section 4.2.1). After scale-up to a STR (section 4.2.2), process intensification strategies were applied to further improve the production process. First, a perfusion process utilizing an ATF system with a standard hollow fiber membrane was established to grow MDCK-PB2(sus) cells to HCD. The perfusion rate was adjusted manually every 12 hours (section 3.4.2). In a next step, the perfusion rate was controlled based on cell concentration measurements using a capacitance probe (section 4.2.4). Lastly, a tubular membrane called VHU was evaluated for its potential to allow a continuous virus harvesting into the permeate during the perfusion process (section 4.2.4).

4.2.1 MODIP screening for DI244 production

Before optimal DIP production was investigated, the growth of MDCK-PB2(sus) and the parental MDCK.Xe.E cells was compared and no significant difference was observed. Next, the impact of the MODIP on DI244 yield was investigated. While earlier DI244 release can be expected for higher MODIPs, infections with higher virus concentrations can result in a strong accumulation of other DI vRNAs (Frensing et al. 2014), which would contaminate the DI244 product. Therefore, four MODIPs ranging from 1E−1 to 1E−4 were tested. For process monitoring, the HA assay, real-time RT-qPCR and plaque assay (DI244 titer) were used. The MODIP screening revealed that the HA and DI244 titer reached their respective maximum value earlier for higher MODIPs (Fig. 4.8a and b). In line with this, the VCC decreased faster for higher MODIPs (Fig. 4.8c). Maximum HA (2.62–2.65 $\log_{10}$HAU/100 µL) and DI244 titers (4.80E+7–1.08E+8 PFU/mL) were comparable for all MODIPs, except for MODIP 1E−1 with slightly lower titers. For each MODIP, a decrease in DI244 titer (PFU/mL) was observed after the respective maximum was reached (Fig. 4.8b). This corresponded to previous findings regarding the decrease of infectious virus titers over cultivation time for wild-type IAV (Genzel et al. 2010), and was observed for OP7 production in section 4.1.1 as well. In this context, to obtain maximum interfering efficacies from biologically active DI244, material was harvested at maximum DI244 plaque titers. In addition, vRNA levels of Seg5, Seg8 and DI244 of the produced virus particles were quantified using real-time RT-qPCR. Surprisingly, maximum DI244 vRNA levels differed strongly for the different MODIPs with highest concentrations achieved for MODIPs 1E-1 and 1E-2 (Fig. 4.8). In contrast, maximum vRNA levels of Seg5 and Seg8 were very comparable for all conditions. DI244 titers, HA titers, and DI244 vRNA levels for the different MODIPs at their respective harvest time are shown in Table 4.2 (production replicate 1).

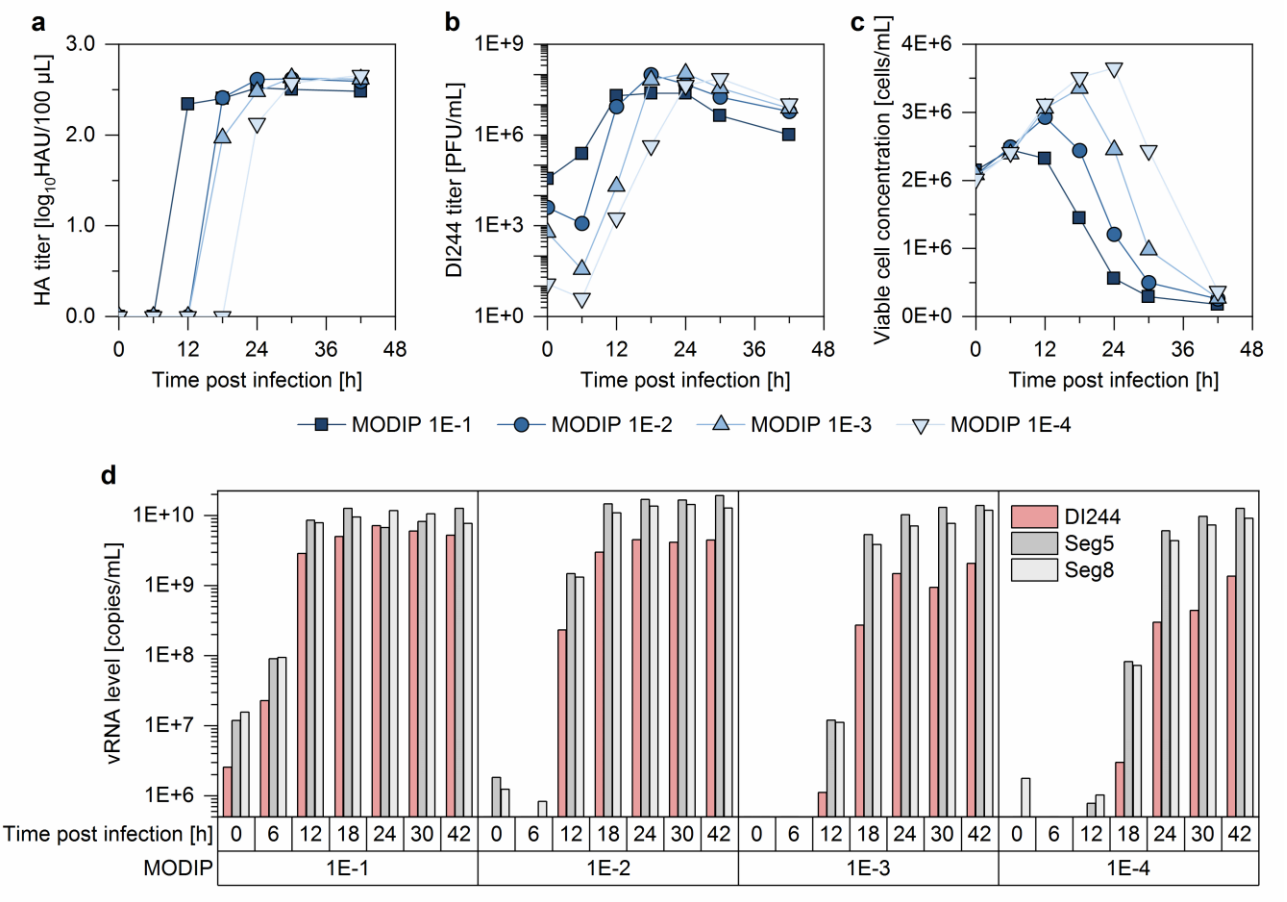

Fig. 4.8 MODIP screening for production of DI244. MDCK-PB2(sus) cells were cultivated in shake flasks (50 mL working volume) and infected at a VCC of 2.0E+6 cells/mL with a purely clonal DI244 seed virus at MODIPs ranging from 1E−1 to 1E−4. (a) HA titers, (b) DI244 titers (plaque assay in MDCK-PB2(adh) cells), (c) VCCs, and (d) vRNA levels of DI244, Seg5, and Seg8.

To control the contamination of the harvested material by defective vRNAs other than DI244 vRNA, a segment-specific RT-PCR was performed (Fig. 4.9). However, no apparent signals indicating deleted vRNAs other than DI244 (Seg1) were observed for any MODIP on any segment.

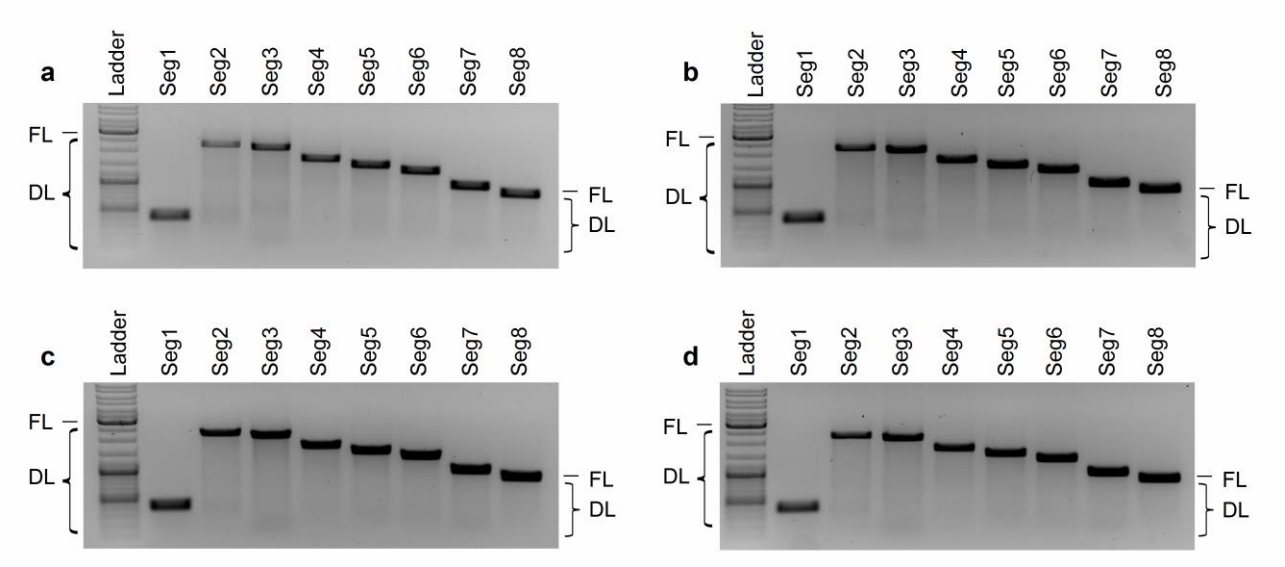

Fig. 4.9 Segment-specific RT-PCR of DI244 material. DI244 material produced at different MODIPs was analyzed for the presence of short vRNAs in Seg1–8. Results for (a) MODIP 1E−1, (b) MODIP 1E−2, (c) MODIP 1E−3 and (d) MODIP 1E−4 are shown. Signals corresponding to full-length (FL) and deleted (DL) vRNAs are indicated (FL size depends on the analyzed vRNA segment). Ladder: upper thick band 3.0 kb, middle thick band 1.0 kb, lower thick band 0.5 kb.

To determine production conditions resulting in material with a high biological efficacy, the *in vitro* interference assay was utilized (Fig. 4.10). The DI244 titers, HA titers, and DI244 vRNA levels for the different DI244 preparations investigated in the interference assay are shown in Table 4.2 (production replicate 2). When STVs were added at MOI 10, addition of DI244 material of any MODIP resulted in a plaque titer reduction of roughly one order of magnitude ($p < 0.01$, unpaired two-tailed t-test). For cells co-infected with STVs at MOI 0.01, larger differences between treated and untreated cells were observed ($p < 0.05$). Here, DI244 material produced at a MODIP of 1E−2 resulted in a reduction in the release of infectious STVs by more than three orders of magnitude. DI244 material produced at the other MODIPs reduced the release of STVs only by less than three (MODIPs 1E−1 and 1E−3) or less than two orders of magnitude (MODIP 1E−4). The difference between MODIP 1E−2 and 1E−1 was significant ($p < 0.01$), the difference between MODIP 1E−2 and 1E−3 was not significant ($p = 0.12$). HA titers of samples from the interference assay showed the same trend as plaque titers. However, this reduction appeared to be less pronounced, most likely as the release of replication deficient DI244 particles themselves also contributed to the HA titer.

Table 4.2 Virus quantification of different DI244 preparations produced at different MODIPs

Assay	DI244 preparation	Production replicate 1	Production replicate 2
HA assay (log10 HA units/100 µL)	MODIP 1E-1 (18 hpi)	2.40	2.28
	MODIP 1E-2 (18 hpi)	2.41	2.31
	MODIP 1E-3 (24 hpi)	2.48	2.42
	MODIP 1E-4 (30 hpi)	2.57	2.50
DI244 titer (PFU/mL)	MODIP 1E-1 (18 hpi)	2.0E+7	2.5E+7
	MODIP 1E-2 (18 hpi)	1.0E+8	8.0E+7
	MODIP 1E-3 (24 hpi)	1.1E+8	7.6E+7
	MODIP 1E-4 (30 hpi)	7.4E+7	6.0E+7
Real-time RT-qPCR (DI244 vRNA copies/mL)	MODIP 1E-1 (18 hpi)	5.0E+9	7.7E+9
	MODIP 1E-2 (18 hpi)	3.0E+9	5.4E+9
	MODIP 1E-3 (24 hpi)	1.5E+9	1.2E+9
	MODIP 1E-4 (30 hpi)	4.4E+8	3.6E+8

With STVs added at MOI 10 and addition of different DI244 preparations, all samples showed comparable vRNA levels for Seg5 and Seg8 in the interference assay (Fig. 4.10b). In contrast, for cells infected at MOI 0.01, strong differences for Seg5 and Seg8 vRNA levels were detected for different DI244 preparations. Here, vRNA levels correlated with the virus titers. For all samples (STV MOIs 10 and 0.01), the vRNA levels of Seg5 and Seg8 were equimolar. In contrast, a lower DI244 vRNA level compared to Seg5 and Seg8 vRNA was observed for the two lowest production MODIPs. This is most pronounced for cells infected with STVs at MOI 10 treated with DI244 produced at MODIP 1E−4, where DI244 vRNA and Seg5 vRNA differ by almost one order of magnitude ($p < 0.005$). As the segment-specific RT-PCR did not indicate accumulation of other vRNAs with a deletion (Fig. 4.9), the interfering effects were solely caused by DI244.

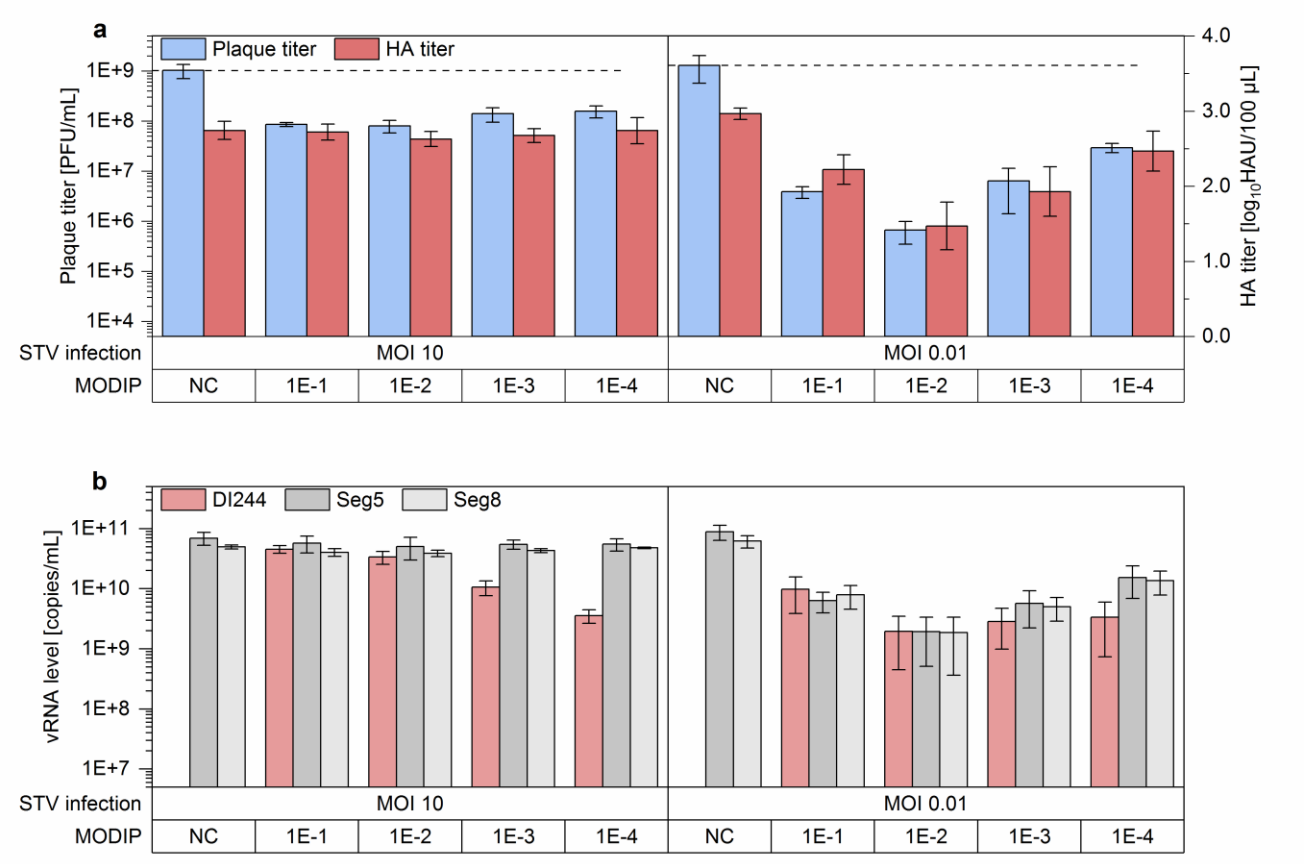

Fig. 4.10 Interfering efficacy of DI244 material produced at different MODIPs. For the interference assay, parental MDCK(adh) cells were infected with STV at MOIs of 10, or 0.01 and co-infected with DI244 material (125 µL), produced at a MODIP ranging from 1E−1 to 1E−4, or medium as negative control (NC). The supernatant was sampled 16 hpi (STV MOI 10) or 24 hpi (STV MOI 0.01). (a) Infectious virus titers were quantified by plaque assay (parental MDCK(adh) cell). The total amount of virus particles was determined by HA assay. (B) vRNA of DI244, Seg5, and Seg8 were investigated using real-time RT-qPCR. The interference assay was performed in independent experiments (n = 3) using one DIP preparation (production replicate 2) for each MODIP; error bars indicate one standard deviation.

In summary, the MODIP affected the DI244 production dynamics with earlier accumulation of DIPs at higher MODIPs. All MODIPs resulted in relatively comparable maximum HA and plaque titers. In contrast, vRNA levels of DI244 differed strongly, with lower quantities at lower production MODIPs. Analysis by segment-specific reverse transcriptase-PCR did not indicate the unwanted accumulation of other vRNAs with deletions, suggesting a clean product. Further, DI244 material produced at different MODIPs showed differences in their interfering efficacies. Here, material produced at a MODIP of 1E−2 showed the highest activity.

4.2.2 DI244 production in a STR batch cultivation

In a next step, production of DI244 material in a STR (500 mL) was investigated (Fig. 4.11). For the process parameters agitation, pH, dissolved oxygen, and temperature, the same setpoints were chosen as previously determined for the parental MDCK.Xe.E cell line (section 4.1.3; 150 rpm, pH 7.4, DO 40%, 37°C). To allow for a comparison with shake flask cultivations, the STR was equally inoculated with a VCC 2E+6 cells/mL. After the DO and pH had stabilized, cells were infected with DI244 at a MODIP of 1E−2 (which resulted in the highest interfering efficacy for the shake flask cultivation (Fig. 4.10)).

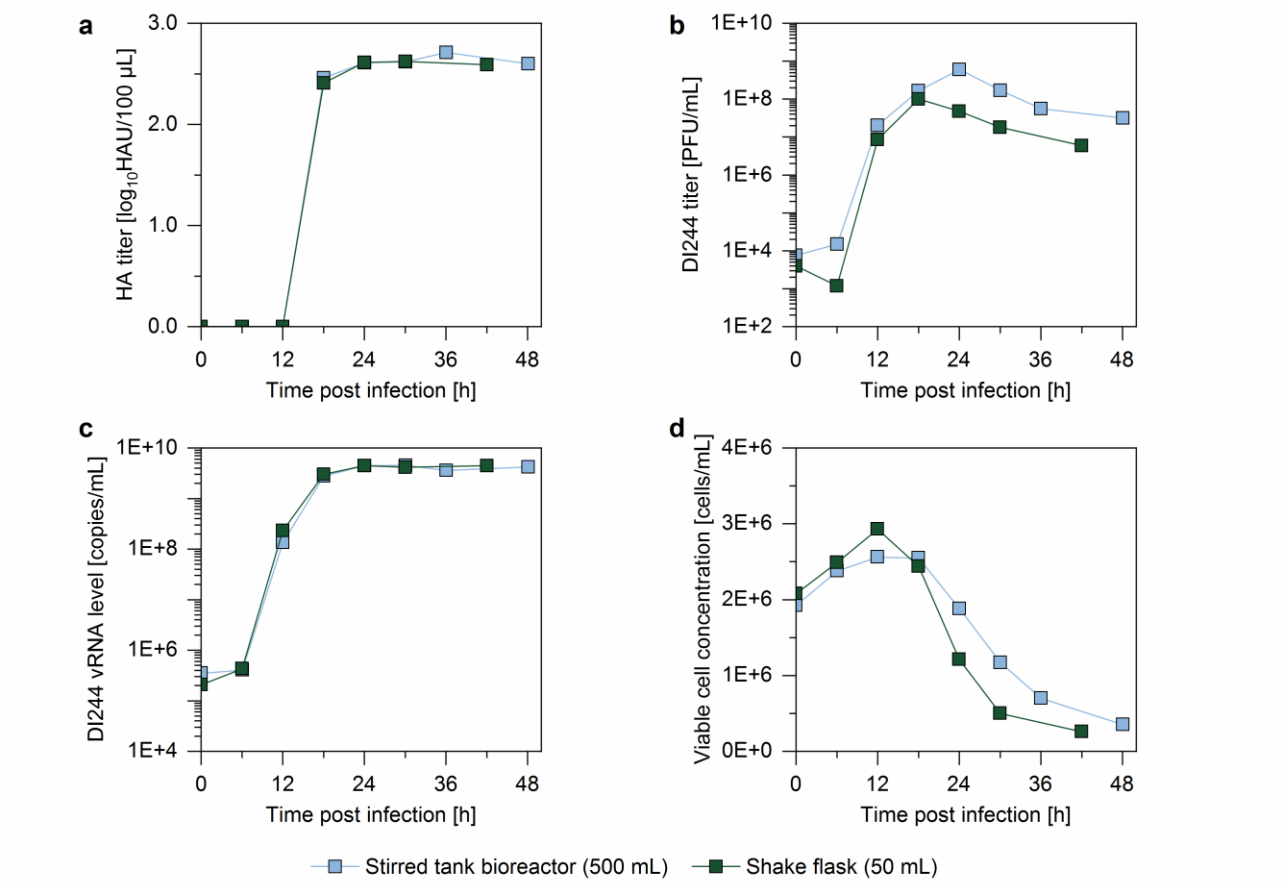

Fig. 4.11 Comparison of DI244 production in a STR and a shake flask. A STR (working volume 500 mL) was inoculated with MDCK-PB2(sus) at a VCC of 2E+6 cells/mL. Cells were infected with purely clonal DI244 seed virus at MODIP 1E−2. (a) HA titers, (b) DI244 titers, (c) DI244 vRNA levels, (d) VCCs. For comparison, DI244 production in a shake flask (see also Fig. 4.8) is shown.

Despite the different production scales, aeration conditions and pH control, very comparable results were achieved for the dynamics in the HA titers and DI244 vRNA levels (Fig. 4.11a and c) with only minor differences for the DI244 titer and the VCC (Fig. 4.11b and d). Here, the shake flask cultivation showed a slightly delayed increase in DI244 titer (Fig. 4.11b) and an earlier decrease in the VCC (Fig. 4.11d) compared to the STR. The observed differences might be explained by the improved control of the cultivation conditions in the STR. More specifically, the pH decreased in the shake flask upon infection, potentially leading to faster cell death and increased virus degradation. In contrast, the pH was kept constant at 7.4 in the STR (controlled by CO_2 and base addition). The DI244 material produced in the STR was then analyzed in the interference assay. Again, a highly similar interfering efficacy was observed compared to DI244 material produced in the shake flask (Fig. 4.12).

In summary, only small differences between a shake flask and a STR cultivation for DI244 production were observed, and large-scale manufacturing of DIPs in STR seems a promising option for future application in antiviral therapy.

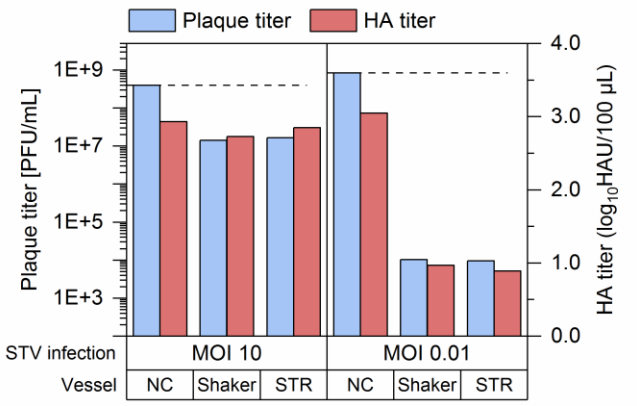

Fig. 4.12 Interfering efficacy of DI244 material produced at MODIP 1E−2 in different cultivation scales. For the interference assay, parental MDCK(adh) cells were infected with STVs at MOI 10, or 0.01 and co-infected with DI244 material (125 µL) or medium as negative control (NC). The supernatant was sampled 16 hpi (STV MOI 10) or 24 hpi (STV MOI 0.01). Infectious virus titers were quantified by plaque assay (MDCK(adh) cells). The total amount of virus particles was determined by HA assay. The interference assay was performed in a single experiment using a preparation of DI244 produced with MODIP 1E−2 either in shake flask (Fig. 4.8; Table 4.2 (production replicate 1)) or in STR (Fig. 4.11).

4.2.3 Establishment of a perfusion process for MDCK-PB2(sus) cells

To evaluate if process intensification strategies that were already used for suspension MDCK cells and IAV STV production (Wu et al. 2021) would be applicable for production of pure DI244 particles, a manually adjusted perfusion process in a STR was implemented (HFM1). For this cultivation, the perfusion rate was adjusted every 12 h, according to a pre-calculated profile (RV exchange regime). The profile was based on the cell-specific growth rate and metabolite uptake rates of the parental MDCK.Xe.E cell line (Fig. 4.6, pH 7.4). Here, it was expected that the MDCK-PB2(sus) cell line would not differ significantly in its metabolic uptake rates from the parental MDCK.Xe.E cell line, as the growth for the two cell lines was shown to be very comparable (Table 4.3). For MDCK.Xe.E cells the cell-specific parameters were calculated in the exponential phase of a previous batch cultivation (Fig. 4.6): μ_{max} 0.0354 1/h (Eq. 1), glucose uptake rate 3.62E–10 mmol/cell/h (Eq. 2), glutamine uptake rate 6.77E–11 mmol/cell/h (Eq. 2). Next, the required perfusion rate was estimated (Eq. 3). Here, it was calculated that a CSPR of 200 pL/cell/day would be sufficient to avoid glucose or glutamine limitations (Eq. 4). According to the estimated perfusion rate a stepwise profile was developed (Fig. 4.13).

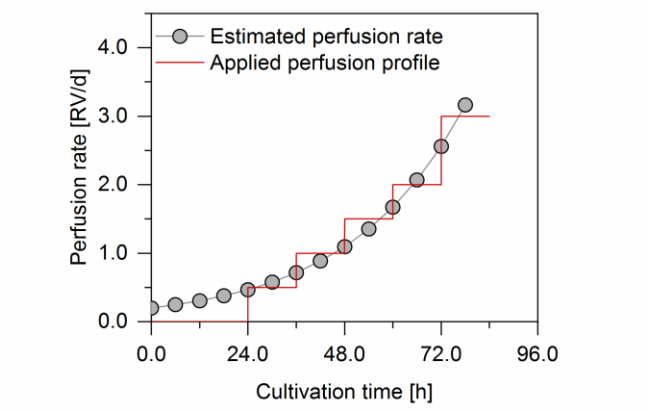

Fig. 4.13 Estimated and manually adjusted perfusion rate for cultivation of MDCK-PB2(sus) cells in a STR (working volume 700 mL; HFM1). For the calculation of the required perfusion rate, the maximum specific growth rate (0.0354 1/h) and the glucose uptake rate (3.62E–10 mmol/cell/h) of MDCK.Xe.E cells cultivated in a batch process were used (Fig. 4.6, pH7.4). Considering the metabolite uptake rates and the glucose concentration in the medium (40 mmol/L), a CSPR of 200 pL/cell/d was calculated. A stepwise perfusion profile was chosen accordingly.

In a next step, a perfusion rate control based on a capacitance probe was established. Here, the signal was correlated to the VCV (Eq. 5) in the STR. For the manually adjusted perfusion cultivation, an average CSPR of 200 pL/cell/d was realized, for the controlled perfusion cultivations a BVSPR of 0.12 pL/µm^3/d was chosen. This would equal a CSPR of 200 pL/cell/d for cells with a diameter of 15 µm. One manually adjusted and three controlled perfusion cultivations were performed in the STR. Moreover, the manually adjusted and one controlled perfusion cultivation were conducted with a commonly used HFM (HFM1 and HFM2). For the following two controlled perfusion cultivations, the VHU was evaluated as a new cell retention membrane (VHU1 and VHU2) to test options for direct harvesting of virus particles through the membrane. Here, similar cell growth was observed for both perfusion rate control strategies and both cell retention membranes, resulting in cell concentrations up to 25.0E+6 cells/mL with viabilities above 95% (Fig. 4.14a). The maximum specific growth rates were very similar to the rate observed for a batch cultivation with MDCK.Xe.E cells (Table 4.3). Further, no membrane fouling or blocking of either membrane was observed, indicating that both membranes are equally suitable for HCD cultivations.

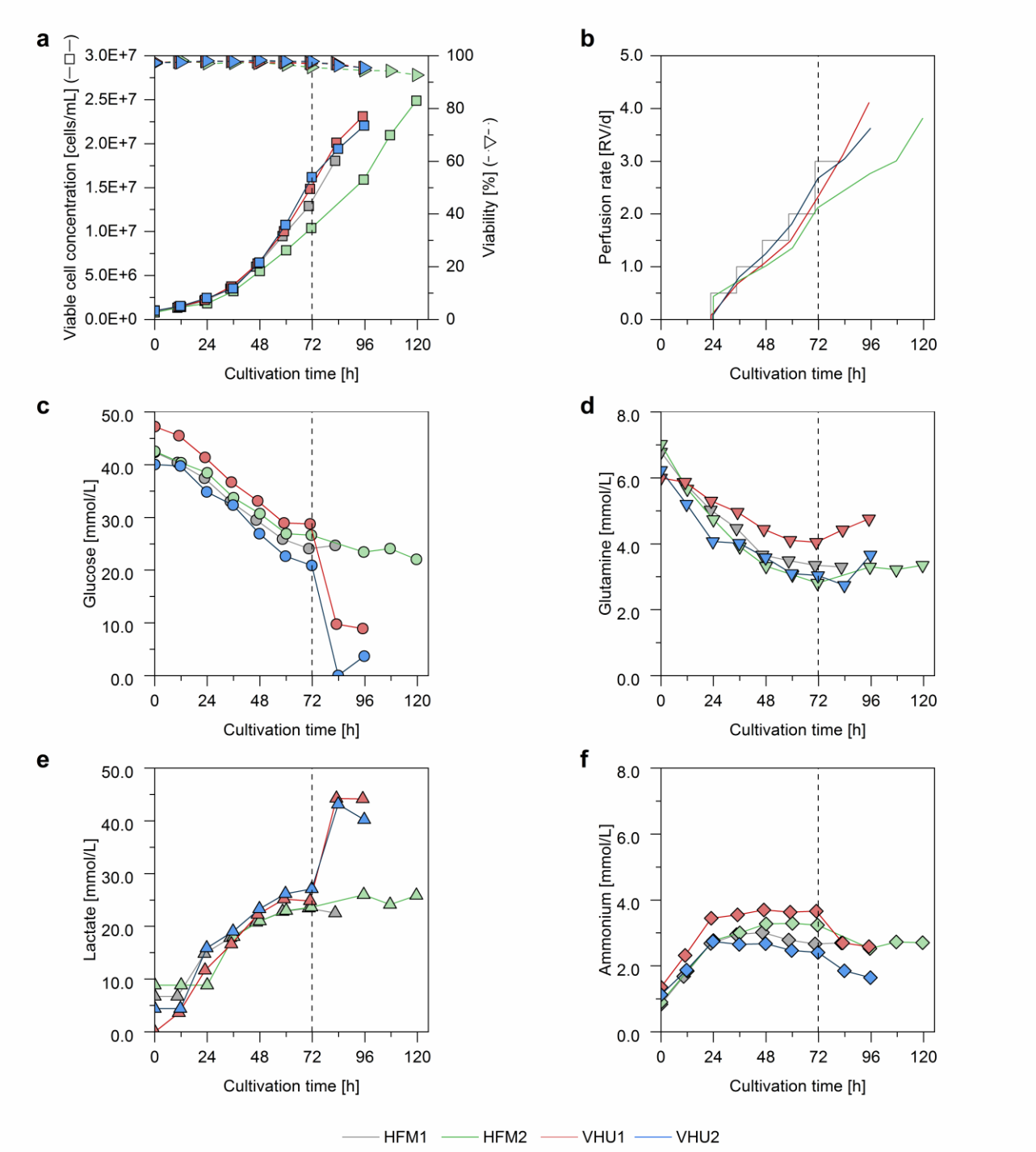

Fig. 4.14 MDCK-PB2(sus) cell cultivations in STRs (working volume 700 mL) coupled to an ATF. The perfusion rate of HFM1 was adjusted manually. The perfusion rates of the other cultivations were controlled based on the VCV in the STR. For HFM2, VHU1 and VHU2, gassing with a micro-sparger was initiated after 72 h (vertical line). (a) VCCs and viabilities, (b) perfusion rate, (c) glucose concentrations, (d) glutamine concentrations, (e) lactate concentrations, and (f) ammonium concentrations.

Table 4.3 Overview of parameters for MDCK-PB2(sus) cells cultivated in a 1 L STR.

	Maximum specific growth rate [1/h]	Glucose uptake rate [mmol/cell/h]	Glutamine uptake rate [mmol/cell/h]
Batch	0.0354	3.62E-10	6.77E-11
HFM1	0.0363	2.37E-10	3.83E-11
HFM2	0.0299	1.61E-10	4.06E-11
VHU1	0.0328	1.99E-10	2.84E-11
VHU2	0.0355	2.30E-10	3.29E-11

For HFM1, HFM2, VHU1, and VHU2, the bioreactor was coupled to an ATF2 system to allow cultivation in perfusion mode. For comparison the maximum specific growth rate and substrate uptake rates of the parental MDCK.Xe.E cell line cultivated in a batch process (Fig. 4.6, pH 7.4) are shown. Rates were determined in exponential cell growth phase.

The controlled perfusion was successfully implemented. The permittivity signal showed a linear correlation with the VCV in the STR (Fig. 4.15) and the perfusion rate increased with increasing VCVs (Fig. 4.14a, b). For all four perfusion cultivations, the metabolite levels were very comparable and no substrate limitation or inhibition by waste products was observed until 72 h post inoculation (Fig. 4.14c–f). The substrate uptake rates were slightly lower than for a previous batch cultivation (Table 4.3). However, the observed substrate concentrations were still in the expected range. For the manually adjusted perfusion cultivation (HFM1), oxygen limitations were observed 84 h post inoculation (data not shown). To circumvent this in the subsequent controllted perfusion cultivations, gassing with an additional micro-sparger was initiated 72 h post inoculation. This did not seem to have an impact on the cell metabolism when the HFM was used (Fig. 4.14c–f). Nevertheless, this cultivation showed a slightly lower specific growth rate, reflected by the perfusion rates of the controlled perfusion cultivations. When the VHU was used, the additional sparging seemed to result in increased glucose uptake and lactate production together with a slight ammonium uptake instead of a release (Fig. 4.14c, e, f). Nevertheless, at this point, differences in cell growth compared to the manually adjusted cultivation seem to be negligible.

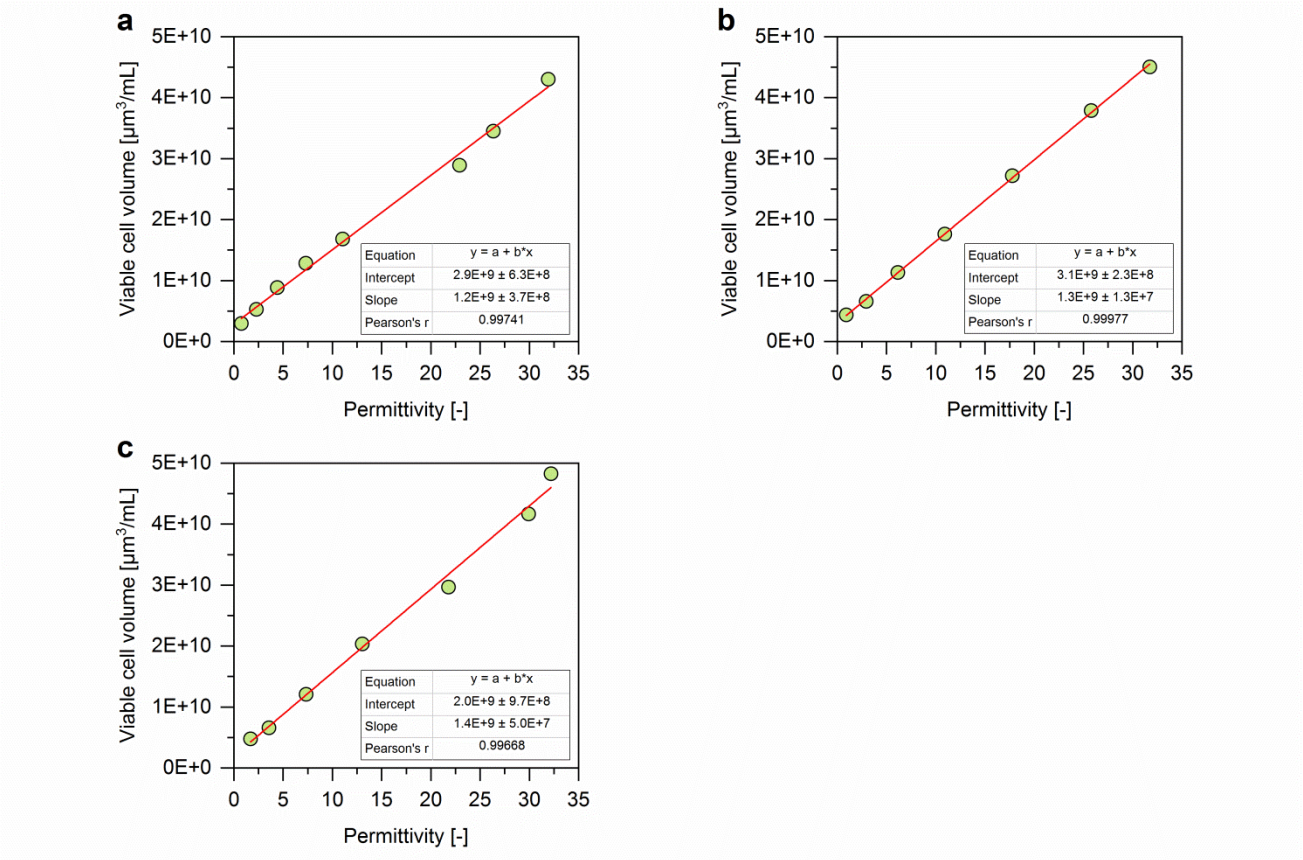

Fig. 4.15 Correlation of permittivity signal and offline measured cell volume. MDCK-PB2(sus) cells were cultivated in a STR (working volume 700 mL) coupled to an ATF. The perfusion rate of the cultivations was controlled using the capacitance probe for cell growth monitoring. (a) HFM2, (b) VHU1, (c) VHU2. For each correlation the equation of the linear regression and the Pearson correlation coefficient are given.

In summary, very comparable cell growth was observed for both cell retention membranes. Further, the control of the perfusion rate could be implemented successfully. The controlled perfusion rate resulted in sufficient metabolite levels, allowing exponential cell growth up to 25.0E+6 cells/mL. When a micro-sparger was used, increased glucose uptake and lactate formation was observed for cultivations utilizing the VHU.

4.2.4 DI244 production in a perfusion cultivation

Next, the cell retention membranes were compared for their ability to allow for harvesting virus particles into the permeate. Cells were infected when the VCC reached concentrations above 20.0E+06 cells/mL (or 25.0E+06 cells/mL for HFM2). Maintaining a constant pH value for cultivation HFM2 at cell concentrations up to 26.8E+6 cells/mL required addition of large amounts of base (7.5% $NaHCO_3$ solution). Therefore, it was decided to infect subsequent cultivations (VHU1 and VHU2) before the VCC exceeded 25.0E+6 cells/mL. For infection a MODIP of 1E–3 was chosen, as this required a much lower volume of seed virus (compared to the previously used MODIP of 1E–2), while resulting in very comparable DI244 titers and interfering efficacies (section 4.2.1). Before virus addition, the medium was fully exchanged and trypsin was added to 20 U/mL. Additionally, the cultivation temperature was reduced from 37°C to 32°C, as this was shown to reduce virus degradation (Fig. 4.16).

Further, the permeate flow was paused for 1 hpi to avoid the loss of trypsin and virus particles into the permeate and to allow for an efficient cell entry of the DIPs. During the virus replication phase, cultivation medium containing 20 U/mL trypsin was used and the perfusion rate was kept constant at 2–3 RV/d. For all four perfusion cultivations, cells continued to grow for the first 6–12 hpi and reached VCCs up to 28.4E+6 cells/mL (Fig. 4.17a). Afterwards, viability and VCC started to decline. HA titers (Fig. 4.17b), vRNA levels (Fig. 4.17c), and PFU titers (Fig. 4.17d) all reached their respective maximum at about 36 hpi. The maximum titer was 7.4E+9 PFU/mL and the maximum DI244 vRNA level was 5.9E+11 copies/mL (HFM2), both being more than 10-fold higher than for the batch production process infected at a VCC of 2.0E+06 cells/mL described before (section 4.2.2). In contrast to previous findings (Fig. 4.8, Fig. 4.11), no decrease in the plaque titers was observed after the respective maximum was reached. The increased virus stability could be explained by the reduced cultivation temperature of 32°C during the virus replication phase as confirmed by small scale experiments (Fig. 4.16d).

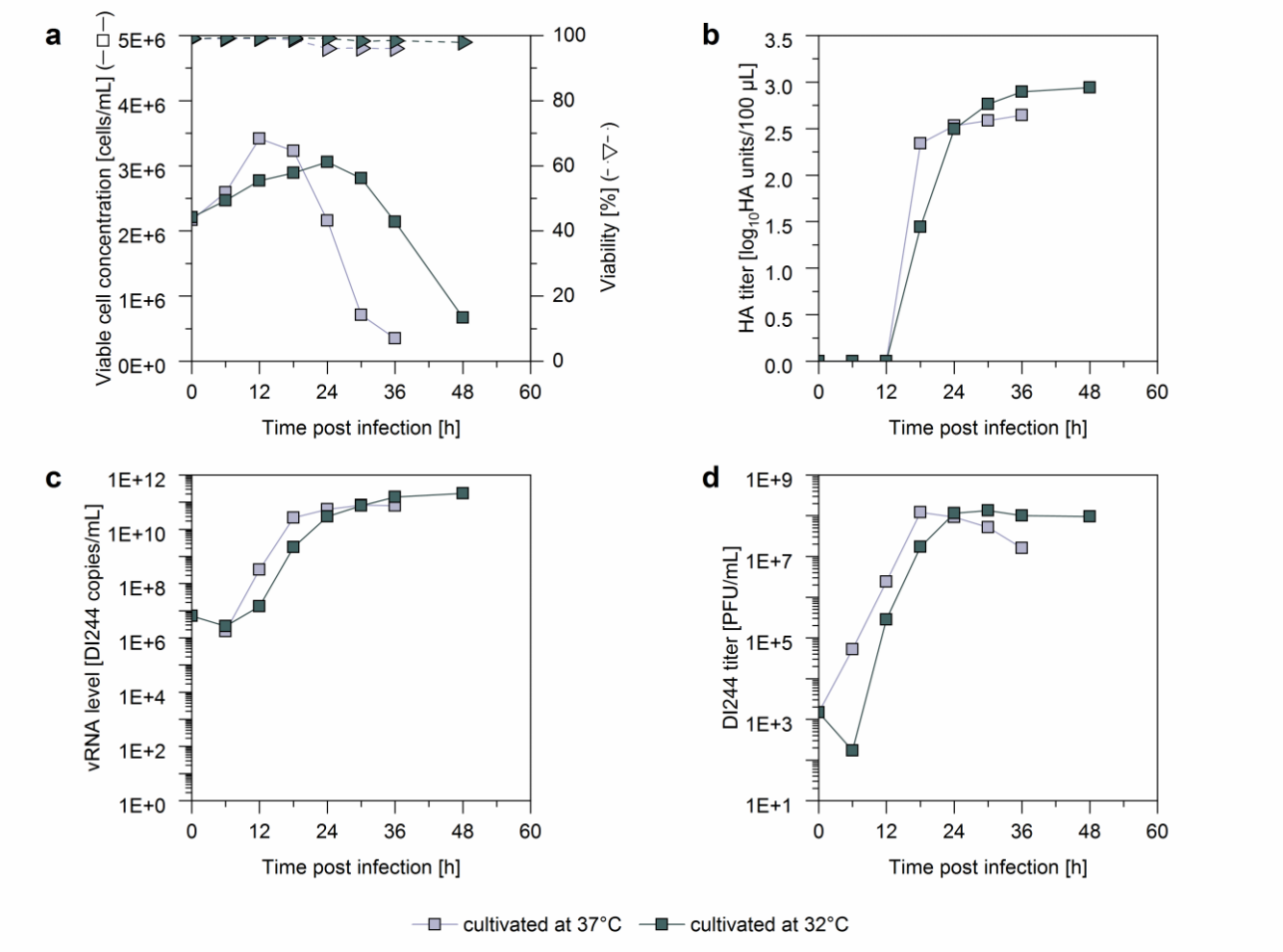

Fig. 4.16 DI244 production at different temperatures. MDCK-PB2(sus) cells were cultivated in shake flasks (50 mL working volume). At time of infection the VCC was adjusted to 2.0E+6 cells/mL and infected with a pure DI244 seed virus at MODIP 1E–3. After infection, the cells were split and either cultivated at 37°C or 32°C. (a) VCCs and viabilities, (b) HA titers, (c) vRNA levels, and (d) DI244 titers.

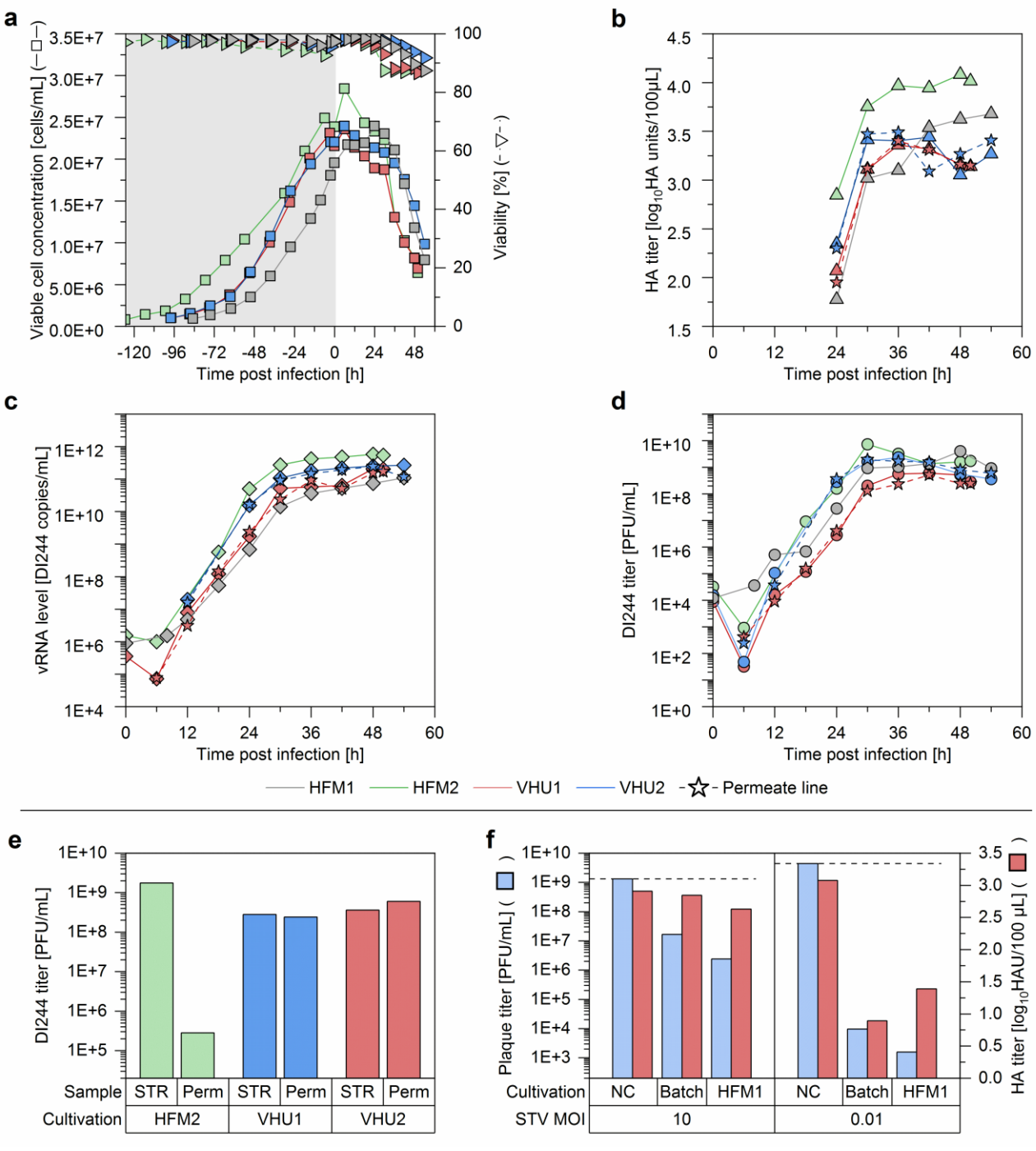

Fig. 4.17 DI244 production in perfusion cultivations. MDCK-PB2(sus) cells were cultivated in STRs (working volume 700 mL) coupled to an ATF. Cells were infected at a VCC of 25.0E+6 cells /mL (HFM2) or 20.0E+6 cells/mL (HFM1, VHU1, VHU2) with a pure DI244 seed virus at MODIP 1E–3. (a) VCCs and viabilities, (b) HA titers, (c) DI244 vRNA levels, (d) DI244 titers. (b, c, and d) Solid lines correspond to virus titers in the STR, dashed lines with star symbols to the virus titers in the permeate line. (e) DI244 titers in STR and permeate line (Perm) at time of harvest (48 hpi). (f) Interference assay. MDCK(adh) cells were infected at MOI 10 or 0.01 with STVs and co-infected with 125 µL of DI244 material produced in HFM1 or a previous batch cultivation (shake flask; Table 4.2, production replicate 2, MODIP 1E–2) and medium as negative control (NC).

Additionally to the virus titers of the STR, titers in the permeate line were determined (Fig. 4.17b–d). For the used HFM it is well established that virus particles of about 40-100 nm in diameter cannot pass through the membrane (Nikolay et al. 2020b). Samples taken shortly before harvesting confirmed this, since only residual virus amounts could be detected in the permeate line (Fig. 4.17e). However when the VHU was used, HA titers, DI244 vRNA levels, and DI244 titers in the STR always equaled the virus titer in the permeate line (Fig. 4.17b–e), suggesting that no virus retention occurred. Further, the virus titer in vessel and permeate stayed very similar until late process times, indicating that no filter fouling or blocking occurred even when high amounts of cell debris were present in the culture broth. This clearly shows the potential of the VHU for continuous virus harvesting during a perfusion cultivation.

For perfusion cultivations with the VHU, virus particles were diluted as they also passed on to the permeate. Therefore, the achieved virus concentrations were lower (Fig. 4.17b–d). For a more detailed comparison of the tested cell retention membranes, the overall process yield, the total amount of virus particles, and the virus yields were calculated (Table 4.4). The total amount of DI244 particles, the total amount of DI244 vRNA, the $CSVY_{PFU}$, and the $CSVY_{vRNA}$ were similar using either membrane. Although the average values of perfusion cultivations using the VHU were a bit higher, the differences were not significant, given the relatively high standard deviation of the virus quantification assays.

Finally, DI244 material produced in a perfusion process (HFM1) and harvested at 48 hpi was tested in an interference assay to verify its antiviral potential compared to material produced previously in a batch cultivation (section 4.2.2; Fig. 4.17f). As the DI244 titer was more than 10-fold higher for material produced in the perfusion cultivation compared to material produced in a batch cultivation, a higher interfering efficacy was expected. Indeed, the DI244 material produced in a perfusion cultivation reduced the plaque titer by almost one order of magnitude more than material produced in a batch cultivation. For the HA titer a similar trend could be observed when STVs were added at MOI 10, but not for STV MOI 0.01. Here, it should be considered that DI244 particles themselves express HA and contribute to the HA titer. Furthermore, the particle-specific interfering efficacy of DI244 material produced in a perfusion and a batch cultivation was compared. Here, both production systems yielded material with a very comparable particle-specific interfering efficacy (Fig. A6), indicating that the production in perfusion mode did not impacted the DIP product quality. Overall, the results clearly demonstrate the antiviral potential of DI244 produced in a perfusion cultivation.

Table 4.4 Overview of process parameters, virus titers and calculated yields for perfusion cultivations.

	HFM1	HFM2	VHU1	VHU2
Color in graphs	■	■	■	■
Perfusion rate control	manual	controlled	controlled	controlled
Working volume [mL]	700	700	700	700
Maximum VCC [cells/mL]	23.96E+06	28.43E+06	23.59E+06	23.97E+06
Virus containing harvest volume [mL]	700	700	3644	4036
Overall DI244 titer at time of harvest [PFU/mL]	9.20E+08	1.74E+09	2.08E+08	5.91E+08
Total DI244 particles [PFU]	6.44E+11	1.22E+12	7.58E+11	2.39E+12
Overall DI244 vRNA level at time of harvest [copies/mL]	1.09E+11	5.38E+11	1.07E+11	7.78E+10
Total DI244 vRNA [copies]	7.66E+13	3.77E+14	3.89E+14	3.14E+14
$CSVY_{PFU}$ [PFU/cell]	**38±17**	**61±27**	**46±20**	**142±63**
$CSVY_{vRNA}$ [1.0E+4 copies/cell]	**4.5±2.4**	**18.5±9.8**	**23.6±12.4**	**18.7±9.9**
PFU in permeate line / PFU in STR [%]	-	**0.03±0.03**	**81±37**	**111±45**
DI244 vRNA in permeate line / DI244 vRNA in STR [%]	-	**0.25±0.16**	**93±43**	**83±20**

MDCK-PB2(sus) cells were cultivated in STRs coupled to an ATF. All cultures were harvested at 48 hpi. For $CSVY_{PFU}$ and $CSVY_{vRNA}$ (Eq. 6), the calculated standard deviation (based on the error propagation of the errors of the used assays) is given. For "PFU or DI244 vRNA in permeate line / PFU or DI244 vRNA in STR" (Eq. 8) the average of the virus replication phase is given with the corresponding standard deviation. "PFU in permeate line / PFU in STR" higher than 100% can be attributed to the high standard deviation of the plaque assays.

In summary, the high VCCs achieved in the perfusion processes resulted in higher virus titers and consequentially higher interfering efficacies compared to the previous batch process. In contrast to the HFM, the VHU allowed to continuously harvest virus particles from the STR without retaining any virus particles. The virus yield of the perfusion process seems to be largely unaffected by the used cell retention membrane.

4.2.5 Protein and DNA retention in a perfusion cultivation

Continuous harvesting of virus particles during a perfusion process theoretically allows the implementation of process integration strategies, where the harvested material can be directly transferred into subsequent downstream processing units without hold times. However, besides virus particles, the cultivation broth contains intact cells, cell debris, and host cell proteins as well as host cell DNA released with cell lysis. The amount of these contaminations that are able to pass through the membrane could have severe implications regarding the performance of downstream processing. Therefore, the protein and dsDNA contamination level in the produced virus material was determined.

For the perfusion with the HFM2, the permeate did not contain significant amounts of virus and only the STR was harvested (700 mL). For the perfusion with the VHU1, virus particles were able to pass through the membrane and were also found in the permeate. Therefore, for the VHU1, the unfiltered cell culture broth from the STR (700 mL) and the collected permeate (2944 mL) was harvested. First, the protein and dsDNA concentration in the virus containing harvest was measured. The VHU appeared to not retain any contaminations, as the protein and dsDNA concentration in the STR and in the collected permeate were more or less the same (Fig. 4.18a). Since proteins and dsDNA were heavily diluted over the time of the cultivation when the VHU was used, their contamination level was very low. In strong contrast, the HFM withheld most of the proteins and dsDNA and much higher levels were observed in the STR. The drastically reduced host cell protein retention of the VHU might also indicate advantages over the HFM for continuous harvesting of recombinant proteins.

Considering the respective harvest volumes (700 mL for HFM2, 3644 mL for VHU1), the total amount of proteins and dsDNA were calculated (Fig. 4.18b). The total amount of dsDNA found in the harvest of the perfusion with HFM2 (only the STR was harvested) equaled the amount of dsDNA found in the harvest of the cultivation with the VHU1 (the STR and the collected permeate were harvested). This indicates that the HFM2 retained the entire dsDNA. In contrast, the HFM appeared to only partly withhold proteins and the total amount of proteins contaminating the virus harvest was much lower.

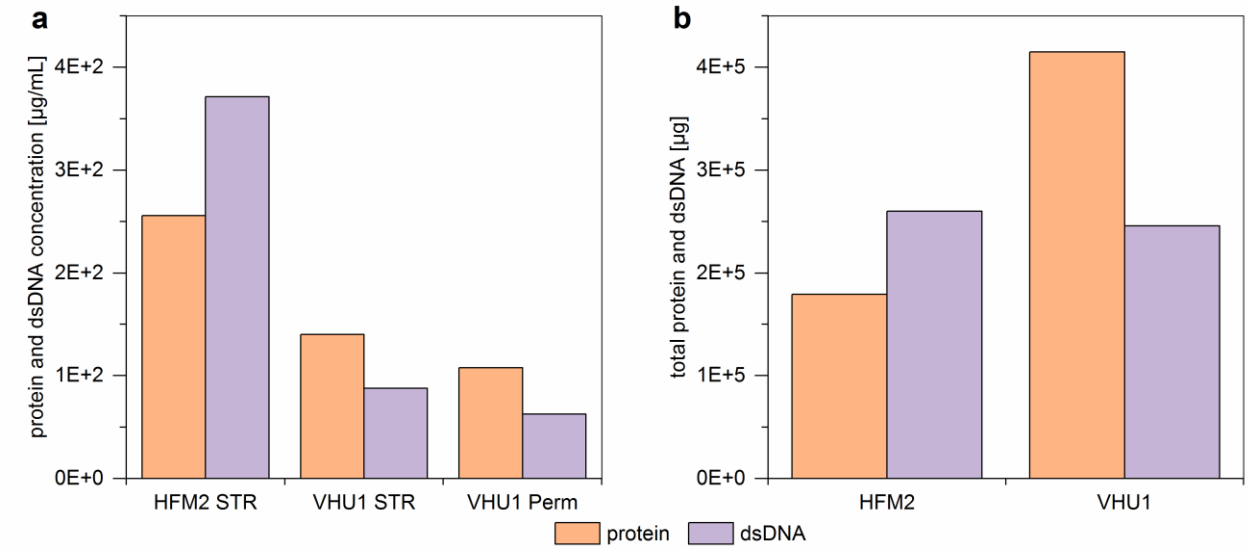

Fig. 4.18 Protein and dsDNA contamination in the DI244 harvest. MDCK-PB2(sus) cells were cultivated in STRs (working volume 700 mL) coupled to an ATF. The harvest (48 hpi) of two perfusion cultivations (HFM2 and VHU1) were analyzed for their (a) protein and dsDNA concentrations. For HFM2, only the STR (700 mL) was harvested; for VHU1, the STR (STR; 700 mL) and the collected permeate (Perm; 2944 mL) were harvested. (b) Total amount of protein and dsDNA based on the respective harvest volume.

In summary, the HFM appeared to retain the dsDNA completely as well as parts of the protein impurities. In contrast, the VHU did not retain any protein or dsDNA impurities, which might also indicate an advantage of the VHU over conventional HFMs for the continuous harvest of recombinant proteins in a perfusion production process.

4.2.6 Discussion

In this PhD work, a cell culture-based production process for purely clonal DI244 particles without STV contamination was established. Here, especially the impact of the MODIP on the interfering efficacy of the produced material was investigated. The production process was scaled up from shake flasks to a laboratory-scale STR. Next, process intensification strategies were applied, resulting in cell concentrations up to 28.4E+06 cells/mL and DI244 titers 10-fold higher than for the batch production process. Further, the perfusion rate was controlled using a capacitance probe monitoring the VCV in the cultivation vessel. Lastly, a novel tubular membrane (VHU) was tested for its potential to continuously harvest virus particles. Here, no retention of the observed virus particles could be detected.

Advantages and opportunities of a cell culture-based production processes

The genetically modified cells used allowed the production of purely clonal DIP preparations (Bdeir et al. 2019; Yamagata et al. 2019), which completely overcame the necessity of STV inactivation. Previously, UV-light was used to disrupt the STV vRNAs in conventionally produced DIP preparations (Dimmock et al. 2008; Wasik et al. 2018). However, it was shown that also the DIP vRNA was damaged by UV light, resulting in a decreased interfering efficacy over UV-inactivation time (Fig. 4.4). In contrast, the interfering efficacy of the purely produced DIP material was maintained at a very high level by avoiding any UV-irradiation. Further, using genetically modified cell lines, concerns regarding biosafety, i.e. the risk of residual infectious STVs due to incomplete inactivation after UV-treatment, can be avoided.

The interfering efficacy of a DIP seems to be affected by many factors including genome length, genome sequence, and breaking point (Duhaut and Dimmock 2002; Duhaut and McCauley 1996; Nayak et al. 1985; Odagiri and Tashiro 1997). Further, the genetically modified MDCK-PB2(sus) can be used for cell-culture based production of any IAV Seg1 DIP (Bdeir et al. 2019). Recently, colleagues identified several IAV Seg1 DIP candidates with different deletion sites and lengths using an evolutionary approach. Some of these candidates appeared to have an improved interfering efficacy compared to DI244 (Pelz et al. 2021). The elucidation of the mechanisms determining the antiviral potential of a DIP is an exciting prospect for future research. Further, the generation of genetically modified cell lines expressing another viral protein, e.g. the viral PB1 or PA protein, would also allow production of purely clonal Seg2 or Seg3 DIPs. These segments are of special interest, as deletions in Seg1–3 are most frequently observed (Davis and Nayak 1979; Nayak et al. 1985) and it was hypothesized that DIPs that originate from Seg1–3 may have advantages over DIPs originating from structural genes (Seg4–8) (Laske et al. 2016). The production and evaluation of Seg2 and Seg3 IAV DIP candidates could be the topic of future research. However, DIPs with a deletion in more than one vRNA segment did not showed an increased interfering efficacy compared to DIPs with a deletion in just one vRNA segment (Bdeir et al. 2021).

The MODIP affected the incorporation of DI244 vRNA in the produced virus particles

In the present PhD work, Seg5 and Seg8 vRNA levels (considered as representative for all STV vRNA segments) were approximately equimolar for each production MODIP and each sampling time point. In contrast, DI244 vRNA levels were often lower. This might suggest that Seg5 and Seg8 vRNAs were present in every virus particle, whereas the DI244 vRNA was absent in some virus particles. Usually, virus assembly and budding was considered a well-organized process, where each of the eight vRNAs is incorporated in the produced virus particle only once (Chou et al. 2012; Noda and Kawaoka 2012). This is facilitated by the packaging sequence, present at the 3' and 5' end of each vRNA segment (Fujii et al. 2003; Hutchinson et al. 2010). Nevertheless, depending on the strain, up to 20% of produced viruses do not package at least one vRNA segment (Nakatsu et al. 2016). This results in the generation of semi-infectious particles (Brooke et al. 2013). Further, also OP7 is a naturally occurring virus variant, which appears to lack several vRNA segments (Kupke et al. 2019).

The MDCK-PB2(sus) cell line used here expressed the viral PB2 protein, encoded by Seg1 vRNA. With the cell line providing the missing PB2 protein, the virus propagation theoretically does not require an intact Seg1 vRNA. Concurrently, also the deleted Seg1 vRNA from DI244 is not essential for replication. Therefore, the MDCK-PB2(sus) cell line might not only allow production of purely clonal Seg1 DIPs, but also propagation of viruses with only seven segments, completely missing the Seg1 vRNA. This could explain the lower levels of DI244 vRNA in the produced virus particles. Furthermore, DI244 vRNA levels decreased with lower MODIPs. A possible explanation may be that higher MODIPs result in overall more co-infections, and therefore a higher probability that all eight segments are present in an infected cell. Here, most produced viruses would incorporate all eight segments. In contrast, in a low MODIP scenario, the likelihood for single-hit infections is increased drastically. Under this condition, cells may occasionally be infected by a virus without DI244 vRNA. Consequentially, those cells could only produce viruses also missing DI244 vRNAs. Additionally, the produced 7-segmented viruses will further accumulate in subsequent infection waves (which are characteristic for low MODIPs).

The lack of DI244 vRNA could also explain the observed differences between the plaque and the interference assay. More specifically, MODIPs of 1E−2 to 1E−4 resulted in very comparable DI244 titers. In contrast, differences in the interfering efficacy were observed, where material produced at

lower MODIPs induced a less pronounced titer reduction. The DI244 titer was evaluated in a plaque assay with MDCK-PB2(adh) cells. Here, virus particles without incorporated DI244 vRNA could still replicate and would therefore contribute to the DI244 titer. On the other hand, particles without DI244 vRNA would not interfere with STV replication. Therefore, these particles would not contribute to the interfering efficacy determined in the interference assay. Consequentially, material produced at a MODIP of 1E−2, showing the highest DI244 vRNA level (for MODIP 1E−2 to 1E−4) resulted in the most pronounced titer reduction. DIP material produced at a MODIP of 1E−1 showed comparable vRNA levels, but lower DI244 titers. A possible explanation could be that the interfering efficacy of this material is lower due to a faster onset of DI244 production, resulting in an earlier onset of degradation of biologically active virus particles and a reduced number of virions carrying DI244 vRNA to the cells.

The mechanism proposed here, where DI vRNAs might not be efficiently incorporated in the produced virus particles, when produced with a complementing cell line, would have implications for the DIP production process. The risk that high amounts of virus particles without any therapeutic effect might be produced, especially at lower MODIPs (usually used for cell culture-based viral vaccine production) is of particular importance. Therefore, optimization of the MODIP seems crucial for the establishment of a production process as it might drastically affect the quality of DIP harvests.

MDCK-PB2(sus) cells can be used for high cell density cultivations

The metabolite uptake rates of MDCK-PB2(sus) cells grown in perfusion cultivations were very comparable to those obtained for the parental MDCK.Xe.E (descendent from a MDCK cell line originally obtained from ECACC). Therefore, expression of PB2 itself did not seem to significantly influence cell metabolism or cell growth. However, the uptake rates were relatively high and consequentially a high CSPR of 200 pL/cell/day was needed for perfusion cultivations. For comparison, when a perfusion process with the same medium but a different MDCK cell line (descendent from a MDCK cell line originally obtained from ATCC) was established, a lower CSPR from 60 pL/cell/day was sufficient (Wu et al. 2021). Furthermore, no oxygen limitations were observed in cultivations with the latter and the optimal pH value for cell growth was much lower (pH 7.4 for MDCK-PB2(sus) and its parental MDCK.Xe.E cell line (ECACC), compared to pH 7.0 for MDCK cells obtained from ATCC). Previous studies compared the cell growth and virus yield of MDCK cells obtained either from ECACC or ATCC grown in Xeno™ medium (Bissinger 2020).

Here, faster cell growth, higher maximum VCCs and a higher $CSVY_{PFU}$ were observed for MDCK cells obtained from ATCC. Therefore, to further improve the process performance, it would be an option to genetically modify MDCK cells from ATCC to express the viral PB2 and evaluate growth and productivity at HCD.

Nevertheless, perfusion control using a capacitance probe for cell growth monitoring was sufficient to maintain high substrate and low waste product levels over the cultivation time. The perfusion rate control allowed for a robust process performance at even higher cell concentrations, as already shown for other cell lines (Nikolay et al. 2018). In the present PhD work, a maximum concentration of 28.4E+06 cells/mL was reached. Here, it should be possible to achieve even higher VCCs with further optimization of the pH and DO control. With the current control regime both parameters were hard to maintain at HCD and it was decided for subsequent cultivations to infect the cells, before the VCC exceeded 25.0E+6 cells/mL. To overcome oxygen limitations observed for the manual perfusion cultivation, aeration with an additional micro-sparger was started 72 h post inoculation for the controlled perfusion cultivations. Here, increased glucose uptake and lactate production was observed, when the VHU was used. The increased lactate formation might indicate increased cell stress. For example, it was reported that cells exposed to shear stress show an increased lactate dehydrogenase activity (Shiragami and Unno 1994). One possible explanation for the increased cell stress could be that the smaller bubbles produced by the micro-sparger could enter the large diameter tubular membrane of the VHU more easily than the membrane of the HFM unit. Therefore, it cannot be excluded that the gas bubbles in combination with the relatively high flow rates in the VHU might result in an increased shear stress. This could have implications on the maximum achievable VCC and should be further investigated.

In summary, MDCK-PB2(sus) cells showed great potential for the design of HCD processes to achieve very high DI244 titers. Further improvements of the cell line could allow for even higher cell concentrations and virus titers.

The VHU allows for continuous virus harvesting

Previous studies investigated different HFMs for their potential to allow continuous virus harvesting (Genzel et al. 2014; Nikolay et al. 2020b). However, almost all tested membranes completely retained the produced virus particles, despite the nominal pore size being much larger than the average virus

diameter. It was concluded that the membrane material and with this, its inner surface, structure, porosity, and hollow fiber wall thickness largely influenced the retention of virus particles. In the present PhD work, these findings were confirmed for a commonly used HFM (nominal pore size 0.2 µm) that retained most IAV DIPs (approximate diameter 80–120 nm). In strong contrast, no virus retention was detected for the VHU. This is especially remarkable since IAV is a lytic virus and, therefore, large amounts of cell debris accumulate towards the end of cultivations. In particular, no filter fouling or blocking was observed over the entire virus production phase. Furthermore, the VHU did not retain host cell proteins in contrast to the used HFM. This might also indicate an advantage over conventional HFM for production and harvest of recombinant proteins (e.g. monoclonal antibodies). The continuous harvesting of virus particles or recombinant proteins would allow the implementation of process integration strategies and could ultimately lead to increased yields by avoiding product degradation due to long holding times at high temperatures.

VHU membrane-based perfusion cultivation vs. non-membrane-based perfusion systems

Besides membrane-based cell retention devices, also other systems exist. The potential of two of these systems (acoustic settler and inclined settler) for continuous virus harvesting was described recently for IAV and MVA production (Coronel et al. 2020; Granicher et al. 2020; Granicher et al. 2021). Choosing one of these systems will depend on many parameters and a detailed comparison of pros and cons was presented before. For the selected production platform, the operation of an ATF system seems to have advantages as no system cooling or complex pumping strategies are required. Further, it was described that the mentioned alternative cell retention systems do not allow for complete cell retention and some cells are lost over the course of the cultivation. Additionally, their separation principles rely on cell settling and therefore longer recirculation times were observed (Chotteau 2015; Coronel et al. 2020; Granicher et al. 2020). In the present PhD work, no cells could be detected in the permeate line of the VHU (data not shown) and the cells only spent a few seconds outside the STR during each pumping cycle of the ATF system. Finally, both the acoustic and the inclined settler do not offer the possibility to retain virus particles. With the ATF system it is now possible to retain or continuously harvest the produced virus particles depending on the membrane chosen for cultivation.

The potential of a perfusion process for IAV DIP production

The DI244 preparations generated in the context of this PhD work were tested in *in vivo* experiments, as outlined in the next section (Hein et al. 2021a). Here, relatively large amounts of DI244 (1.5E+6 PFU per dose) needed to be administered. Therefore, it was important to establish a production process that could supply the needed quantities. The average amount of produced DI244 for a perfusion cultivation with a working volume of 700 mL was 1.25E+12 PFU. This would be enough to treat almost one million mice. While the dose for humans is currently unknown, it seems very likely that even a small scale perfusion process could be used to generate a high number of DI244 doses for human use. Further, perfusion cultivations show a drastically improved STY (Eq. 7) compared to a batch cultivation process. The STY was calculated for all conducted perfusion cultivations and for a batch cultivation with the same cultivation conditions as used for the perfusion cultivation (working volume 700 mL, 1.0E+6 cells/mL at time of inoculation). Here, the STY was in average 200-fold higher for the perfusion cultivations (Table 4.5). Overall, this provides further evidence for the feasibility of cell culture-based perfusion process for the production of DIP material.

Table 4.5 STY for different DI244 production cultivations

	Cell growth phase [h]	Infection phase[h]	Total DI244 particles [PFU]	STY [PFU/h/mL]	Fold improvement in STY compared to batch
Batch	19.50	24.00	4.20E+11	1.38E+7	**1**
HFM1	84.65	48.00	7.66E+13	8.25E+8	**60**
HFM2	125.25	48.00	3.77E+14	3.11E+9	**225**
VHU1	97.75	48.00	3.89E+14	3.81E+9	**276**
VHU2	98.00	48.00	3.14E+14	3.07E+9	**223**

For HFM1, HFM2, VHU1, and VHU2, the bioreactor was coupled to an ATF2 system to allow cultivation in perfusion mode (see section 4.2.4). For the batch cultivation, the STY (Eq. 7) was calculated using the maximum virus titer of a previous batch production (Fig. 4.11), but assuming an increased working volume (700 mL instead 500 mL) and an initial growth phase from 1.0E+6 to 2.0E+6 cells/mL (using the growth rate of an non-infected batch cultivation; Table 4.3).

4.2.7 Subsequent experiments with produced DI244 material

DI244 material produced using the established cell culture-based platform was used by colleagues and collaboration partners for subsequent experiments to investigate (i) the feasibility of virus purification methods (Hein et al. 2021a), (ii) the antiviral effectivity in animal experiments (Hein et al. 2021a), (iii) the replication dynamics of DI244 and STVs in defined co-infection experiments (Ruediger et al. 2021), and (iv) the interfering efficacy against SARS-CoV-2 (Rand et al. 2021).

DI244 material produced in shake flasks was purified by membrane-based SXC. Here, a DI244 yield of 92.3% was achieved. This is consistent with previous results for downstream processing of IAV (Marichal-Gallardo et al. 2017). The clearance of host cell DNA was 97.1%, and could be increased to 99.95% by adding a DNA digestion step prior to SXC. The total protein clearance was 97.2%, which is also consistent with previously reported data (Marichal-Gallardo et al. 2017). Further, the DI244 material was concentrated approximately 40-fold, resulting in a drastically increased *in vitro* interfering efficacy (Hein et al. 2021a).

Studies in a mouse infection model were performed to evaluate the antiviral efficacy of DI244 material *in vivo* by a collaboration partner (IG group at the HZI). The tested material was cell culture-derived unpurified DI244 produced in shake flasks. Treatment of mice with DI244 alone did not result in any body weight loss, and therefore DI244 did not appear to be highly toxic. Mice infected with an otherwise lethal dose of IAV showed a reduced body weight loss and all animals survived the infection upon treatment with unpurified DI244, clearly demonstrating the antiviral potential (Hein et al. 2021a).

The established production platform allowed for the first time to produce large quantities of pure DIP material, which was used for defined co-infection experiments with pure STV preparations. A set of experiments using various MOIs and MODIPs was conducted to elucidate the complex interplay between STVs and DIPs. The obtained data was used for the development of a multiscale model, describing DIP and STV replication on cellular and population level. One observation was that the DIP to STV ratio required to completely prevent STV replication seems to be approximately 10,000 to 1 (Ruediger et al. 2021).

Lastly, the antiviral efficacy of produced DI244 against SARS-CoV-2 was investigated by a collaboration partner (VAM group at the HZI). Calu-3 cells were co-infected with SARS-CoV-2

STVs and SXC-purified DI244 produced in a STR. Depending on the applied amount of DI244 it was possible to completely abolish SARS-CoV-2 replication. As demonstrated by the induction of the interferon system, it was concluded that the unspecific innate immune response majorly contributed to the antiviral effect. This study suggested that IAV DIPs might confer protection against a variety of other heterologous interferon-sensitive viruses (Rand et al. 2021), which would be in line with previous claims (Dimmock and Easton 2015; Easton et al. 2011; Scott et al. 2011). However, as discussed earlier (section 4.1.4), the innate immune response cannot solely explain the antiviral effects of IAV DIPs and observed interfering effects in the interference assay are much more likely explained by DIP vRNA interfering with the replication of the STVs.

5 CONCLUSION AND OUTLOOK

In the presented PhD work, cell culture-based production processes for two types of DIPs (OP7 and DI244) were established. For the recently discovered DIP OP7 (point mutations in Seg7 vRNA), a seed virus containing the OP7 and infectious STVs was used. First, the production conditions were investigated in small scale, before the process was scaled up to a laboratory-scale STR. Next, to inactivate the STVs in the produced material, UV-irradiation was utilized, which also reduced the interfering efficacy of the OP7 material. The contamination of DIP material with STVs is a well-known problem and therefore other groups developed systems for production of purely clonal DIP preparations (without STVs) to circumvent the necessity of a STV inactivation (Bdeir et al. 2019; Yamagata et al. 2019). Here, in a first step, adherent MDCK cells were genetically engineered to express the viral protein PB2 encoded by the deleted Seg1 of DI244. Subsequentially, a similar production system with genetically modified suspension MDCK cells, was used in the presented PhD work to establish a more easily scalable production process for pure DI244 preparations. Optimal infection conditions were first determined in shake flasks. Afterwards, the production process was scaled up to a laboratory-scale STR and process intensification strategies were applied. More specifically, a HCD perfusion cultivation was established utilizing an ATF system. The perfusion cultivation was further improved by controlling the perfusion rate using an online capacitance probe, which measured the VCV in the STR. Lastly, different cell retention membranes were investigated for their potential to continuously harvest DI244 particles. Overall, the production processes for both DIPs allowed production of DIP material with a high titer and high interfering efficacy.

5.1 Cell culture-based production of OP7

The optimal infection conditions for production of OP7 were first investigated in shake flasks. Here, the production yield of OP7 particles was highly depended on the applied MOI. This was shown to be caused by the interplay of STV and DI vRNA and could be observed in the infectious virus titers, HA titers, OP7 vRNA levels, and the mutated OP7-M1. The established process resulted in very high OP7 vRNA levels and high interfering efficacies. However, this was partially mitigated due to the required UV-irradiation to inactivate STVs in the production background. Here, it would be desirable

to develop a system for production of pure OP7 particles without STVs to avoid any kind of inactivation step. One option would be to genetically modify MDCK cells to express the viral wild-type M1 and M2 protein encoded by Seg7 vRNA to potentially allow replication of pure OP7 particles, analogous to the DI244 production system. However, in contrast to conventional DI vRNAs, the OP7 vRNA can be translated into (mutated) proteins. Those proteins might contribute to the interfering efficacy, as hypothesized earlier (Kupke et al. 2019) and therefore the rescue of pure OP7 particles may be more complicated than for DIPs with an internal deletion. Nevertheless, the development of a production process for pure OP7 preparations without any STV contamination should be further pursued considering the high interfering potency of OP7. More specifically, treatment with OP7 material without any UV-inactivation reduced the infectious virus release in the interference assay approximately two orders of magnitude more than UV-treated OP7 or DI244 (without UV-treatment). This illustrates the tremendous potential of OP7 for antiviral therapy. The development of a production system for pure OP7 particles would not only improve the interfering efficacy of the final material, but could also be an important step towards clinical trials. More specifically, concerns of the safety of DIP material due to residual STV contaminations were discussed before, but could be avoided by production of pure DIP preparations.

The antiviral efficacy of the produced and UV-inactivated OP7 was not only shown *in vitro* but also *in vivo*. Here, OP7 treatment protected mice against an otherwise lethal dose of IAV and completely prevented any bodyweight loss. To our knowledge, this was the first time the antiviral effect of a DIP solely containing point mutations was shown in animal experiments (Hein et al. 2021c). Further, an antiviral effect of the OP7 material, produced in the context of this PhD work, against the heterologous virus SARS-CoV-2 could be shown *in vitro* (Rand et al. 2021). This is in line with previous findings, which suggested a broad efficacy of IAV DIPs against many other heterologous interferon-sensitive viruses due to an unspecific stimulation of the innate immune response by IAV DIP infection (Dimmock and Easton 2015; Easton et al. 2011; Scott et al. 2011).

The established production process for OP7 showed a very good scalability, demonstrated by scale-up experiments from the shake flask to the STR. The improved scalability, the possibility to apply process intensification strategies, and the possibility to genetically modify the production cell line to allow production of pure OP7 particles clearly demonstrates the advantage of using cell culture-based production systems, rather than egg-based systems.

Overall, a high-yield production process for OP7 was successfully established that shows great potential to be further improved in the future, i.e. using genetically modified cell lines and process intensification strategies. Given the very high antiviral efficacy of OP7 observed in *in vitro* and *in vivo* experiments, clinical trials could be aspired.

5.2 Cell culture-based production of DI244

Previously, a production system for pure DI244 particles, using a genetically modified adherent MDCK cell line and a pure DI244 seed virus was developed by others (Bdeir et al. 2019). Later, also a suspension MDCK cell line was genetically modified to express the viral PB2 (MDCK-PB2(sus)), which was used in the present PhD work to establish a production process for large quantities of DI244 material.

The production of pure DI244 was first investigated in shake flasks. Surprisingly, the MODIP impacted the interfering efficacy of the produced material. This was caused by a reduced DI244 vRNA content per virus particle for lower MODIPs. This phenomenon, where DI vRNAs might not be efficiently incorporated in the produced virus particles, when produced with a complementing cell line, needs to be considered for future DIP production. Specifically, there may be the risk that high amounts of virus particles without any therapeutic effect are produced, especially at lower MODIPs. Therefore, optimization of the MODIP seems crucial for the establishment of a pure DIP production process.

DI244 material produced in shake flasks proved to be a very promising antiviral agent. More specifically, 100% of mice infected with an otherwise lethal dose of IAV STV survived the infection upon treatment with the produced DI244 material. As far as we know, this was the first time purely clonal IAV DIP material that did not require UV-inactivation positively demonstrated its antiviral potential in an animal model (Hein et al. 2021a). Here, it would be desirable to conduct infection experiments in ferrets, as they are susceptible to human IAV and air-borne virus transmission (Barnard 2009; Richard et al. 2020; Whitley 2010). In a next step, infection experiments in macaques could be carried out, as their clinical symptoms closely resemble those found in humans (Rimmelzwaan et al. 2001) and as a final step towards clinical trials.

While the animal experiments showed very promising results, relatively large DIP quantities were required for a complete protection, i.e. 1.5E+06 PFU per mouse (Hein et al. 2021a). To investigate if higher amounts (e.g. needed for a potential clinical application) can be supplied, a scale-up of the production process to a laboratory-scale STR was investigated. The infections experiments in the STR showed very similar virus replication dynamics and final titers compared to shake flask experiments. Therefore, large-scale manufacturing of DIPs seems to be a promising prospect.

In a next step, to further improve the production process of DI244, process intensification strategies were applied. More specifically, using an ATF system, a HCD perfusion process was developed. To our knowledge, this was the first time DIP preparations were produced in a perfusion cultivation. First, the perfusion rate was adjusted manually, before a control based on the signal of a capacitance probe, which measured the VCV in the bioreactor, was established. Here, both the manually adjusted and the controlled perfusion resulted in sufficient metabolite concentrations and VCCs up to 28.4E+6 cells/mL were reached. Consequentially, very high DIP titers up to 7.4E+9 PFU/mL were achieved in the perfusion cultivation, clearly demonstrating the feasibility of cell culture-based DIP production for antiviral therapy. Further, the use of different cell retention membranes was investigated. A commonly used HFM (pore size 0.2 µm) and the novel tubular VHU (pore size ~10 µm), showed very comparable performances for the cell growth phase, both allowing cell growth to HCD, without any blockage. During the virus replication phase, the VHU, in contrast to the HFM, allowed a continuous virus harvesting. As far as we are aware, this is the first time a continuous virus harvesting for a membrane-based perfusion was described and opens up new possibilities for process integration, where the virus harvest is directly transferred to subsequent downstream processing units. The assessment of these strategies is very timely as process intensification, process integration, and continuous manufacturing will be of high importance in any virus production process.

Another opportunity for future research is the investigation of other DIP candidates for antiviral therapy. More specifically, the MDCK-PB2(sus) cell line used here, also allows the replication of other DIP candidates with a deletion in Seg1. Very recently, three such DIP candidates were produced and two appeared to have an increased interfering efficacy compared to DI244 (Pelz et al. 2021). Moreover, it is also possible to genetically engineer MDCK cells to express the viral PB1 or PA, encoded by Seg2 and Seg3 vRNA, respectively. Such cell lines would allow the production of DIPs with deletions in these segments. Since the interfering efficacy of DIPs seems to be affected by many factors including genome length, genome sequence, and breaking point (Duhaut and Dimmock 2002;

Duhaut and McCauley 1996; Nayak et al. 1985; Odagiri and Tashiro 1997), those DIP candidates may have a higher interfering efficacy than DI244 and should be further investigated. Here, the established production process could be easily adapted to produce other DIP candidates, which could then be further investigated *in vitro* or *in vivo*.

The above mentioned potential research topics could be pursued almost immediately. While these are all of interest to better understand DIPs or their cell culture-based production, the long term goal has to be clinical studies to promote the introduction of DIPs to the market to provide a new class of antiviral therapeutics. The steps required for this involve the generation of a good manufacturing practice (GMP)-certified cell line and seed virus. This would allow the generation of DIP preparations, which could be investigated in clinical trials. Both, the generation of a GMP-certified cell line and the conduction of clinical trials are very expensive and might be only possible in collaboration with an industrial partner.

Overall, a high-yield production process for DI244 was first established in small scale and then scaled up, before process intensification strategies were applied. The established process yielded very high DIP titers, clearly demonstrating the feasibility of cell culture-based processes for production of DIPs for antiviral therapy. Further, the proposed production process could be easily adapted to produce other DIP candidates. The presented proof-of-principle study represents a first important step to promote the introduction of DIPs as a novel antiviral therapeutic to the market.

LIST OF FIGURES

LIST OF TABLES

BIBLIOGRAPHY

Ahn WS, Jeon JJ, Jeong YR, Lee SJ, Yoon SK (2008) Effect of culture temperature on erythropoietin production and glycosylation in a perfusion culture of recombinant CHO cells. Biotechnol Bioeng 101(6):1234-44 doi:10.1002/bit.22006

Alnaji FG, Brooke CB (2020) Influenza virus DI particles: Defective interfering or delightfully interesting? PLoS Pathog 16(5):e1008436 doi:10.1371/journal.ppat.1008436

Alnaji FG, Reiser WK, Rivera-Cardona J, Te Velthuis AJW, Brooke CB (2021) Influenza A Virus Defective Viral Genomes Are Inefficiently Packaged into Virions Relative to Wild-Type Genomic RNAs. mBio:e0295921 doi:10.1128/mBio.02959-21

An Y, Rininger JA, Jarvis DL, Jing X, Ye Z, Aumiller JJ, Eichelberger M, Cipollo JF (2013) Comparative glycomics analysis of influenza Hemagglutinin (H5N1) produced in vaccine relevant cell platforms. J Proteome Res 12(8):3707-20 doi:10.1021/pr400329k

Barnard DL (2009) Animal models for the study of influenza pathogenesis and therapy. Antiviral Res 82(2):A110-22 doi:10.1016/j.antiviral.2008.12.014

Barrett AD, Dimmock NJ (1986) Defective interfering viruses and infections of animals. Curr Top Microbiol Immunol 128:55-84 doi:10.1007/978-3-642-71272-2_2

Barrett PN, Mundt W, Kistner O, Howard MK (2009) Vero cell platform in vaccine production: moving towards cell culture-based viral vaccines. Expert Rev Vaccines 8(5):607-18 doi:10.1586/erv.09.19

Baum A, Garcia-Sastre A (2011) Differential recognition of viral RNA by RIG-I. Virulence 2(2):166-9 doi:10.4161/viru.2.2.15481

Baxby D (1999) Edward Jenner's inquiry after 200 years. BMJ 318(7180):390 doi:10.1136/bmj.318.7180.390

Bdeir N, Arora P, Gartner S, Hoffmann M, Reichl U, Poehlmann S, Winkler M (2019) A system for production of defective interfering particles in the absence of infectious influenza A virus. PLoS One 14(3):e0212757 doi:10.1371/journal.pone.0212757

Bdeir N, Arora P, Gärtner S, Poehlmann S, Winkler M (2021) Evidence that two instead of one defective interfering RNA in influenza A virus-derived defective interfering particles (DIPs) does not enhance antiviral activity. Scientific Reports 11(1):20477 doi:10.1038/s41598-021-99691-1

Belicha-Villanueva A, Rodriguez-Madoz JR, Maamary J, Baum A, Bernal-Rubio D, Minguito de la Escalera M, Fernandez-Sesma A, Garcia-Sastre A (2012) Recombinant influenza A viruses with enhanced levels of PB1 and PA viral protein expression. J Virol 86(10):5926-30 doi:10.1128/JVI.06384-11

Bielser JM, Wolf M, Souquet J, Broly H, Morbidelli M (2018) Perfusion mammalian cell culture for recombinant protein manufacturing - A critical review. Biotechnol Adv 36(4):1328-1340 doi:10.1016/j.biotechadv.2018.04.011

Bissinger T (2020) Evaluation of MDCK suspension cell lines for influenza A virus production : media, metabolism, and process conditions,

Bissinger T, Fritsch J, Mihut A, Wu Y, Liu X, Genzel Y, Tan WS, Reichl U (2019) Semi-perfusion cultures of suspension MDCK cells enable high cell concentrations and efficient influenza A virus production. Vaccine 37(47):7003-7010 doi:10.1016/j.vaccine.2019.04.054

Blume S, Geesink I (2000) A brief history of polio vaccines. Science 288(5471):1593-4 doi:10.1126/science.288.5471.1593

Bock A, Sann H, Schulze-Horsel J, Genzel Y, Reichl U, Mohler L (2009) Growth behavior of number distributed adherent MDCK cells for optimization in microcarrier cultures. Biotechnol Prog 25(6):1717-31 doi:10.1002/btpr.262

Bock A, Schulze-Horsel J, Schwarzer J, Rapp E, Genzel Y, Reichl U (2011) High-density microcarrier cell cultures for influenza virus production. Biotechnol Prog 27(1):241-50 doi:10.1002/btpr.539

Boycott AE (1920) Sedimentation of Blood Corpuscles. Nature 104(2621):532-532 doi:10.1038/104532b0

Brooke CB, Ince WL, Wrammert J, Ahmed R, Wilson PC, Bennink JR, Yewdell JW (2013) Most influenza a virions fail to express at least one essential viral protein. J Virol 87(6):3155-62 doi:10.1128/JVI.02284-12

Calder LJ, Wasilewski S, Berriman JA, Rosenthal PB (2010) Structural organization of a filamentous influenza A virus. Proc Natl Acad Sci U S A 107(23):10685-90 doi:10.1073/pnas.1002123107

Castro R, Fernandes P, Laske T, Sousa MF, Genzel Y, Scharfenberg K, Alves PM, Coroadinha AS (2015) Production of canine adenovirus type 2 in serum-free suspension cultures of MDCK cells. Appl Microbiol Biotechnol 99(17):7059-68 doi:10.1007/s00253-015-6636-8

Cattaneo MV, Spanjaard RA (2017) Perfusion filtration systems, US20190300833A1. US Patent,

Cattaneo R, Schmid A, Eschle D, Baczko K, ter Meulen V, Billeter MA (1988) Biased hypermutation and other genetic changes in defective measles viruses in human brain infections. Cell 55(2):255-65 doi:10.1016/0092-8674(88)90048-7

Chen C, Wong HE, Goudar CT (2018) Upstream process intensification and continuous manufacturing. Current Opinion in Chemical Engineering 22:191-198 doi:https://doi.org/10.1016/j.coche.2018.10.006

Chotteau V (2015) Perfusion Processes. In: Al-Rubeai M (ed) Animal Cell Culture. vol 9. Springer, Cham, Cell Engineering, pp 407-443

Chou YY, Vafabakhsh R, Doganay S, Gao Q, Ha T, Palese P (2012) One influenza virus particle packages eight unique viral RNAs as shown by FISH analysis. Proc Natl Acad Sci U S A 109(23):9101-6 doi:10.1073/pnas.1206069109

Chu C, Lugovtsev V, Golding H, Betenbaugh M, Shiloach J (2009) Conversion of MDCK cell line to suspension culture by transfecting with human siat7e gene and its application for influenza virus production. Proc Natl Acad Sci U S A 106(35):14802-7 doi:10.1073/pnas.0905912106

Cianci C, Tiley L, Krystal M (1995) Differential activation of the influenza virus polymerase via template RNA binding. J Virol 69(7):3995-9

Clincke M-F, Mölleryd C, Samani PK, Lindskog E, Fäldt E, Walsh K, Chotteau V (2013) Very high density of Chinese hamster ovary cells in perfusion by alternating tangential flow or tangential

flow filtration in WAVE bioreactor™—part II: Applications for antibody production and cryopreservation. Biotechnology Progress 29(3):768-777 doi:https://doi.org/10.1002/btpr.1703

Coahran DR, Buzzell A, Lauffer MA (1962) The effect of ultraviolet irradiation on nucleic acid isolated from tobacco mosaic virus. Biochim Biophys Acta 55:755-67 doi:10.1016/0006-3002(62)90854-5

Colman PM (2009) New antivirals and drug resistance. Annu Rev Biochem 78:95-118 doi:10.1146/annurev.biochem.78.082207.084029

Compans RW, Content J, Duesberg PH (1972) Structure of the ribonucleoprotein of influenza virus. J Virol 10(4):795-800 doi:10.1128/JVI.10.4.795-800.1972

Coronel J, Granicher G, Sandig V, Noll T, Genzel Y, Reichl U (2020) Application of an Inclined Settler for Cell Culture-Based Influenza A Virus Production in Perfusion Mode. Front Bioeng Biotechnol 8:672 doi:10.3389/fbioe.2020.00672

Cox MM, Patriarca PA, Treanor J (2008) FluBlok, a recombinant hemagglutinin influenza vaccine. Influenza Other Respir Viruses 2(6):211-9 doi:10.1111/j.1750-2659.2008.00053.x

Cros JF, Palese P (2003) Trafficking of viral genomic RNA into and out of the nucleus: influenza, Thogoto and Borna disease viruses. Virus Res 95(1-2):3-12 doi:10.1016/s0168-1702(03)00159-x

Davis AR, Nayak DP (1979) Sequence relationships among defective interfering influenza viral RNAs. Proc Natl Acad Sci U S A 76(7):3092-6 doi:10.1073/pnas.76.7.3092

De BK, Nayak DP (1980) Defective interfering influenza viruses and host cells: establishment and maintenance of persistent influenza virus infection in MDBK and HeLa cells. J Virol 36(3):847-59 doi:10.1128/JVI.36.3.847-859.1980

Deyde VM, Xu X, Bright RA, Shaw M, Smith CB, Zhang Y, Shu Y, Gubareva LV, Cox NJ, Klimov AI (2007) Surveillance of resistance to adamantanes among influenza A(H3N2) and A(H1N1) viruses isolated worldwide. J Infect Dis 196(2):249-57 doi:10.1086/518936

Dimmock NJ, Beck S, McLain L (1986) Protection of mice from lethal influenza: evidence that defective interfering virus modulates the immune response and not virus multiplication. J Gen Virol 67 (Pt 5):839-50 doi:10.1099/0022-1317-67-5-839

Dimmock NJ, Dove BK, Meng B, Scott PD, Taylor I, Cheung L, Hallis B, Marriott AC, Carroll MW, Easton AJ (2012) Comparison of the protection of ferrets against pandemic 2009 influenza A virus (H1N1) by 244 DI influenza virus and oseltamivir. Antiviral Res 96(3):376-85 doi:10.1016/j.antiviral.2012.09.017

Dimmock NJ, Easton AJ (2014) Defective interfering influenza virus RNAs: time to reevaluate their clinical potential as broad-spectrum antivirals? J Virol 88(10):5217-27 doi:10.1128/JVI.03193-13

Dimmock NJ, Easton AJ (2015) Cloned Defective Interfering Influenza RNA and a Possible Pan-Specific Treatment of Respiratory Virus Diseases. Viruses 7(7):3768-88 doi:10.3390/v7072796

Dimmock NJ, Rainsford EW, Scott PD, Marriott AC (2008) Influenza virus protecting RNA: an effective prophylactic and therapeutic antiviral. J Virol 82(17):8570-8 doi:10.1128/JVI.00743-08

Doroshenko A, Halperin SA (2009) Trivalent MDCK cell culture-derived influenza vaccine Optaflu® (Novartis Vaccines). Expert Review of Vaccines 8(6):679-688 doi:10.1586/erv.09.31

Dowd JE, Jubb A, Kwok KE, Piret JM (2003) Optimization and control of perfusion cultures using a viable cell probe and cell specific perfusion rates. Cytotechnology 42(1):35-45 doi:10.1023/A:1026192228471

Dowd JE, Kwok KE, Piret JM (2001) Glucose-based optimization of CHO-cell perfusion cultures. Biotechnol Bioeng 75(2):252-6 doi:10.1002/bit.10013

Ducommun P, Kadouri A, von Stockar U, Marison IW (2002) On-line determination of animal cell concentration in two industrial high-density culture processes by dielectric spectroscopy. Biotechnol Bioeng 77(3):316-23 doi:10.1002/bit.1197

Duhaut SD, Dimmock NJ (1998) Heterologous protection of mice from a lethal human H1N1 influenza A virus infection by H3N8 equine defective interfering virus: comparison of defective RNA sequences isolated from the DI inoculum and mouse lung. Virology 248(2):241-53 doi:10.1006/viro.1998.9267

Duhaut SD, Dimmock NJ (2002) Defective segment 1 RNAs that interfere with production of infectious influenza A virus require at least 150 nucleotides of 5' sequence: evidence from a plasmid-driven system. J Gen Virol 83(Pt 2):403-411 doi:10.1099/0022-1317-83-2-403

Duhaut SD, McCauley JW (1996) Defective RNAs inhibit the assembly of influenza virus genome segments in a segment-specific manner. Virology 216(2):326-37 doi:10.1006/viro.1996.0068

Easton AJ, Scott PD, Edworthy NL, Meng B, Marriott AC, Dimmock NJ (2011) A novel broad-spectrum treatment for respiratory virus infections: influenza-based defective interfering virus provides protection against pneumovirus infection in vivo. Vaccine 29(15):2777-84 doi:10.1016/j.vaccine.2011.01.102

Eaton MD, Scala AR (1961) Inhibitory effect of glutamine and ammonia on replication of influenza virus in ascites tumor cells. Virology 13:300-7 doi:10.1016/0042-6822(61)90149-0

Elsayed EA, Wagner R (2011) Application of hydrocyclones for continuous cultivation of SP-2/0 cells in perfusion bioreactors: Effect of hydrocyclone operating pressure. BMC Proceedings 5(8):P65 doi:10.1186/1753-6561-5-S8-P65

Enders JF, Weller TH, Robbins FC (1949) Cultivation of the Lansing Strain of Poliomyelitis Virus in Cultures of Various Human Embryonic Tissues. Science 109(2822):85-7 doi:10.1126/science.109.2822.85

Esclade LR, Carrel S, Peringer P (1991) Influence of the screen material on the fouling of spin filters. Biotechnol Bioeng 38(2):159-68 doi:10.1002/bit.260380208

Fineberg HV (2014) Pandemic preparedness and response--lessons from the H1N1 influenza of 2009. N Engl J Med 370(14):1335-42 doi:10.1056/NEJMra1208802

Fodor E (2013) The RNA polymerase of influenza a virus: mechanisms of viral transcription and replication. Acta Virol 57(2):113-22 doi:10.4149/av_2013_02_113

Fodor E, Pritlove DC, Brownlee GG (1994) The influenza virus panhandle is involved in the initiation of transcription. J Virol 68(6):4092-6 doi:10.1128/JVI.68.6.4092-4096.1994

Fournier E, Moules V, Essere B, Paillart JC, Sirbat JD, Isel C, Cavalier A, Rolland JP, Thomas D, Lina B, Marquet R (2012) A supramolecular assembly formed by influenza A virus genomic RNA segments. Nucleic Acids Res 40(5):2197-209 doi:10.1093/nar/gkr985

Frazzati-Gallina NM, Paoli RL, Mourao-Fuches RM, Jorge SA, Pereira CA (2001) Higher production of rabies virus in serum-free medium cell cultures on microcarriers. J Biotechnol 92(1):67-72 doi:10.1016/s0168-1656(01)00362-5

Frensing T (2015) Defective interfering viruses and their impact on vaccines and viral vectors. Biotechnol J 10(5):681-9 doi:10.1002/biot.201400429

Frensing T, Heldt FS, Pflugmacher A, Behrendt I, Jordan I, Flockerzi D, Genzel Y, Reichl U (2013) Continuous Influenza Virus Production in Cell Culture Shows a Periodic Accumulation of Defective Interfering Particles. Plos One 8(9) doi:ARTN e72288 10.1371/journal.pone.0072288

Frensing T, Pflugmacher A, Bachmann M, Peschel B, Reichl U (2014) Impact of defective interfering particles on virus replication and antiviral host response in cell culture-based influenza vaccine production. Appl Microbiol Biotechnol 98(21):8999-9008 doi:10.1007/s00253-014-5933-y

Fujii Y, Goto H, Watanabe T, Yoshida T, Kawaoka Y (2003) Selective incorporation of influenza virus RNA segments into virions. Proc Natl Acad Sci U S A 100(4):2002-7 doi:10.1073/pnas.0437772100

Gallo-Ramirez LE, Nikolay A, Genzel Y, Reichl U (2015) Bioreactor concepts for cell culture-based viral vaccine production. Expert Rev Vaccines 14(9):1181-95 doi:10.1586/14760584.2015.1067144

Gaush CR, Hard WL, Smith TF (1966) Characterization of an established line of canine kidney cells (MDCK). Proc Soc Exp Biol Med 122(3):931-5 doi:10.3181/00379727-122-31293

Genzel Y, Behrendt I, Rodig J, Rapp E, Kueppers C, Kochanek S, Schiedner G, Reichl U (2013) CAP, a new human suspension cell line for influenza virus production. Appl Microbiol Biotechnol 97(1):111-22 doi:10.1007/s00253-012-4238-2

Genzel Y, Dietzsch C, Rapp E, Schwarzer J, Reichl U (2010) MDCK and Vero cells for influenza virus vaccine production: a one-to-one comparison up to lab-scale bioreactor cultivation. Appl Microbiol Biotechnol 88(2):461-75 doi:10.1007/s00253-010-2742-9

Genzel Y, Olmer RM, Schafer B, Reichl U (2006) Wave microcarrier cultivation of MDCK cells for influenza virus production in serum containing and serum-free media. Vaccine 24(35-36):6074-87 doi:10.1016/j.vaccine.2006.05.023

Genzel Y, Reichl U (2007) Vaccine Production. In: Pörtner R (ed) Animal Cell Biotechnology: Methods and Protocols. Humana Press, Totowa, NJ, pp 457-473

Genzel Y, Reichl U (2009) Continuous cell lines as a production system for influenza vaccines. Expert Rev Vaccines 8(12):1681-92 doi:10.1586/erv.09.128

Genzel Y, Vogel T, Buck J, Behrendt I, Ramirez DV, Schiedner G, Jordan I, Reichl U (2014) High cell density cultivations by alternating tangential flow (ATF) perfusion for influenza A virus production using suspension cells. Vaccine 32(24):2770-81 doi:10.1016/j.vaccine.2014.02.016

Giachetti C, Holland JJ (1988) Altered replicase specificity is responsible for resistance to defective interfering particle interference of an Sdi- mutant of vesicular stomatitis virus. J Virol 62(10):3614-21 doi:10.1128/JVI.62.10.3614-3621.1988

Golob JL, Lugogo N, Lauring AS, Lok AS (2021) SARS-CoV-2 vaccines: a triumph of science and collaboration. JCI Insight 6(9) doi:10.1172/jci.insight.149187

Gorenflo VM, Chow VS, Chou C, Piret JM (2005) Optical analysis of perfusion bioreactor cell concentration in an acoustic separator. Biotechnol Bioeng 92(4):514-8 doi:10.1002/bit.20693

Goto H, Kawaoka Y (1998) A novel mechanism for the acquisition of virulence by a human influenza A virus. Proc Natl Acad Sci U S A 95(17):10224-8 doi:10.1073/pnas.95.17.10224

Granicher G, Coronel J, Trampler F, Jordan I, Genzel Y, Reichl U (2020) Performance of an acoustic settler versus a hollow fiber-based ATF technology for influenza virus production in perfusion. Appl Microbiol Biotechnol 104(11):4877-4888 doi:10.1007/s00253-020-10596-x

Granicher G, Tapia F, Behrendt I, Jordan I, Genzel Y, Reichl U (2021) Production of Modified Vaccinia Ankara Virus by Intensified Cell Cultures: A Comparison of Platform Technologies for Viral Vector Production. Biotechnol J 16(1):e2000024 doi:10.1002/biot.202000024

Grohskopf LA, Alyanak E, Broder KR, Blanton LH, Fry AM, Jernigan DB, Atmar RL (2020) Prevention and Control of Seasonal Influenza with Vaccines: Recommendations of the Advisory Committee on Immunization Practices - United States, 2020-21 Influenza Season. MMWR Recomm Rep 69(8):1-24 doi:10.15585/mmwr.rr6908a1

Gröner A, Vorlop J (1996) Animal cells and processes for the replication of influenza viruses US Patent,

Gubareva LV, Trujillo AA, Okomo-Adhiambo M, Mishin VP, Deyde VM, Sleeman K, Nguyen HT, Sheu TG, Garten RJ, Shaw MW, Fry AM, Klimov AI (2010) Comprehensive assessment of 2009 pandemic influenza A (H1N1) virus drug susceptibility in vitro. Antivir Ther 15(8):1151-9 doi:10.3851/IMP1678

Guy B, Guirakhoo F, Barban V, Higgs S, Monath TP, Lang J (2010) Preclinical and clinical development of YFV 17D-based chimeric vaccines against dengue, West Nile and Japanese encephalitis viruses. Vaccine 28(3):632-49 doi:10.1016/j.vaccine.2009.09.098

Hagen M, Chung TD, Butcher JA, Krystal M (1994) Recombinant influenza virus polymerase: requirement of both 5' and 3' viral ends for endonuclease activity. J Virol 68(3):1509-15

Hampson AW, Mackenzie JS (2006) The influenza viruses. Med J Aust 185(S10):S39-43 doi:10.5694/j.1326-5377.2006.tb00705.x

Han J, Perez J, Schafer A, Cheng H, Peet N, Rong L, Manicassamy B (2018) Influenza Virus: Small Molecule Therapeutics and Mechanisms of Antiviral Resistance. Curr Med Chem 25(38):5115-5127 doi:10.2174/0929867324666170920165926

Handa-Corrigan A, Nikolay S, Jeffery D, Heffernan B, Young A (1992) Controlling and predicting monoclonal antibody production in hollow-fiber bioreactors. Enzyme and Microbial Technology 14(1):58-63 doi:https://doi.org/10.1016/0141-0229(92)90027-L

Harding AT, Heaton NS (2018) Efforts to Improve the Seasonal Influenza Vaccine. Vaccines (Basel) 6(2) doi:10.3390/vaccines6020019

Harris A, Cardone G, Winkler DC, Heymann JB, Brecher M, White JM, Steven AC (2006) Influenza virus pleiomorphy characterized by cryoelectron tomography. Proc Natl Acad Sci U S A 103(50):19123-7 doi:10.1073/pnas.0607614103

Harty RN, Holden VR, O'Callaghan DJ (1993) Transcriptional and translational analyses of the UL2 gene of equine herpesvirus 1: a homolog of UL55 of herpes simplex virus type 1 that is maintained in the genome of defective interfering particles. J Virol 67(4):2255-65 doi:10.1128/JVI.67.4.2255-2265.1993

Hassanzadeh SM, Zavareh A, Shokrgozar MA, Ramezani A, Fayaz A (2011) High vero cell density and rabies virus proliferation on fibracel disks versus cytodex-1 in spinner flask. Pak J Biol Sci 14(7):441-8 doi:10.3923/pjbs.2011.441.448

Hegde NR (2015) Cell culture-based influenza vaccines: A necessary and indispensable investment for the future. Hum Vaccin Immunother 11(5):1223-34 doi:10.1080/21645515.2015.1016666

Heidemann R, Zhang C, Qi H, Larrick Rule J, Rozales C, Park S, Chuppa S, Ray M, Michaels J, Konstantinov K, Naveh D (2000) The use of peptones as medium additives for the production of a recombinant therapeutic protein in high density perfusion cultures of mammalian cells. Cytotechnology 32(2):157-167 doi:10.1023/A:1008196521213

Hein MD, Arora P, Marichal-Gallardo P, Winkler M, Genzel Y, Poehlmann S, Schughart K, Kupke SY, Reichl U (2021a) Cell culture-based production and in vivo characterization of purely clonal defective interfering influenza virus particles. BMC Biol 19(1):91 doi:10.1186/s12915-021-01020-5

Hein MD, Chawla A, Cattaneo M, Kupke SY, Genzel Y, Reichl U (2021b) Cell culture-based production of defective interfering influenza A virus particles in perfusion mode using an alternating tangential flow filtration system. Appl Microbiol Biotechnol 105(19):7251-7264 doi:10.1007/s00253-021-11561-y

Hein MD, Kollmus H, Marichal-Gallardo P, Puttker S, Benndorf D, Genzel Y, Schughart K, Kupke SY, Reichl U (2021c) OP7, a novel influenza A virus defective interfering particle: production, purification, and animal experiments demonstrating antiviral potential. Appl Microbiol Biotechnol 105(1):129-146 doi:10.1007/s00253-020-11029-5

Henao-Restrepo AM, Camacho A, Longini IM, Watson CH, Edmunds WJ, Egger M, Carroll MW, Dean NE, Diatta I, Doumbia M, Draguez B, Duraffour S, Enwere G, Grais R, Gunther S, Gsell PS, Hossmann S, Watle SV, Konde MK, Keita S, Kone S, Kuisma E, Levine MM, Mandal S, Mauget T, Norheim G, Riveros X, Soumah A, Trelle S, Vicari AS, Rottingen JA, Kieny MP (2017) Efficacy and effectiveness of an rVSV-vectored vaccine in preventing Ebola virus disease: final results from the Guinea ring vaccination, open-label, cluster-randomised trial (Ebola Ca Suffit!). Lancet 389(10068):505-518 doi:10.1016/S0140-6736(16)32621-6

Hiller GW, Clark DS, Blanch HW (1993) Cell retention-chemostat studies of hybridoma cells-analysis of hybridoma growth and metabolism in continuous suspension culture in serum-free medium. Biotechnol Bioeng 42(2):185-95 doi:10.1002/bit.260420206

Hoffmann E, Neumann G, Kawaoka Y, Hobom G, Webster RG (2000) A DNA transfection system for generation of influenza A virus from eight plasmids. Proc Natl Acad Sci U S A 97(11):6108-13 doi:10.1073/pnas.100133697

Hoffmann E, Stech J, Guan Y, Webster RG, Perez DR (2001) Universal primer set for the full-length amplification of all influenza A viruses. Arch Virol 146(12):2275-89 doi:10.1007/s007050170002

Hu AY, Weng TC, Tseng YF, Chen YS, Wu CH, Hsiao S, Chou AH, Chao HJ, Gu A, Wu SC, Chong P, Lee MS (2008) Microcarrier-based MDCK cell culture system for the production of influenza H5N1 vaccines. Vaccine 26(45):5736-40 doi:10.1016/j.vaccine.2008.08.015

Huang AS, Baltimore D (1970) Defective viral particles and viral disease processes. Nature 226(5243):325-7 doi:10.1038/226325a0

Huang D, Peng WJ, Ye Q, Liu XP, Zhao L, Fan L, Xia-Hou K, Jia HJ, Luo J, Zhou LT, Li BB, Wang SL, Xu WT, Chen Z, Tan WS (2015) Serum-Free Suspension Culture of MDCK Cells for Production of Influenza H1N1 Vaccines. PLoS One 10(11):e0141686 doi:10.1371/journal.pone.0141686

Huang D, Zhao L, Tan W (2011) [Adherent and single-cell suspension culture of Madin-Darby canine kidney cells in serum-free medium]. Sheng Wu Gong Cheng Xue Bao 27(4):645-52

Hundt B, Molle N, Stefaniak S, Durrwald R, Weyand J (2011) Large pilot scale cultivation process study of adherent MDBK cells for porcine Influenza A virus propagation using a novel disposable stirred-tank bioreactor. BMC Proc 5 Suppl 8:P128 doi:10.1186/1753-6561-5-S8-P128

Huo C, Cheng J, Xiao J, Chen M, Zou S, Tian H, Wang M, Sun L, Hao Z, Hu Y (2020) Defective Viral Particles Produced in Mast Cells Can Effectively Fight Against Lethal Influenza A Virus. Front Microbiol 11:553274 doi:10.3389/fmicb.2020.553274

Hutchinson EC, von Kirchbach JC, Gog JR, Digard P (2010) Genome packaging in influenza A virus. J Gen Virol 91(Pt 2):313-28 doi:10.1099/vir.0.017608-0

Hutter J, Rodig JV, Hoper D, Seeberger PH, Reichl U, Rapp E, Lepenies B (2013) Toward animal cell culture-based influenza vaccine design: viral hemagglutinin N-glycosylation markedly impacts immunogenicity. J Immunol 190(1):220-30 doi:10.4049/jimmunol.1201060

Iuliano AD, Roguski KM, Chang HH, Muscatello DJ, Palekar R, Tempia S, Cohen C, Gran JM, Schanzer D, Cowling BJ, Wu P, Kyncl J, Ang LW, Park M, Redlberger-Fritz M, Yu H, Espenhain L, Krishnan A, Emukule G, van Asten L, Pereira da Silva S, Aungkulanon S, Buchholz U, Widdowson MA, Bresee JS, Global Seasonal Influenza-associated Mortality Collaborator N (2018) Estimates of global seasonal influenza-associated respiratory mortality: a modelling study. Lancet 391(10127):1285-1300 doi:10.1016/S0140-6736(17)33293-2

Jang J, Bae S-E (2018) Comparative Co-Evolution Analysis Between the HA and NA Genes of Influenza A Virus. Virology: Research and Treatment 9:1178122X18788328 doi:10.1177/1178122X18788328

Jaworski E, Routh A (2017) Parallel ClickSeq and Nanopore sequencing elucidates the rapid evolution of defective-interfering RNAs in Flock House virus. PLoS Pathog 13(5):e1006365 doi:10.1371/journal.ppat.1006365

Jennings PA, Finch JT, Winter G, Robertson JS (1983) Does the higher order structure of the influenza virus ribonucleoprotein guide sequence rearrangements in influenza viral RNA? Cell 34(2):619-27 doi:10.1016/0092-8674(83)90394-x

Jericevic Z, Kucan I, Chambers RW (1982) Photochemical cleavage of phosphodiester bonds in oligoribonucleotides. Biochemistry 21(25):6563-7 doi:10.1021/bi00268a037

Johnson M, Lanthier S, Massie B, Lefebvre G, Kamen AA (1996) Use of the Centritech Lab Centrifuge for Perfusion Culture of Hybridoma Cells in Protein-Free Medium. Biotechnology Progress 12(6):855-864 doi:https://doi.org/10.1021/bp960072n

Johnson NP, Mueller J (2002) Updating the accounts: global mortality of the 1918-1920 "Spanish" influenza pandemic. Bull Hist Med 76(1):105-15 doi:10.1353/bhm.2002.0022

Jorba N, Coloma R, Ortin J (2009) Genetic trans-complementation establishes a new model for influenza virus RNA transcription and replication. PLoS Pathog 5(5):e1000462 doi:10.1371/journal.ppat.1000462

Kalbfuss B, Knochlein A, Krober T, Reichl U (2008) Monitoring influenza virus content in vaccine production: precise assays for the quantitation of hemagglutination and neuraminidase activity. Biologicals 36(3):145-61

Kärber G (1931) Beitrag zur kollektiven Behandlung pharmakologischer Reihenversuche. Naunyn-Schmiedebergs Archiv für experimentelle Pathologie und Pharmakologie 162(4):480-483 doi:10.1007/BF01863914

Karst DJ, Serra E, Villiger TK, Soos M, Morbidelli M (2016) Characterization and comparison of ATF and TFF in stirred bioreactors for continuous mammalian cell culture processes. Biochemical Engineering Journal 110:17-26 doi:https://doi.org/10.1016/j.bej.2016.02.003

Karst DJ, Steinebach F, Soos M, Morbidelli M (2017a) Process performance and product quality in an integrated continuous antibody production process. Biotechnol Bioeng 114(2):298-307 doi:10.1002/bit.26069

Karst DJ, Steinhoff RF, Kopp MRG, Serra E, Soos M, Zenobi R, Morbidelli M (2017b) Intracellular CHO Cell Metabolite Profiling Reveals Steady-State Dependent Metabolic Fingerprints in Perfusion Culture. Biotechnol Prog 33(4):879-890 doi:10.1002/btpr.2421

Kawahara H, Mitsuda S, Kumazawa E, Takeshita Y (1994) High-density culture of FM-3A cells using a bioreactor with an external tangential-flow filtration device. Cytotechnology 14(1):61-6 doi:10.1007/BF00772196

Kawakami E, Watanabe T, Fujii K, Goto H, Watanabe S, Noda T, Kawaoka Y (2011) Strand-specific real-time RT-PCR for distinguishing influenza vRNA, cRNA, and mRNA. J Virol Methods 173(1):1-6 doi:10.1016/j.jviromet.2010.12.014

Kelley B (2009) Industrialization of mAb production technology: the bioprocessing industry at a crossroads. MAbs 1(5):443-52 doi:10.4161/mabs.1.5.9448

Killip MJ, Young DF, Gatherer D, Ross CS, Short JA, Davison AJ, Goodbourn S, Randall RE (2013) Deep sequencing analysis of defective genomes of parainfluenza virus 5 and their role in interferon induction. J Virol 87(9):4798-807 doi:10.1128/JVI.03383-12

Kirnbauer R, Booy F, Cheng N, Lowy DR, Schiller JT (1992) Papillomavirus L1 major capsid protein self-assembles into virus-like particles that are highly immunogenic. Proc Natl Acad Sci U S A 89(24):12180-4 doi:10.1073/pnas.89.24.12180

Konstantinov K, Goudar C, Ng M, Meneses R, Thrift J, Chuppa S, Matanguihan C, Michaels J, Naveh D (2006) The "push-to-low" approach for optimization of high-density perfusion cultures of animal cells. Adv Biochem Eng Biotechnol 101:75-98 doi:10.1007/10_016

Konstantinov KB, Cooney CL (2015) White Paper on Continuous Bioprocessing May 20–21 2014 Continuous Manufacturing Symposium. Journal of Pharmaceutical Sciences 104(3):813-820 doi:https://doi.org/10.1002/jps.24268

Krammer F, Smith GJD, Fouchier RAM, Peiris M, Kedzierska K, Doherty PC, Palese P, Shaw ML, Treanor J, Webster RG, García-Sastre A (2018) Influenza. Nature Reviews Disease Primers 4(1):3 doi:10.1038/s41572-018-0002-y

Kupke SY (2020) Single-cell analysis of influenza A virus replication : sources of cell-to-cell heterogeneity and discoverey of a novel type of defective interfering particle,

Kupke SY, Riedel D, Frensing T, Zmora P, Reichl U (2019) A Novel Type of Influenza A Virus-Derived Defective Interfering Particle with Nucleotide Substitutions in Its Genome. J Virol 93(4) doi:10.1128/JVI.01786-18

Kyung YS, Peshwa MV, Gryte DM, Hu WS (1994) High density culture of mammalian cells with dynamic perfusion based on on-line oxygen uptake rate measurements. Cytotechnology 14(3):183-90 doi:10.1007/BF00749615

Lackenby A, Besselaar TG, Daniels RS, Fry A, Gregory V, Gubareva LV, Huang W, Hurt AC, Leang SK, Lee RTC, Lo J, Lollis L, Maurer-Stroh S, Odagiri T, Pereyaslov D, Takashita E, Wang D, Zhang W, Meijer A (2018) Global update on the susceptibility of human influenza viruses to neuraminidase inhibitors and status of novel antivirals, 2016-2017. Antiviral Res 157:38-46 doi:10.1016/j.antiviral.2018.07.001

Laske T, Heldt FS, Hoffmann H, Frensing T, Reichl U (2016) Modeling the intracellular replication of influenza A virus in the presence of defective interfering RNAs. Virus Res 213:90-99 doi:10.1016/j.virusres.2015.11.016

Lazzarini RA, Keene JD, Schubert M (1981) The origins of defective interfering particles of the negative-strand RNA viruses. Cell 26(2 Pt 2):145-54 doi:10.1016/0092-8674(81)90298-1

Li D, Aaskov J (2014) Sub-genomic RNA of defective interfering (D.I.) dengue viral particles is replicated in the same manner as full length genomes. Virology 468-470:248-255 doi:10.1016/j.virol.2014.08.013

Linder A, Bothe V, Linder N, Schwarzlmueller P, Dahlstrom F, Bartenhagen C, Dugas M, Pandey D, Thorn-Seshold J, Boehmer DFR, Koenig LM, Kobold S, Schnurr M, Raedler J, Spielmann G, Karimzadeh H, Schmidt A, Endres S, Rothenfusser S (2021) Defective Interfering Genomes and the Full-Length Viral Genome Trigger RIG-I After Infection With Vesicular Stomatitis Virus in a Replication Dependent Manner. Front Immunol 12:595390 doi:10.3389/fimmu.2021.595390

Liu J, Shi X, Schwartz R, Kemble G (2009) Use of MDCK cells for production of live attenuated influenza vaccine. Vaccine 27(46):6460-3 doi:10.1016/j.vaccine.2009.06.024

Lohr V, Genzel Y, Behrendt I, Scharfenberg K, Reichl U (2010) A new MDCK suspension line cultivated in a fully defined medium in stirred-tank and wave bioreactor. Vaccine 28(38):6256-64 doi:10.1016/j.vaccine.2010.07.004

Lohr V, Rath A, Genzel Y, Jordan I, Sandig V, Reichl U (2009) New avian suspension cell lines provide production of influenza virus and MVA in serum-free media: studies on growth, metabolism and virus propagation. Vaccine 27(36):4975-82 doi:10.1016/j.vaccine.2009.05.083

Lopez CB (2014) Defective viral genomes: critical danger signals of viral infections. J Virol 88(16):8720-3 doi:10.1128/JVI.00707-14

Losa J (2018) Packed-bed reactors for the production of yellow fever virus vaccines. Max Planck Institute Magdeburg

Lundquist RE, Sullivan M, Maizel JV, Jr. (1979) Characterization of a new isolate of poliovirus defective interfering particles. Cell 18(3):759-69 doi:10.1016/0092-8674(79)90129-6

Marichal-Gallardo P, Borner K, Pieler MM, Sonntag-Buck V, Obr M, Bejarano D, Wolff MW, Krausslich HG, Reichl U, Grimm D (2021) Single-Use Capture Purification of Adeno-Associated Viral Gene Transfer Vectors by Membrane-Based Steric Exclusion Chromatography. Hum Gene Ther 32(17-18):959-974 doi:10.1089/hum.2019.284

Marichal-Gallardo P, Pieler MM, Wolff MW, Reichl U (2017) Steric exclusion chromatography for purification of cell culture-derived influenza A virus using regenerated cellulose membranes and polyethylene glycol. J Chromatogr A 1483:110-119 doi:10.1016/j.chroma.2016.12.076

Matlin KS, Reggio H, Helenius A, Simons K (1981) Infectious entry pathway of influenza virus in a canine kidney cell line. J Cell Biol 91(3 Pt 1):601-13 doi:10.1083/jcb.91.3.601

Matsuzaki Y, Katsushima N, Nagai Y, Shoji M, Itagaki T, Sakamoto M, Kitaoka S, Mizuta K, Nishimura H (2006) Clinical features of influenza C virus infection in children. J Infect Dis 193(9):1229-35 doi:10.1086/502973

Meijer A, Lackenby A, Hungnes O, Lina B, van-der-Werf S, Schweiger B, Opp M, Paget J, van-de-Kassteele J, Hay A, Zambon M, European Influenza Surveillance S (2009) Oseltamivir-resistant influenza virus A (H1N1), Europe, 2007-08 season. Emerg Infect Dis 15(4):552-60 doi:10.3201/eid1504.181280

Mendes M, Russell AB (2021) Library-based analysis reveals segment and length dependent characteristics of defective influenza genomes. bioRxiv:2021.09.06.459165 doi:10.1101/2021.09.06.459165

Mercille S, Johnson M, Lemieux R, Massie B (1994) Filtration-based perfusion of hybridoma cultures in protein-free medium: Reduction of membrane fouling by medium supplementation with DNase I. Biotechnol Bioeng 43(9):833-46 doi:10.1002/bit.260430902

Meuwly F, Papp F, Ruffieux PA, Bernard AR, Kadouri A, von Stockar U (2006) Use of glucose consumption rate (GCR) as a tool to monitor and control animal cell production processes in packed-bed bioreactors. J Biotechnol 122(1):122-9 doi:10.1016/j.jbiotec.2005.08.005

Milian E, Kamen AA (2015) Current and emerging cell culture manufacturing technologies for influenza vaccines. Biomed Res Int 2015:504831 doi:10.1155/2015/504831

Mura M, Combredet C, Najburg V, Sanchez David RY, Tangy F, Komarova AV (2017) Nonencapsidated 5' Copy-Back Defective Interfering Genomes Produced by Recombinant Measles Viruses Are Recognized by RIG-I and LGP2 but Not MDA5. J Virol 91(20) doi:10.1128/JVI.00643-17

Nakatsu S, Sagara H, Sakai-Tagawa Y, Sugaya N, Noda T, Kawaoka Y (2016) Complete and Incomplete Genome Packaging of Influenza A and B Viruses. mBio 7(5) doi:10.1128/mBio.01248-16

Naruse T, Fukuda T, Tanabe T, Ichikawa M, Oda Y, Tochihara S, Kimachi K, Kino Y, Ueda K (2015) A clinical phase I study of an EB66 cell-derived H5N1 pandemic vaccine adjuvanted with AS03. Vaccine 33(45):6078-84 doi:10.1016/j.vaccine.2015.09.022

Nayak DP, Chambers TM, Akkina RK (1985) Defective-interfering (DI) RNAs of influenza viruses: origin, structure, expression, and interference. Curr Top Microbiol Immunol 114:103-51 doi:10.1007/978-3-642-70227-3_3

Nayak DP, Hui EK, Barman S (2004) Assembly and budding of influenza virus. Virus Res 106(2):147-65 doi:10.1016/j.virusres.2004.08.012

Nerome K, Ishida M (1978) The multiplication of an influenza C virus in an established line of canine kidney (MDCK) cells. J Gen Virol 39(1):179-81 doi:10.1099/0022-1317-39-1-179

Nikolay A, Bissinger T, Granicher G, Wu Y, Genzel Y, Reichl U (2020a) Perfusion Control for High Cell Density Cultivation and Viral Vaccine Production. Methods Mol Biol 2095:141-168 doi:10.1007/978-1-0716-0191-4_9

Nikolay A, de Grooth J, Genzel Y, Wood JA, Reichl U (2020b) Virus harvesting in perfusion culture: Choosing the right type of hollow fiber membrane. Biotechnol Bioeng 117(10):3040-3052 doi:10.1002/bit.27470

Nikolay A, Leon A, Schwamborn K, Genzel Y, Reichl U (2018) Process intensification of EB66(R) cell cultivations leads to high-yield yellow fever and Zika virus production. Appl Microbiol Biotechnol 102(20):8725-8737 doi:10.1007/s00253-018-9275-z

Noda T, Kawaoka Y (2012) Packaging of influenza virus genome: robustness of selection. Proc Natl Acad Sci U S A 109(23):8797-8 doi:10.1073/pnas.1206736109

Noda T, Sagara H, Yen A, Takada A, Kida H, Cheng RH, Kawaoka Y (2006) Architecture of ribonucleoprotein complexes in influenza A virus particles. Nature 439(7075):490-2 doi:10.1038/nature04378

Noh JY, Kim WJ (2013) Influenza vaccines: unmet needs and recent developments. Infect Chemother 45(4):375-86 doi:10.3947/ic.2013.45.4.375

Noll T, Biselli M (1998) Dielectric spectroscopy in the cultivation of suspended and immobilized hybridoma cells. J Biotechnol 63(3):187-98 doi:10.1016/s0168-1656(98)00080-7

Odagiri T, Tashiro M (1997) Segment-specific noncoding sequences of the influenza virus genome RNA are involved in the specific competition between defective interfering RNA and its progenitor RNA segment at the virion assembly step. J Virol 71(3):2138-45

Olsen B, Munster VJ, Wallensten A, Waldenström J, Osterhaus ADME, Fouchier RAM (2006) Global Patterns of Influenza A Virus in Wild Birds. Science 312(5772):384 doi:10.1126/science.1122438

Opitz L, Salaklang J, Buttner H, Reichl U, Wolff MW (2007) Lectin-affinity chromatography for downstream processing of MDCK cell culture derived human influenza A viruses. Vaccine 25(5):939-47 doi:10.1016/j.vaccine.2006.08.043

Oxford JS (2007) Antivirals for the treatment and prevention of epidemic and pandemic influenza. Influenza Other Respir Viruses 1(1):27-34 doi:10.1111/j.1750-2659.2006.00006.x

Ozturk SS (1996) Engineering challenges in high density cell culture systems. Cytotechnology 22(1-3):3-16 doi:10.1007/BF00353919

Pau MG, Ophorst C, Koldijk MH, Schouten G, Mehtali M, Uytdehaag F (2001) The human cell line PER.C6 provides a new manufacturing system for the production of influenza vaccines. Vaccine 19(17-19):2716-21 doi:10.1016/s0264-410x(00)00508-9

Paules CI, Sullivan SG, Subbarao K, Fauci AS (2018) Chasing Seasonal Influenza - The Need for a Universal Influenza Vaccine. N Engl J Med 378(1):7-9 doi:10.1056/NEJMp1714916

Pelz L, Ruediger D, Dogra T, Alnaji FG, Genzel Y, Brooke CB, Kupke SY, Reichl U (2021) Semi-continuous propagation of influenza A virus and its defective interfering particles: analyzing the dynamic competition to select candidates for antiviral therapy. J Virol:JVI0117421 doi:10.1128/JVI.01174-21

Perez Rubio A, Eiros JM (2018) Cell culture-derived flu vaccine: Present and future. Hum Vaccin Immunother 14(8):1874-1882 doi:10.1080/21645515.2018.1460297

Perrault J (1981) Origin and replication of defective interfering particles. Curr Top Microbiol Immunol 93:151-207 doi:10.1007/978-3-642-68123-3_7

Peschel B, Frentzel S, Laske T, Genzel Y, Reichl U (2013) Comparison of influenza virus yields and apoptosis-induction in an adherent and a suspension MDCK cell line. Vaccine 31(48):5693-9 doi:10.1016/j.vaccine.2013.09.051

Petiot E, El-Wajgali A, Esteban G, Geny C, Pinton H, Marc A (2012) Real-time monitoring of adherent Vero cell density and apoptosis in bioreactor processes. Cytotechnology 64(4):429-41 doi:10.1007/s10616-011-9421-2

Pieler MM, Heyse A, Wolff MW, Reichl U (2017) Specific ion effects on the particle size distributions of cell culture-derived influenza A virus particles within the Hofmeister series. Eng Life Sci 17(5):470-478 doi:10.1002/elsc.201600153

Ping J, Lopes TJS, Nidom CA, Ghedin E, Macken CA, Fitch A, Imai M, Maher EA, Neumann G, Kawaoka Y (2015) Development of high-yield influenza A virus vaccine viruses. Nat Commun 6:8148 doi:10.1038/ncomms9148

Pinto RCV, Medronho RA, Castilho LR (2008) Separation of CHO cells using hydrocyclones. Cytotechnology 56(1):57-67 doi:10.1007/s10616-007-9108-x

Plotkin S (2014) History of vaccination. Proc Natl Acad Sci U S A 111(34):12283-7 doi:10.1073/pnas.1400472111

Pohlscheidt M, Langer U, Minuth T, Bodeker B, Apeler H, Horlein HD, Paulsen D, Rubsamen-Waigmann H, Henzler HJ, Reichl U (2008) Development and optimisation of a procedure for the production of Parapoxvirus ovis by large-scale microcarrier cell culture in a non-animal, non-human and non-plant-derived medium. Vaccine 26(12):1552-65 doi:10.1016/j.vaccine.2008.01.032

Pollock J, Ho SV, Farid SS (2013) Fed-batch and perfusion culture processes: economic, environmental, and operational feasibility under uncertainty. Biotechnol Bioeng 110(1):206-19 doi:10.1002/bit.24608

Rajendran R, Lingala R, Vuppu SK, Bandi BO, Manickam E, Macherla SR, Dubois S, Havelange N, Maithal K (2014) Assessment of packed bed bioreactor systems in the production of viral vaccines. AMB Express 4:25 doi:10.1186/s13568-014-0025-z

Raman S, Brian DA (2005) Stem-loop IV in the 5' untranslated region is a cis-acting element in bovine coronavirus defective interfering RNA replication. J Virol 79(19):12434-46 doi:10.1128/JVI.79.19.12434-12446.2005

Rand U, Kupke SY, Shkarlet H, Hein MD, Hirsch T, Marichal-Gallardo P, Cicin-Sain L, Reichl U, Bruder D (2021) Antiviral Activity of Influenza A Virus Defective Interfering Particles against SARS-CoV-2 Replication In Vitro through Stimulation of Innate Immunity. Cells 10(7) doi:10.3390/cells10071756

Rehwinkel J, Tan CP, Goubau D, Schulz O, Pichlmair A, Bier K, Robb N, Vreede F, Barclay W, Fodor E, Reis e Sousa C (2010) RIG-I detects viral genomic RNA during negative-strand RNA virus infection. Cell 140(3):397-408 doi:10.1016/j.cell.2010.01.020

Reiter M, Mundt W (2005) Method for large scale production of virus antigen, US6951752B2. US Patent,

Remsen JF, Miller N, Cerutti PA (1970) Photohydration of uridine in the RNA of coliphage R17. II. The relationship between ultraviolet inactivation and uridine photohydration. Proc Natl Acad Sci U S A 65(2):460-6 doi:10.1073/pnas.65.2.460

Rey M, Girard MP (2008) The global eradication of poliomyelitis: progress and problems. Comp Immunol Microbiol Infect Dis 31(2-3):317-25 doi:10.1016/j.cimid.2007.07.013

Richard M, van den Brand JMA, Bestebroer TM, Lexmond P, de Meulder D, Fouchier RAM, Lowen AC, Herfst S (2020) Influenza A viruses are transmitted via the air from the nasal respiratory epithelium of ferrets. Nat Commun 11(1):766 doi:10.1038/s41467-020-14626-0

Rimmelzwaan GF, Kuiken T, van Amerongen G, Bestebroer TM, Fouchier RA, Osterhaus AD (2001) Pathogenesis of influenza A (H5N1) virus infection in a primate model. J Virol 75(14):6687-91 doi:10.1128/JVI.75.14.6687-6691.2001

Robertson JS, Schubert M, Lazzarini RA (1981) Polyadenylation sites for influenza virus mRNA. J Virol 38(1):157-63 doi:10.1128/JVI.38.1.157-163.1981

Rourou S, Ben Ayed Y, Trabelsi K, Majoul S, Kallel H (2014) An animal component free medium that promotes the growth of various animal cell lines for the production of viral vaccines. Vaccine 32(24):2767-9 doi:10.1016/j.vaccine.2014.02.040

Ruediger D, Pelz L, Hein MD, Kupke SY, Reichl U (2021) Multiscale model of defective interfering particle replication for influenza A virus infection in animal cell culture. PLoS Comput Biol 17(9):e1009357 doi:10.1371/journal.pcbi.1009357

Rumschlag-Booms E, Rong L (2013) Influenza a virus entry: implications in virulence and future therapeutics. Adv Virol 2013:121924 doi:10.1155/2013/121924

Salk JE, Suriano PC (1949) Importance of antigenic composition of influenza virus vaccine in protecting against the natural disease; observations during the winter of 1947-1948. Am J Public Health Nations Health 39(3):345-55 doi:10.2105/ajph.39.3.345

Schubert M, Lazzarini RA (1981) Structure and origin of a snapback defective interfering particle RNA of vesicular stomatitis virus. J Virol 37(2):661-72 doi:10.1128/JVI.37.2.661-672.1981

Scott PD, Meng B, Marriott AC, Easton AJ, Dimmock NJ (2011) Defective interfering influenza A virus protects in vivo against disease caused by a heterologous influenza B virus. J Gen Virol 92(Pt 9):2122-32 doi:10.1099/vir.0.034132-0

Seitz C, Frensing T, Hoper D, Kochs G, Reichl U (2010) High yields of influenza A virus in Madin-Darby canine kidney cells are promoted by an insufficient interferon-induced antiviral state. J Gen Virol 91(Pt 7):1754-63 doi:10.1099/vir.0.020370-0

Seitz C, Isken B, Heynisch B, Rettkowski M, Frensing T, Reichl U (2012) Trypsin promotes efficient influenza vaccine production in MDCK cells by interfering with the antiviral host response. Appl Microbiol Biotechnol 93(2):601-11 doi:10.1007/s00253-011-3569-8

Shaw A (2012) New technologies for new influenza vaccines. Vaccine 30(33):4927-33 doi:10.1016/j.vaccine.2012.04.095

Shaw ML, Palese P (2013) Orthomyxovidae. In: Kipe DMH, P.M.; Griffin, D.E. (ed) Fields Virology. vol 1. Lippincott Williams & Wilkins, Philadelphia, pp 1151-1185

Shevitz J (2000) Fluid filtration system, US6544424B1. United States Patent,

Shiragami N, Unno H (1994) Effect of shear stress on activity of cellular enzyme in animal cell. Bioprocess Engineering 10(1):43-45 doi:10.1007/BF00373534

Shirgaonkar IZ, Lanthier S, Kamen A (2004) Acoustic cell filter: a proven cell retention technology for perfusion of animal cell cultures. Biotechnol Adv 22(6):433-44 doi:10.1016/j.biotechadv.2004.03.003

Silva AC, Roldão A, Teixeira A, Fernandes P, Sousa MFQ, P.M. A (2015) Cell Immobilization for the Production of Viral Vaccines. In: M. A-R (ed) Animal Cell Culture. vol 9. Springer, Cham., Cell Engineering, pp 541-563

Skehel JJ, Wiley DC (2000) Receptor binding and membrane fusion in virus entry: the influenza hemagglutinin. Annu Rev Biochem 69:531-69 doi:10.1146/annurev.biochem.69.1.531

Smith GJ, Vijaykrishna D, Bahl J, Lycett SJ, Worobey M, Pybus OG, Ma SK, Cheung CL, Raghwani J, Bhatt S, Peiris JS, Guan Y, Rambaut A (2009) Origins and evolutionary genomics of the 2009 swine-origin H1N1 influenza A epidemic. Nature 459(7250):1122-5 doi:10.1038/nature08182

Smith J, Dutkowski R, Ward P (2006) Antivirals for influenza in healthy adults. Lancet 367(9522):1571; author reply 1573 doi:10.1016/S0140-6736(06)68683-2

Spearman C (1909) Review of The Method of 'Right and Wrong Cases' ('Constant Stimuli') without Gauss's Formula. Psychological Bulletin 6(1):27-28 doi:10.1037/h0063767

Strahle L, Garcin D, Kolakofsky D (2006) Sendai virus defective-interfering genomes and the activation of interferon-beta. Virology 351(1):101-11 doi:10.1016/j.virol.2006.03.022

Strassburg MA (1982) The global eradication of smallpox. Am J Infect Control 10(2):53-9 doi:10.1016/0196-6553(82)90003-7

Su Y, Wei Z, Miao Y, Sun L, Shen Y, Tang Z, Li L, Quan Y, Yu H, Wang WC, Zhou W, Tian J (2021) Optimized process operations reduce product retention and column clogging in ATF-based perfusion cell cultures. Appl Microbiol Biotechnol doi:10.1007/s00253-021-11662-8

Swick A, Baltes A, Yin J (2014) Visualizing infection spread: dual-color fluorescent reporting of virus-host interactions. Biotechnol Bioeng 111(6):1200-9 doi:10.1002/bit.25170

Tan J, Asthagiri Arunkumar G, Krammer F (2018) Universal influenza virus vaccines and therapeutics: where do we stand with influenza B virus? Current Opinion in Immunology 53:45-50 doi:https://doi.org/10.1016/j.coi.2018.04.002

Tapia F, Laske T, Wasik MA, Rammhold M, Genzel Y, Reichl U (2019) Production of Defective Interfering Particles of Influenza A Virus in Parallel Continuous Cultures at Two Residence Times-Insights From qPCR Measurements and Viral Dynamics Modeling. Front Bioeng Biotechnol 7:275 doi:10.3389/fbioe.2019.00275

Tapia F, Vazquez-Ramirez D, Genzel Y, Reichl U (2016) Bioreactors for high cell density and continuous multi-stage cultivations: options for process intensification in cell culture-based viral vaccine production. Appl Microbiol Biotechnol 100(5):2121-32 doi:10.1007/s00253-015-7267-9

Tapia F, Vogel T, Genzel Y, Behrendt I, Hirschel M, Gangemi JD, Reichl U (2014) Production of high-titer human influenza A virus with adherent and suspension MDCK cells cultured in a single-use hollow fiber bioreactor. Vaccine 32(8):1003-11 doi:10.1016/j.vaccine.2013.11.044

Taubenberger JK, Reid AH, Fanning TG (2000) The 1918 influenza virus: A killer comes into view. Virology 274(2):241-5 doi:10.1006/viro.2000.0495

Thomassen YE, Rubingh O, Wijffels RH, van der Pol LA, Bakker WA (2014) Improved poliovirus D-antigen yields by application of different Vero cell cultivation methods. Vaccine 32(24):2782-8 doi:10.1016/j.vaccine.2014.02.022

Thomassen YE, van der Welle JE, van Eikenhorst G, van der Pol LA, Bakker WAM (2012) Transfer of an adherent Vero cell culture method between two different rocking motion type bioreactors with respect to cell growth and metabolic rates. Process Biochemistry 47(2):288-296 doi:https://doi.org/10.1016/j.procbio.2011.11.006

Tiley LS, Hagen M, Matthews JT, Krystal M (1994) Sequence-specific binding of the influenza virus RNA polymerase to sequences located at the 5' ends of the viral RNAs. J Virol 68(8):5108-16

Tobita K (1975) Permanent canine kidney (MDCK) cells for isolation and plaque assay of influenza B viruses. Med Microbiol Immunol 162(1):23-7 doi:10.1007/BF02123574

Tobita K, Sugiura A, Enomote C, Furuyama M (1975) Plaque assay and primary isolation of influenza A viruses in an established line of canine kidney cells (MDCK) in the presence of trypsin. Med Microbiol Immunol 162(1):9-14 doi:10.1007/BF02123572

Trampler F, Sonderhoff SA, Pui PW, Kilburn DG, Piret JM (1994) Acoustic cell filter for high density perfusion culture of hybridoma cells. Biotechnology (N Y) 12(3):281-4 doi:10.1038/nbt0394-281

Ulmer JB, Mason PW, Geall A, Mandl CW (2012) RNA-based vaccines. Vaccine 30(30):4414-8 doi:10.1016/j.vaccine.2012.04.060

Ulmer JB, Sadoff JC, Liu MA (1996) DNA vaccines. Curr Opin Immunol 8(4):531-6 doi:10.1016/s0952-7915(96)80042-2

Valenzuela P, Medina A, Rutter WJ, Ammerer G, Hall BD (1982) Synthesis and assembly of hepatitis B virus surface antigen particles in yeast. Nature 298(5872):347-50 doi:10.1038/298347a0

van Wielink R, Kant-Eenbergen HC, Harmsen MM, Martens DE, Wijffels RH, Coco-Martin JM (2011) Adaptation of a Madin-Darby canine kidney cell line to suspension growth in serum-free media and comparison of its ability to produce avian influenza virus to Vero and BHK21 cell lines. J Virol Methods 171(1):53-60 doi:10.1016/j.jviromet.2010.09.029

Vasin AV, Temkina OA, Egorov VV, Klotchenko SA, Plotnikova MA, Kiselev OI (2014) Molecular mechanisms enhancing the proteome of influenza A viruses: an overview of recently discovered proteins. Virus Res 185:53-63 doi:10.1016/j.virusres.2014.03.015

Velez D, Miller L, Macmillan JD (1989) Use of tangential flow filtration in perfusion propagation of hybridoma cells for production of monoclonal antibodies. Biotechnol Bioeng 33(7):938-40 doi:10.1002/bit.260330721

Von Magnus P (1951) Propagation of the PR8 strain of influenza A virus in chick embryos. III. Properties of the incomplete virus produced in serial passages of undiluted virus. Acta Pathol Microbiol Scand 29(2):157-81 doi:10.1111/j.1699-0463.1951.tb00114.x

Wang MD, Yang M, Huzel N, Butler M (2002) Erythropoietin production from CHO cells grown by continuous culture in a fluidized-bed bioreactor. Biotechnol Bioeng 77(2):194-203 doi:10.1002/bit.10144

Warnock JN, Al-Rubeai M (2006) Bioreactor systems for the production of biopharmaceuticals from animal cells. Biotechnol Appl Biochem 45(Pt 1):1-12 doi:10.1042/BA20050233

Wasik MA, Eichwald L, Genzel Y, Reichl U (2018) Cell culture-based production of defective interfering particles for influenza antiviral therapy. Appl Microbiol Biotechnol 102(3):1167-1177 doi:10.1007/s00253-017-8660-3

Webster RG, Bean WJ, Gorman OT, Chambers TM, Kawaoka Y (1992) Evolution and ecology of influenza A viruses. Microbiological Reviews 56(1):152

White KA, Morris TJ (1994) Nonhomologous RNA recombination in tombusviruses: generation and evolution of defective interfering RNAs by stepwise deletions. J Virol 68(1):14-24 doi:10.1128/JVI.68.1.14-24.1994

Whitley RJ (2010) Of ferrets and humans: influenza pathogenesis. J Infect Dis 201(7):976-7 doi:10.1086/651133

Wu P, Ozturk SS, Blackie JD, Thrift JC, Figueroa C, Naveh D (1995) Evaluation and applications of optical cell density probes in mammalian cell bioreactors. Biotechnol Bioeng 45(6):495-502 doi:10.1002/bit.260450606

Wu Y, Bissinger T, Genzel Y, Liu X, Reichl U, Tan WS (2021) High cell density perfusion process for high yield of influenza A virus production using MDCK suspension cells. Appl Microbiol Biotechnol 105(4):1421-1434 doi:10.1007/s00253-020-11050-8

Yamagata Y, Muramoto Y, Miyamoto S, Shindo K, Nakano M, Noda T (2019) Generation of a purely clonal defective interfering influenza virus. Microbiol Immunol 63(5):164-171 doi:10.1111/1348-0421.12681

Yanguez E, Nieto A (2011) So similar, yet so different: selective translation of capped and polyadenylated viral mRNAs in the influenza virus infected cell. Virus Res 156(1-2):1-12 doi:10.1016/j.virusres.2010.12.016

York A, Fodor E (2013) Biogenesis, assembly, and export of viral messenger ribonucleoproteins in the influenza A virus infected cell. RNA Biol 10(8):1274-82 doi:10.4161/rna.25356

Zahoor MA, Khurshid M, Qureshi R, Naz A, Shahid M (2016) Cell culture-based viral vaccines: current status and future prospects. Future Virology 11(7):549-562 doi:10.2217/fvl-2016-0006

Zhang S, Handa-Corrigan A, Spier RE (1993) A comparison of oxygenation methods fro high-density perfusion culture of animal cells. Biotechnol Bioeng 41(7):685-92 doi:10.1002/bit.260410702

Zhang Y, Stobbe P, Silvander CO, Chotteau V (2015) Very high cell density perfusion of CHO cells anchored in a non-woven matrix-based bioreactor. Journal of Biotechnology 213:28-41 doi:https://doi.org/10.1016/j.jbiotec.2015.07.006

Zhao H, To KKW, Chu H, Ding Q, Zhao X, Li C, Shuai H, Yuan S, Zhou J, Kok KH, Jiang S, Yuen KY (2018) Dual-functional peptide with defective interfering genes effectively protects mice against avian and seasonal influenza. Nat Commun 9(1):2358 doi:10.1038/s41467-018-04792-7

Zheng W, Tao YJ (2013) Structure and assembly of the influenza A virus ribonucleoprotein complex. FEBS Lett 587(8):1206-14 doi:10.1016/j.febslet.2013.02.048

Zost SJ, Parkhouse K, Gumina ME, Kim K, Diaz Perez S, Wilson PC, Treanor JJ, Sant AJ, Cobey S, Hensley SE (2017) Contemporary H3N2 influenza viruses have a glycosylation site that alters binding of antibodies elicited by egg-adapted vaccine strains. Proc Natl Acad Sci U S A 114(47):12578-12583 doi:10.1073/pnas.1712377114

LIST OF PUBLICATIONS

Peer-reviewed journal articles

Hein MD, Kollmus H, Marichal-Gallardo P, Puttker S, Benndorf D, Genzel Y, Schughart K, Kupke SY, Reichl U (2021) OP7, a novel influenza A virus defective interfering particle: production, purification, and animal experiments demonstrating antiviral potential. *Appl Microbiol Biotechnol* 105(1):129-146
Contribution: Conceptualization, Methodology, Investigation, Writing (original draft; review and editing), Project Administration

Hein MD, Arora P, Marichal-Gallardo P, Winkler M, Genzel Y, Pöhlmann S, Schughart K, Kupke SY, Reichl U (2021) Cell culture-based production and in vivo characterization of purely clonal defective interfering influenza virus particles. *BMC Biol* 19(1):91
Contribution: Conceptualization, Methodology, Investigation, Writing (original draft; review and editing), Project Administration

Hein MD, Chawla A, Cattaneo M, Kupke SY, Genzel Y, Reichl U (2021) Cell culture-based production of defective interfering influenza A virus particles in perfusion mode using an alternating tangential flow filtration system. *Appl Microbiol Biotechnol* 105(19):7251-7264
Contribution: Conceptualization, Methodology, Investigation, Writing (original draft; review and editing), Project Administration

Rand U, Kupke SY, Shkarlet H, **Hein MD**, Hirsch T, Marichal-Gallardo P, Cicin-Sain L, Reichl U, Bruder D (2021) Antiviral activity of influenza A virus defective interfering particles against SARS-CoV-2 replication *in vitro* through stimulation of innate immunity. *Cells* 10(7), 1756
Contribution: Investigation, Writing (review and editing)

Rüdiger D, Pelz L, **Hein MD**, Kupke SY, Reichl U (2021) Multiscale model of defective interfering particle replication for influenza A virus infection in animal cell culture. *PLOS Computational Biology* 17(9): e1009357
Contribution: Data curation, Formal analysis, Investigation, Methodology, Writing (review and editing)

Talks

Kupke SY, Riedel D, Frensing T, Kollmus H, Zmora P, Schughart K, Reichl U (2019) A Novel Type of Defective Interfering Particle for Antiviral Therapy. *26th ESACT Meeting*. Copenhagen, Denmark (poster spotlight presentation; presenter **Hein MD)**

Hein MD, Kollmus H, Genzel Y, Kupke SY, Schughart K, Reichl U (2019) Production of a novel class of influenza A virus-derived defective interfering particle as an antiviral agent. *14th PEACe.* Newport, USA (short oral presentation)

Hein MD, Tapia F, Kollmus H, Genzel Y, Kupke SY, Schughart K, Reichl U (2019) Continuous mode of production for two classes of defective interfering particles as antiviral candidates. *Integrated Continuous Biomanufacturing IV.* Massachusetts, USA

Hein MD, Chawla A, Cattaneo M, Kupke SY, Genzel Y, Reichl U (2021) Continuous virus harvesting of influenza A virus particles in perfusion mode using an alternating tangential flow filtration system. AdBIOPRO Workshop 2021 Bioproduction of Therapeutic Biologics. Bosön, Sweden

Posters

Hein MD, Genzel Y, Kupke SY, Reichl U (2019) Producing a new class of defective interfering particles as antiviral. *26th ESACT Meeting*. Copenhagen, Denmark

Hein MD, Kollmus H, Genzel Y, Kupke SY, Schughart K, Reichl U (2019) Production of a novel class of influenza A virus-derived defective interfering particle as an antiviral agent. *14th PEACe.* Newport, USA

Hein MD, Arora P, Marichal-Gallardo P, Winkler M, Genzel Y, Pöhlmann S, Schughart K, Kupke SY, Reichl U (2021) Defective interfering particles as antivirals: Production, purification, and animal testing. *30th Annual Meeting of the Society for Virology.* Hannover, Germany

Supervised thesis

Chawla, A (2021) High cell density perfusion process for the production of defective interfering influenza virus particles- DI244. *Master thesis.* Faculty of Sciences I – Biosciences, Martin-Luther-Universität Halle-Wittenberg, Halle, Germany

Patent

Rand U, Kupke SY, **Hein MD**, Bruder D, Reichl U (2021) Influenza virus defective interfering particles for use in the prophylactic or therapeutic treatment of *coronaviridae* infection. (EP21157812.5, pending)

APPENDIX

Appendix A – Supplementary information

Appendix A.1 – Optimal harvest time point for OP7 production

The impact of the harvest time point on the interfering efficacy of the produced OP7 material was investigated using an interference assay. However, no significant improvements were observed when compared to 32 hpi (Fig. A1).

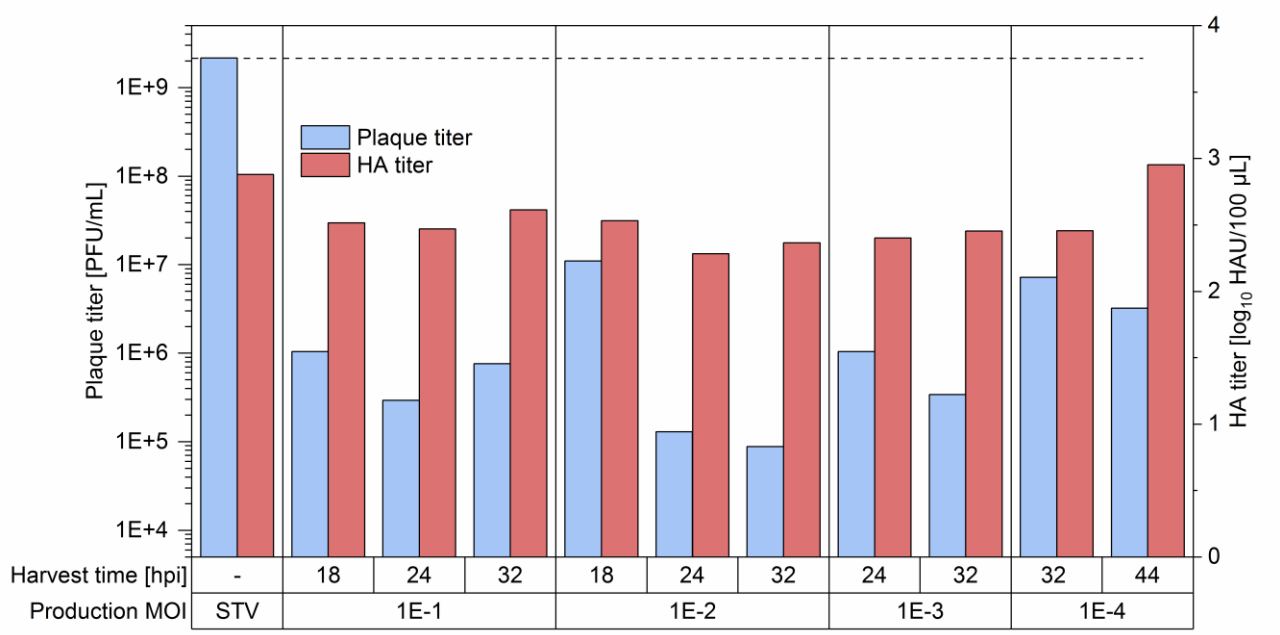

Fig. A1 Interfering efficacy of OP7 material produced at different MOIs and harvested at different time points. For the interference assay MDCK(adh) cells were infected at MOI 10 with STVs and co-infected with 125 µL of OP7 material, produced at a MOI ranging from 1E−1 to 1E−4 (and harvested at different time points) or medium as negative control (NC). At 16 hpi, plaque titers and HA titers were determined.

Appendix A.2 – VCC screening for OP7 production

To investigate the impact of the VCC at time of infection on the OP7 yield, screening experiments were carried out. For this, MDCK.Xe.E cells were cultivated in shake flasks (50 mL working volume) and infected with OP7 seed virus. Here, it was hypothesized that the optimal production MOI might

differ depending on the VCC at time of infection. Therefore, four MOIs ranging from 1E−1 to 1E−4 were tested for each VCC (Fig. A2 − Fig. A4). However, no strong impact of the VCC at time of infection on the interfering efficacy of the produced OP7 was observed (Fig. A5). Here, the accumulation of waste products (e.g. ammonium) may affected the virus propagation for higher VCCs. This was later circumvented by performing perfusion cultivations with a high perfusion rate and an additional medium exchange before infection.

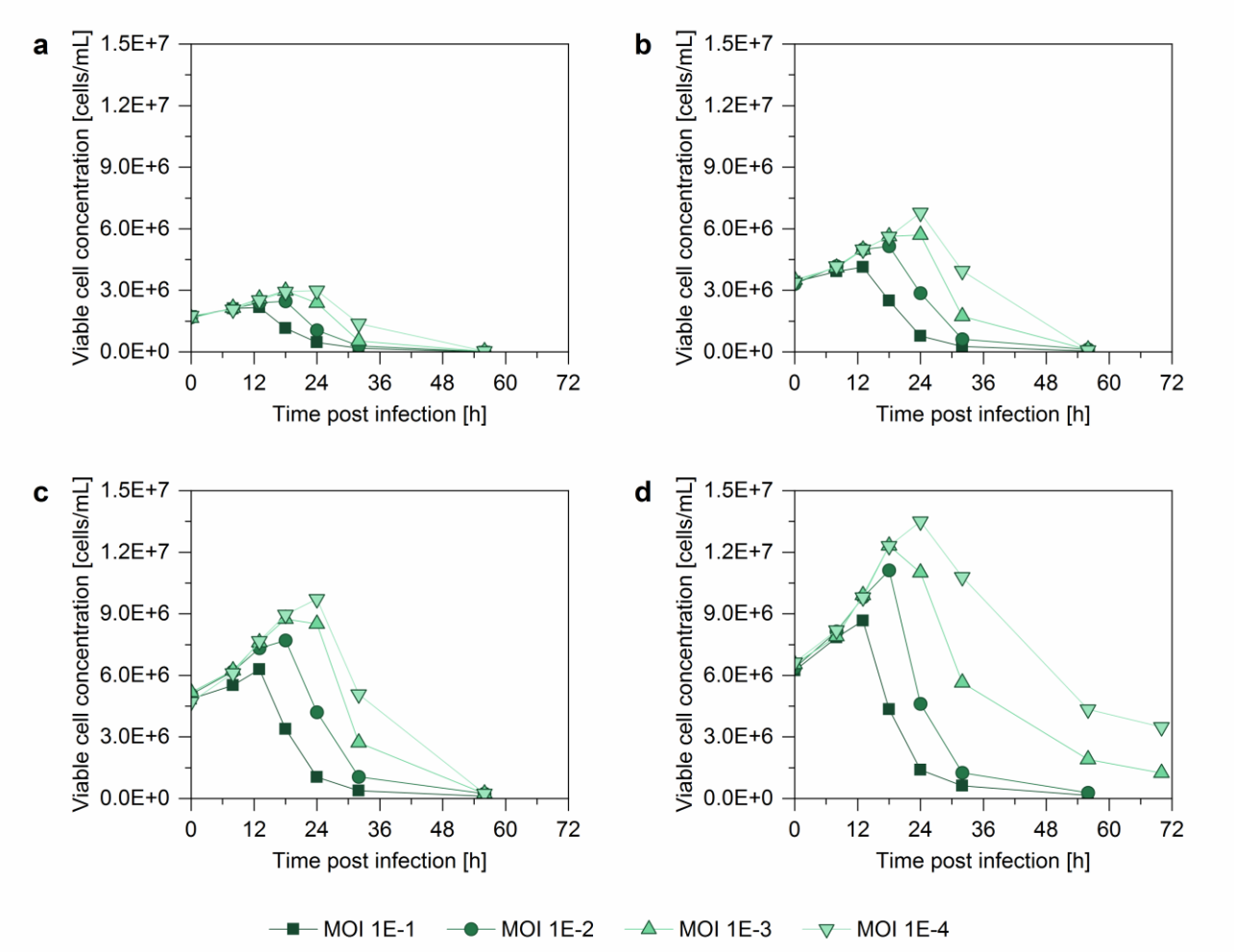

Fig. A2 VCC screening for batch mode production of OP7. MDCK.Xe.E cells were cultivated in shake flasks (50 mL working volume) and infected at different VCCs with OP7 seed virus at different MOIs. The VCC at time of infection was (a) 1.5E+6 cells/mL, (b) 3.0E+6 cells/mL, (c) 4.5E+6 cells/mL, and (d) 6.0E+6 cells/mL.

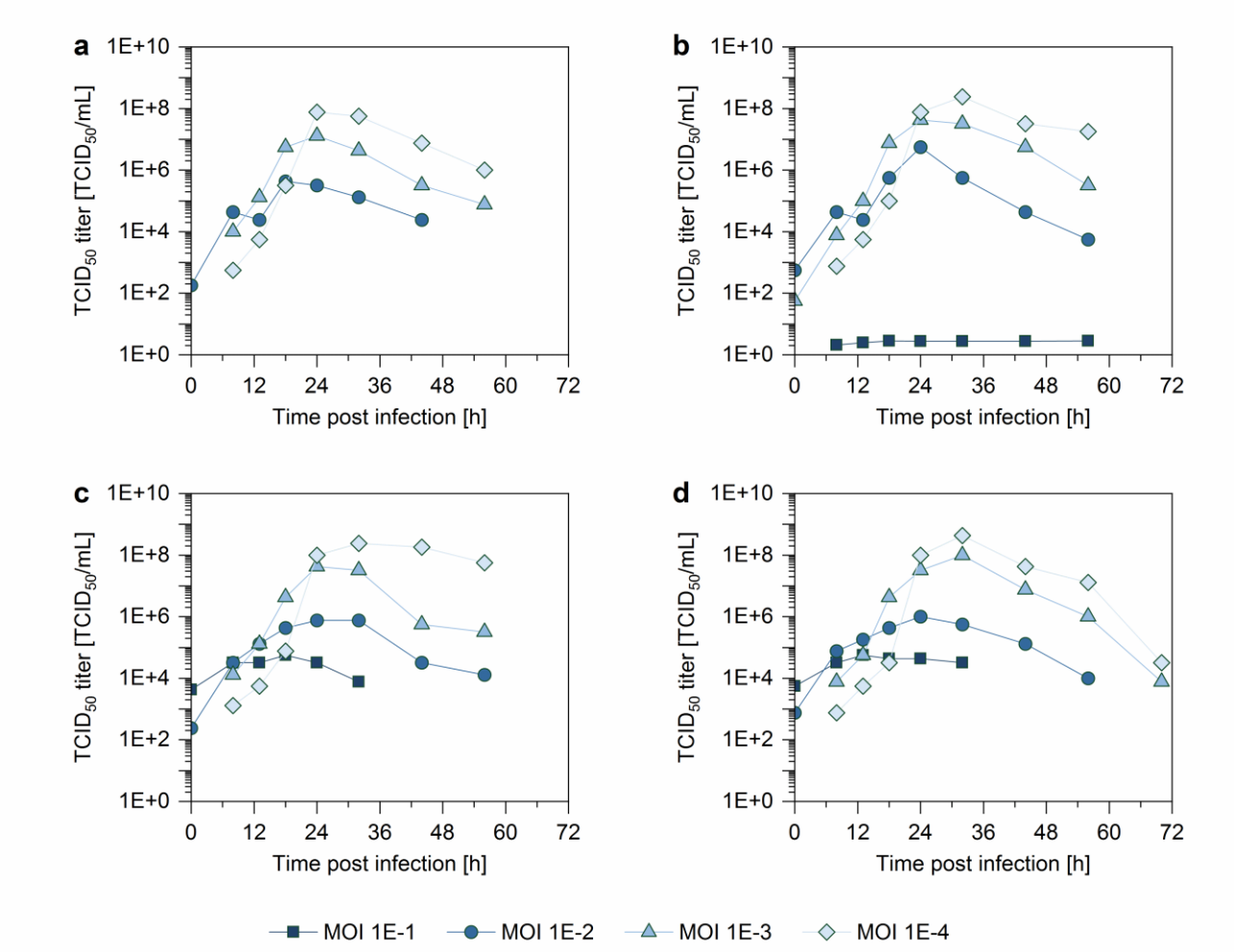

Fig. A3 $TCID_{50}$ of the VCC screening for batch mode production of OP7. MDCK.Xe.E cells were cultivated in shake flasks (50 mL working volume) and infected at different VCCs with OP7 seed virus at different MOIs. The VCC at time of infection was (a) 1.5E+6 cells/mL, (b) 3.0E+6 cells/mL, (c) 4.5E+6 cells/mL, and (d) 6.0E+6 cells/mL.

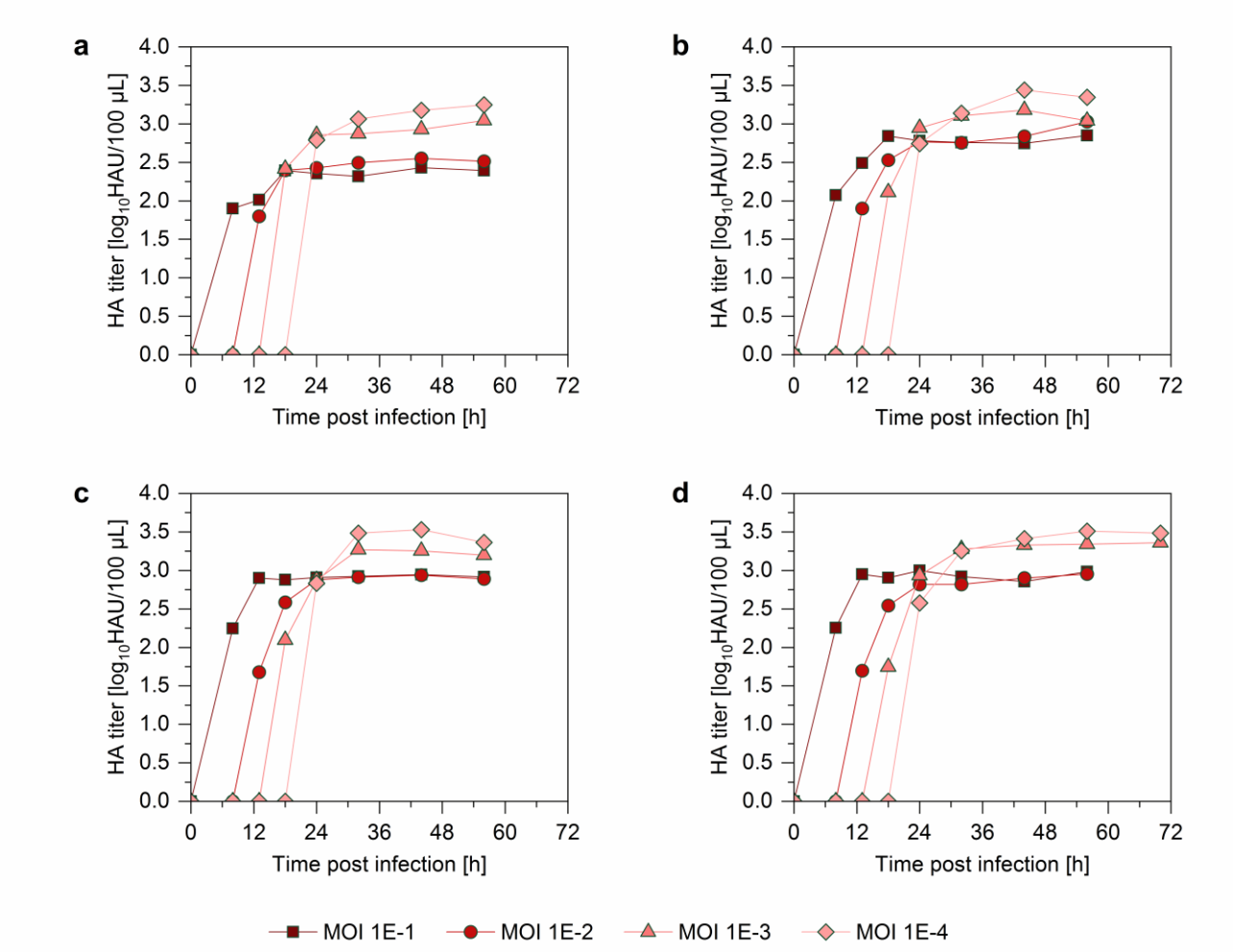

Fig. A4 HA titers of the VCC screening for batch mode production of OP7. MDCK.Xe.E cells were cultivated in shake flasks (50 mL working volume) and infected at different VCCs with OP7 seed virus at different MOIs. The VCC at time of infection was (a) 1.5E+6 cells/mL, (b) 3.0E+6 cells/mL, (c) 4.5E+6 cells/mL, and (d) 6.0E+6 cells/mL.

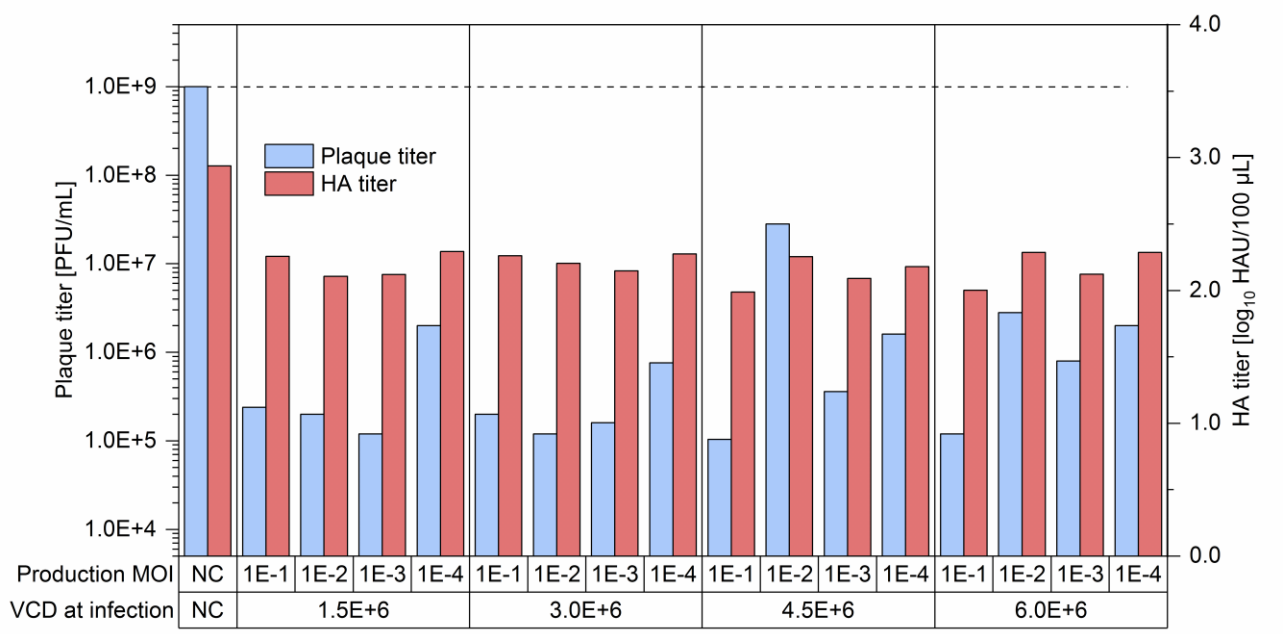

Fig. A5 Interference assay of the VCC screening for batch mode production of OP7. MDCK.Xe.E cells were cultivated in shake flasks (50 mL working volume) and infected at different VCCs with OP7 seed virus at different MOIs. The generated material was analyzed in an interference assay. Here, MDCK(adh) cells were infected at MOI 10 with STVs and co-infected with 125 µL of OP7 material or medium as negative control (NC). At 16 hpi, plaque titers and HA titers were determined.

Appendix A.3 – Particle-specific interfering efficacy of DI244 produced in batch and perfusion cultivations

To investigate the impact of the used production system on the interfering efficacy of produced DI244 material per particle, the DIP material was applied to the interference assay with a fixed MODIP of 100. Here, very comparable particle-specific interfering efficacies were observed for both production systems (Fig. A6).

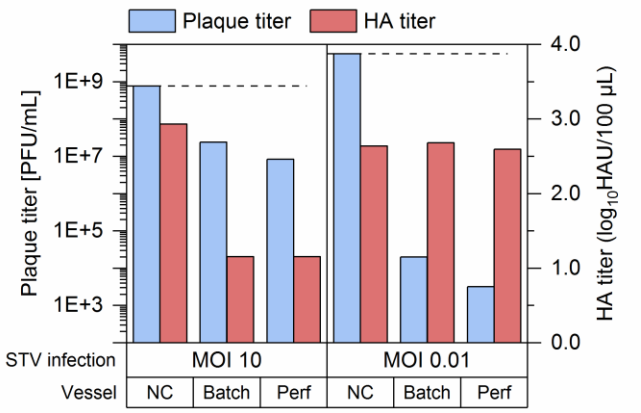

Fig. A6 Particle-specific interference assay of DI244 material. DI244 material was produced with MDCK-PB2(sus) cells cultivated in a STR (700 mL working volume) operated in perfusion mode (VHU1, Table 4.4) or in shake flask (50 mL working volume) operated in batch mode (Table 4.2, production replicate 2, MODIP 1E–2). For the interference Assay, MDCK(adh) cells were infected at MOI 10 or 0.01 with STVs and co-infected with DI244 material at MODIP 100 or medium as negative control (NC).

Appendix B – Preparation for Xeno™ medium

(1) Add the final volume of deionized or distilled water at 28–32°C
(2) Start stirring, but avoid bubbles
(3) Gently add Xeno™-CD001S powder at 21.04 g/L to water and mix for 20–30 min
(4) Adjust pH to 6.2–6.7 with 5 mol/L NaOH solution and mix for 10–20 min
(5) Precisely add 2.00 g/L sodium bicarbonate powder and mix for 10–20 min
(6) When everything is completely dissolved, adjust pH to 7.0–7.4 (if needed)
(7) Filter sterilize by 0.22 μm pore size membrane filtration
(8) After filtration, store at 2–8°C for up to one month. Protect from light.
(9) Add glutamine before usage

Appendix C – Lists of consumables, reagents, and equipment

Table C.1 List of consumables

Consumable	Manufacturer	Article number
6-well plates	Greiner BioOne	M8562
Bottle-top sterile filter	Nalgene	Z358215
PES membrane (0.2 µm, 470 cm^2)	Spectrum Labs	-
Shake flasks (baffled, 125 mL)	Thermo Fisher Scientific	4116-0125
Shake flasks (baffled, 250 mL)	Thermo Fisher Scientific	4116-0250
T175 flasks	Greiner BioOne	C7356
T75 flasks	Greiner BioOne	C7231
VHU membrane (~10 µm, 62 cm^2)	Artemis Biosystems	-

Table C.2 List of reagents

Reagent	Manufacturer	Article number
Agarose	AppliChem	A2114
Bovine serum albumin	Sigma-Aldrich	A1391
Bradford assay	BioRad Laboratories	500-0006
Crystal violet	Roth	C.I. 42555
dNTPs	Thermo Fisher Scientific	R0193
EDTA	Sigma-Aldrich	EDS-100g
FastDigest Green Buffer	Thermo Fisher Scientific	B72
FBS	Pan Biotech	10270-106
GeneRuler DNA Ladder Mix	Thermo Fisher Scientific	SM0333
GMEM powder	Gibco	22100-093
Isopropanol	Merck	1096342511
Lambda DNA	Promega	D1501
Maxima H Minus Reverse Transcriptase 5xRT buffer	Thermo Fisher Scientific	EP0753
Methanol	Roth	CP43.1
NucleoSpin RNA Virus kit	Macherey-Nagel	740956.250
Peptone	Lab M	LAB204
Phusion High-Fidelity DNA Polymerase 5x Phusion HF buffer MgCl2	Thermo Fisher Scientific	F530L
Primers	Thermo Fisher Scientific	-
Quant-iT PicoGreen assay	Life Technologies	P7581
RiboLock RNase Inhibitor	Thermo Fisher Scientific	EO0382
Roti-GelStain	Roth	3865.2
Rotor-Gene SYBR Green PCR Kit	Qiagen	204074
Trypan blue	Merck	1117320025
Trypsin	Gibco Sigma-Aldrich	1188797 T7409, T1426

Table C.3 List of equipment

Equipment	Manufacturer	Model name
3-D mixer	Heidolph	Duomax 1030
Agarose gel electrophoresis equipment	Biomed Analytics	Agagel Maxi Biometra
	VWR	Power Source 300V
	Gibco	BRL UV Transilluminator
	Biometra	BioDocAnalyzer
Autoclave	HP Medizintechnik	Varioklav 65T
ATF and controller	Repligen	ATF 2 with C24U-v2.0 controller
Balance	Satorius	TE1502S
		Cubis precisuion
Cell counter	Beckman Coulter	ViCell XR cell counter
Centrifuge	Thermo Fisher Scientific	Heraeus BiofugePrimoR, Fresco 17
	Beckman Coulter	Avanti J 20, Optima LE 80K
DO probe	Hamilton	78108039
Heat block	Grant Instruments	-
Incubator	Heraeus	Heracell 240
Laminar hood	Thermo Fisher Scientific	Safe 2020
Metabolite analyzer	Nova Biomedical	Bioprofile 100 Plus
Microplate reader	Tecan	Infinite 200 Pro NanoQuant
Microscope	Zeiss	Axioskop 2
pH meter	WTW	inoLab pH meter
pH probe	Hamilton	78103230
Pipetting robot	Qiagen	QIAgility
Pump	Watson-Marlow	120 U/DV
Real-time PCR cycler	Qiagen	Rotor-Gene Q
STR System	Eppendorf AG	DASGIP® Parallel Bioreactor System
Temperature probe	Eppendorf AG	78103304
Thermocycler	Biometra	T Professional Thermocycler
Water purification system	Millipore	Milli-Q Advantage A10